MODELLING AND CONTROL OF A FLUIDIZED BED GASIFIER

by

MOSHE KUTTEN

A dissertation submitted to the Graduate Faculty in Engineering in partial fulfillment of the requirements for the degree of Doctor of Philosophy, The City University of New York

1978

This manuscript has been read and accepted for the Graduate Faculty in Engineering in satisfaction of the dissertation requirement for the degree of Doctor of Philosophy.

8/15/78
date

Chairman of Examining Committee

8/15/78
date

Executive Officer

Professor R. Shinnar, Chairman

Professor J. Yerushalmi

Professor F.E. Thau
Supervisory Committee

The City University of New York

ABSTRACT

MODELLING AND CONTROL OF
A FLUIDIZED BED GASIFIER

by

Moshe Kutten

Advisor: Professor Ruel Shinnar

The thesis deals with an evaluation of the steady state and the dynamic behavior of an air blown fluidized bed coal gasifier to producing low BTU gas. There is a considerable current effort to develop low pollution, coal fired, power plants based on an integrated gasifier and a combined cycle system. The demands of the power industry for fast response to large fluctuations in demand put control requirements on such plants which are not encountered in the process industries. The thesis is concerned with the suitability of fluid bed gasifiers for this purpose and the way that the design of the gasifier affects its dynamic behavior and controllability.

A simplified model of such a gasifier is presented that allows evaluation of both the steady state and dynamic control strategies of such a gasifier. Fluidized beds have a limited range of steady state operation due to the velocity required for good fluidization. Our results indicate that even within this range there are potential

control problems that have to be taken into account in the development of such gasifiers.

It is shown that the steady state range of control can be sometimes considerably smaller than indicated by purely hydrodynamic consideration, as lower flow rates can lead to higher conversions.

The dynamic behavior shows a short time response dominated by the thermal inertia of the coal bed and a long time response, which is a function of the adjustment of the bed ash content to different flow rates. For good controllability it is important to be able to adjust ash removal rate. The short time response has the potential to exhibit an inverse response in the total fuel production to changes in air rate. This feature is important in the development of proper control schemes. The adjustment of the ash removal rate could introduce slow drifts with large time constants and could reduce the efficiency of the system at low production rates or during swings.

Both the dynamic and steady state features of the system strongly depend on the design of the system. It is therefore important that in the development of the gasifier there demands are taken into account. The results of the thesis illustrates the type of problems that may be encountered and suggests some potential solutions.

DEDICATION

To Nehama, whose love, encouragement and patience contributed more than anything else to the completion of this work.

ACKNOWLEDGMENT

The author wishes to express his profound appreciation and gratitude to Professor R. Shinnar, his Graduate Advisor, for his guidance, inspiration and assistance at all times during the course of this work. He would like to thank his parents for their help and encouragement.

Financial assistance was made available by the National Science Foundation. This aid is gratefully acknowledged.

TABLE OF CONTENTS

LIST OF TABLES

LIST OF FIGURES

Figure

Figure

Figure

Figure

Figure

Figure

Figure

Figure

Figure

Figure

Figure

I. Introduction

Coal gasification leading to either medium or low BTU gas is one of the options considered for future coal fired power plants. Followed by a combined cycle power plant, it will provide clean power generation at reasonable efficiencies. At present, such plants are still on the drawing board. They present some interest challenges for the process control engineer.

Coal gasifier followed by a scrubber is a complex chemical plant. By combining the gasification system with a power plant, we force it to follow loan variations. There is a difference between a power plant and a chemical plant. Power plants experience variable outputs and have to be able to adapt to relatively fast load changes over large ratios of output. In the terminology of the power plant engineer, the ratio between the maximum and minimum capacity at which the power plant is required to be operable is called the turndown ratio. Desirable turndown ratios for power plants are from frou to eight, whereas even a ratio of two is large for any chemical reactor. Following such changes is especially difficult if they occur over short time spans.

This is a challenging control peoblem, and it might have some implications on the final design choice. In a previous paper by the advisor (Shinnar and Silverstein, 1977), the effect that steady state design has on controllability is reviewed by discussing the design of a hydrocracker. One of the conclusions drawn was that taking the control problem into

account in the initial design and development is justified in cases where control is expected to be difficult.

Different coat gasifiers under consideration have totally different dynamic behavior. To make intelligent choices one needs to understand the way each one behaves under strong fluctuations of the inputs. In this paper our goals are somewhat more modest. We intend to concentrate on fluidized bed gasifiers, investigate their steady state behavior and correlate their dynamic behavior under different conditions.

Here, we face a problem similar to the one faced in the investigation and design of hydrocrackers. The kinetics, as well as the fluid dynamic behavior of the fluidized bed gasifiers, are complex, not well known, and will change from coal to coal. What we need is not an exact process model, but rather an understanding of the critical parameters of the system and its general behavior. We can reach this goal by looking at a set of simplified models that incorporate the basic physics and chemistry of the process and find the parameters which dominate the steady state and the dynamic behavior of the process (see also Kestenbaum et al (1976) and Palmor and Shinnar (1977)).

2. Fluidized Bed Gasifiers

Let us start with a short description of the gasifier, envisioned in Figure 1 as part of a combined cycle power plant, and discuss some of our assumptions as to the modelling and the design of the reactor.

At the bottom the gasifier is fed with preheated steam and air. Part or all of the steam needed for gasification can be produced at the exit of the gasifier where the gas is cooled for the cleaning process. The air is supplied to the gasifier by the gas turbine compressor. Being connected on line with the power cycle, the amount of air being supplied to the gasifier by the compressor is a function of the power demand imposed on the power cycle. The air input to the gasifier in this case is, therefore, the main input variable determining the output of the gasifier. Other manipulated variables are needed to control the condition in the gasifier.

At the top the gases are passed through a heat exchanger in which steam is generated and then through a H_2S absorption column. Coal may be fed into the fluid bed at either the top or in the bottom of the bed. The location of the feeding point is essential from two points of view. Feeding the coal at the top serves to increase the amount of CH_4 produced during the devolatilization process due to the higher H_2 partial pressure. It also increases the formation of tars. Rapid mixing of the fresh coal with hot char will minimize or eliminate tar production and, therefore, a feeding point closer to the hotter zone of combustion at the bottom of the bed is probably desirable. For our purposes we will assume that the coal is immediately mixed with hot char and no tar is formed.

We assume that the solid in the gasifier is well mixed and due to the large movement of solid, most of the gasification section of the bed is reasonably isothermal. In the combustion zone at the bottom there are local zones of higher temperature.

Due to the short gas resident time, the thermal holdup of the gas can be neglected. At any instant, therefore, the outlet composition of the gas is given by the instantaneous bed condition and the inlet composition and flow rate of the gas.

One of the important design considerations in a fluid bed gasifier is the way that coal is added, ash is removed and the amount of solid in the bed is controlled. Various schemes have been proposed (Westinghouse and IGT), in which the ash agglomerates and is removed, preferentially while the unreacted char remains in the bed. For our model, we assume that the solids removed are identical to the solids in the bed and solids carried over with the gas are returned to the bed. We further assume that the coal feedrate can be adjusted and the amount of char in the bed, measured by differential pressure gauges, is adjusted by controlling the feed rate. Removal rate can be independently controlled, but as it is much harder to monitor and adjust, we make the assumption that adjustment of removal rate is a slow process, and that during fast changes the rate of solid removal stays constant. A simple mass balance shows that the ash concentration in the bed is uniquely determined by the ratio of feed rate to removal rate.

We consider here as our base case a one-stage fluid bed of considerable height (10-20 feet unexpanded height), fed with coal of about 1/8" average particle size and operating without ash agglomeration. (Analysis of the coal is given in Table 1). Ash is removed from the bed at rather a constant or an adjustable rate. The gas feed is a mixture of a preheated air and steam operating at linear velocities of 2-5

feet/sec. To avoid excessive tar formation, the bed would have to operate above 1600°F. There is also an upper limit on the temperature (about 1800-1900°F) if we assume no agglomeration.

We state these conditions in advance as any simplified modelling procedure is valid only in a certain range of conditions. We can now develop the basic equations of our model.

3. Modelling of a Fluid Bed

The various gasification reactions can be lumped into three main lumps according to the relative rates of the chemical phenomena.

3.1 Devolatilization of Coal

Upon entering the bed, the coal decomposes instantaneously into volatile matter and char. This process, at the given temperature range, occurs in the order of magnitude of few seconds (Wen et al, 1974). Kinetics can be neglected therefore as the time scale of the total response is larger due to the large holdup of char in the bed.

The products of devolatilization are assumed to be mainly CH_4, CO_2, CO, H_2, H_2O, and H_2S (Anthony (1976), Menster (1974), Wen (1974), Johnson (1977)). We assume here, for simplicity, that all oxygen and sulfur is emitted in the volatiles, that the amount of CH_4 formed is a function of hydrogen pressure and the type of coal only and that the remaining char contains only hydrogen. The thermal decomposition of CH_4 is

neglected here and the devolatilization is considered to be thermally neutral. The exact balances for the decomposition assumed for our model are given in Table 2.

Devolatilization coefficients change from coal to coal and also depend on temperature, heating rate and total pressure. Methane, at these temperatures, might partially decompose to char and H_2. The ash may have catalytic properties, which could effect both the formation and decomposition of methane. There are insufficient data in the literature to accurately estimate these coefficients at actual gasifier conditions. Our set of parameters was chosen, therefore, to give a reasonable estimate of the process, based on the available data.

3.2 Combustion of Char With Air or Oxygen

$$CH_a + (1+\tfrac{1}{4}a)O_2 \rightarrow CO_2 + \tfrac{1}{2}a\ H_2O \qquad (1)$$

Air or oxygen entering the bed contacts mainly devolatilized char which is assumed to be completely combusted to CO_2 and H_2O. This reaction is assumed to occur mainly in the lower section of the bed (first foot) and can, therefore, be assumed to be immediate. At temperatures above 1600°F combustion reactions are fast and as long as the bed contains a significant concentration of carbon (above 20%), most of the oxygen will be consumed at the bottom. To confirm that assumption, the consumption of oxygen in the air was computed at different conditions and at temperature range above 1500°F, using reaction rates given in the literature (Field (1967)), (see example in Appendix 1).

When carbon or char reacts with oxygen, it forms a mixture of CO and CO_2 (Caram (1976), Avedesian (1973), Field (1967)). At temperatures above 1600°F mostly CO is formed, but the reaction between CO and O_2 is practically immediate in terms of the residence time in the bed. The oxygen diffusing into the particle will convert most of the escaping CO and CO_2, in the boundary layer around the particle.

3.3 Gasification Reactions

The controlling reactions of the gasifier are:

2a. $CH_a + H_2O \rightleftarrows CO + (1+\frac{1}{2}a)H_2$

2b. $CH_a + CO_2 \rightleftarrows 2CO + \frac{1}{2}aH_2$

2c. $CO + H_2O \rightleftarrows CO_2 + H_2$

Reaction rates and rate constants suggested by various investigators for reactions (2a) and (2b) are also not accurately known. The scatter in figures 2a and 2b is large, particularly with respect to the reactivity of the coal.

Reaction (2c) is rather fast as compared to the residence time and other reactions. We assumed, therefore, that at each point the gas is shifted to equilibrium with respect to reaction (2c).

Reaction rate depends strongly, not only on the coal being used, but also on the surface area available for reaction, on the conversion of the carbon in the bed and on the thermal history of the char particles. At high temperatures the reaction becomes diffusion controlled for large particles, but for the particle sizes and temperatures involved in the

fluid bed treated here, diffusional resistance is small for the gasification reaction. We will try to overcome some of those uncertainties by looking at the behavior of the bed at different activation energies for reactions (2a) and (2b), and by using different reactivities for the coal.

Having outlined the chemical reactions, we come to the description of the flow regime in the bed. The problem is compounded by the complexity of the process and the lack of supporting data on large scale gasifiers where high pressures, high gas velocities, large solid inventories and relatively large particle sizes are being utilized. However, we are saved by the fact that we deal with a process which is not very sensitive to the flow model.

Two main factors determine the sensitivity of the product composition to the model assumed for the reactor. The first is the conversion. The second is the flow regime and the mixing in the reactor. If high conversions are desired, than any reaction becomes very sensitive to the flow regime. For the type of reactor we are discussion (uniform mixed solids and temperature), the highest conversion is achieved under plug flow conditions. For very high conversions, even small deviations from plug flow are important. For conversions below 60%, this sensitivity is strongly decreased. While the conversion of the oxygen is complete, the conversion of the two controlling reactions (reactions (2a) and (2b)), is going to be incomplete in the gasifiers discussed.

The combustion reaction occurs at the bottom, both at the solid surface and inside the bubbles. As it is fast in this temperature range, there is very little chance of any by-pass of oxygen in the bubble phase, as oxygen will react with any gasification products present in the gas phase. If oxygen reacts with some of the hydrogen or CH_4 released instead of char, then the total heat released by the combustion of oxygen would increase and the conversion of char to fuel gas would be slightly reduced.

This brings us to the second criterion, namely, the sensitivity of a kinetic model to mixing and flow phenomena. If we consider a single reaction (such as 2b), then by plotting the product composition in a composition space as a function of the space velocity, we get a trajectory independent of the flow regime. The trajectory will be identical for a stirred tank, a plug flow reactor, or any of the complex bubble models mentioned in the literature. The only difference will be in the location of the points on the trajectory for different space velocities. A desired conversion represented by a specific point on the trajectory will require a lower space velocity in a stirred tank than in a plug flow reactor.

For consecutive reactions this is not true, especially in the region where the intermediates dominate. There, the trajectory is very sensitive to the mixing regime. The same applies to all complex reaction systems. One can test this by plotting the trajectory for both a plug flow reactor and a stirred tank reactor and note whether or not they superimpose.

Our system is more complex than a single reaction as it contains consecutive reactions. However, in the region of interest, the trajectories in the composition space for a stirred tank and a plug flow models are identical, as can be seen from Figure 3a. The type of flow model being used to characterize the behavior of the reactor is therefore not of prime significance, at least in the range of conversions below 80%. As previously mentioned, we lack experimental information about the behavior of large fluidized beds of this type. Good contact between solids and gas exists in such beds though, at any instant of time, some of the solid is not well accessible (see Krambeck, (1969)). A reasonable good approximate model for fluidized beds of this type is simply a plug flow reactor with an apparently lower reaction rate (about 50-60% of that of a packed bed).

Using complex models for our purpose would not ensure, therefore, more accurate description of the fluidized bed reactor.

To illuminate the above discussion we replot, in Figure 4, some of the results of Kato and Wen (1969). In the region of moderate conversions, the difference between their bubble model and the modified plug flow is not very large and both models fit the available data reasonably well. We should, however, remember that none of these experiments are from industrial sized beds, which involve much higher bed heights and higher gas velocities.

The main problem in predicting the behavior of such a gasifier does not relate to the gas flow, but rather to the behavior of the solids. The rates of the gasification reactions, (2a) and (2b), are dependent on product composition, and reaction rates given in the literature often include Langmuir type terms in the denominator. Thus, for (2a), the rate may be given by:

$$r = \frac{K_1 \cdot P_{H_2C}}{1 + K_2 \cdot P_{H_2} + K_3 \cdot P_{H_2O}} \qquad (3)$$

In a fixed bed at a steady state the concentrations in the denominator are the local concentrations. In a fluid bed the solid moves and continuously sees a different environment. There is indication that this might effect gasification (Squires, 1961). Most Kinetic data for fluid bed gasification are obtained in heated beds using steam or steam and CO_2 mixtures as the sole gasification medium. The combustion reaction at the bottom could influence the inhibition effects of the products. Rate equations obtained in fixed beds or in fluid bed with low conversion and uniform gas concentration are, therefore, of questionable value for large scale fluid beds, especially with respect to overall pressure dependence.

For our purpose, pressure dependence is only important in one sense. In some of the control schemes envisioned, the overall pressure is reduced when the air feed is reduced. Here, we need a reliable overall pressure dependence for the gasification rate to make useful predictions. We intend to investigate the problem by comparing the steady state behavior and the

dynamic response for different pressure sensitivities of the gasification rate.

There is another insufficiency in our model in the sense that real fluid beds are never isothermal, especially if very fast exothermic reactions such as the combustion reactions are involved. Individual particles might ignite, especially inside the bubble, and may reach much higher temperatures (Gordon and Amundson (1976), Luss and Amundson (1969)). This would cause agglomeration which might be detrimental to the overall operation. Those effects of temperature non-uniformities which might be stronger at lower gas velocities are important from the control point of view, as it could lead to strong constraints on our ability to vary the load. Modelling in this case can only point out potential difficulties. The problem is too complex and too dependent on system parameters and design, and can't lend itself to accurate predictions.

On the gas composition itself, as well as on the average temperature behavior, the non-uniformities at the bottom have very little effect as we will show later.

Having outlined our basic model, we can now present its equations in terms of mass and heat balances. A summary of the model equations is given in Table 4.

4. Steady State Behavior of the Gasifier

Let us first look at the overall steady state behavior of such a gasifier in terms of the design and operating parameters involved, assuming air as the gasifying medium.

The behavior of three major outputs should be examined both by the steady state and the unsteady state analysis:

1. The temperature of the bed which has to be in rather reasonable limits because of the constraints mentioned earlier.
2. The BTU content of the gas given in BTU/SCF.
3. The total energy output of the clean fuel gas supplied to the turbine, given in BTU/Hr.

The important input variables potentially at our disposal at which we have to look are:

1. air flow rate
2. steam flow rate
3. coal feed rate
4. solid holdup in bed
5. withdrawal rate of ash
6. pressure

Other inputs, such as the coal properties and the inlet temperatures, are assumed to be known and fixed.

In Figure 3b we show the effect of the inverse space velocity (or the bed holdup) on the output variables for the base case, both for a plug flow and a stirred tank reactor. The variable used here as a reference is defined by the ratio: Solid inventory/gas feed flow rate (air + steam).

In Figure 3c we plot the output variables to show that the results are really quite insensitive to the flow regime, in the sense that for a constant inlet composition, the outlet

composition is a unique function of the bed temperature. What backmixing does is that it changes the holdup required to achieve a given conversion (or bed temperature, which is a function of the gas conversion). This is another way of showing that we are dealing here with a single trajectory in the component space. As we have several reactions, it seems incorrect at first glance. It can be explained as follows: the combustion process is very fast and goes to completion regardless of mixing phenomena. The same applies to the devolitization reaction. The controlling reactions are the two gasification reactions. These are coupled to each other via the shift reaction and, therefore, act as if they are a single reaction. One of the output variables plotted in Figure 3c is the H_2 content of the gas. In a power plant we are actually only interested in the total BTU/Hr and the heating value and not in the detailed composition, but H_2 content is measured rather easily and could serve as a control variable.

In the above figures the carbon content of the bed is kept constant (30%) and so is the input gas composition (steam/oxygen = 2.0 mole ratio).

In Figure 5a we give similar results for another main variable, namely, the steam to oxygen ratio. (To get the steam/air ratio, one has to multiply by 0.21.) This ratio is the main control variable of the system. We plot the temperature, the heating value and the cold gas efficiency, assuming constant linear velocity. We will use similar representation for all other plots when comparisons between the base case of the plug flow reactor and other models are given.

In Figure 5a the holdup is held constant and so is the carbon content of the bed (30%). Feed and withdrawal rates are adjusted accordingly. The steady state characteristics of the model in which gasification reactions assumed to reach equilibrium are also presented. It is evident that within the high temperature region (above 2000°F, low steam/oxygen ratios), the kinetic model approaches the equilibrium model, while the composition is far from equilibrium at the lower range of temperatures.

We note that the temperature decreases continuously with increasing steam to air ratio. As our temperature range is constrained by other criteria, only a small portion of the curve will be useful for operation. This range will change according to the reactivity of the coal and can also be affected by the bed holdup. We give therefore (Figures 6a-6d) the steady state curves for different activities and bed holdups.

The heating value in Figure 5a attains a maximum at a rather high steam to air ratio. This maximum exists due to the low reactivity of the coal at low temperatures.

The cold gas efficiency -η, increases monotonously with the steam to air ratio. However, this does not necessarily mean that higher steam to air ratios leads to higher thermal efficiencies. When judging thermal efficiency we have to take also into account the need to raise the steam. We defined an approximate expression for the net thermal efficiency as follows:

Denoting: Total BTU = L.H.V. of dry gas x output flow rate (4)

We get that:

$$\eta_{net} = \frac{\text{Total BTU of output gas} + E_G - E_S}{\text{L.H.V. of coal} \times \text{lb coal gasified}} \quad (5)$$

where E_G is the sensible heat that can be generated by cooling the gases to 400°F and E_S is the energy needed to raise the steam.

Equation 5 is slightly arbitrary. The efficiency and the losses of the gasifier strongly depend on the boundries of the unit thermal balances and the way that low quality heat is being used. What we want to express here, in a quantitative way, is the fact that if we supply excess high quality steam at high temperature and condense it in a diluted form, we lose free energy in the sense that the energy recovered does not have the same value as the energy supplied. We express it by neglecting the heat recovered from the condensation of the steam in the product gas which might be slightly over-conservative.

In Figure 5b we plot the net thermal efficiency together with the cold gas efficiency for two different reactivities. The overall efficiency decreases with the steam to air ratio. Highest values are achieved at low steam to air ratios. On the other hand, η increases with the steam/air ratio. A compromise should be chosen, as we want a high fraction of the BTU in the form of fuel gas and not in the form of steam. The limiting parameters are the temperature and the fluid bed operability. Figure 5b illustrates clearly the efficiency penalties involved in different types of operation.

In Figure 7 we compare our base case with similar curves for a case where the gas flow is represented by a stirred tank. The difference is not significant. The largest deviations are obtained at the region where the conversions are high (high heating value).

In that sense our results are not sensitive to the exact mixing regime in the bed. However, we have to qualify that statement. At low gas velocities the quality of the fluidization changes. Low velocity fluid bed draws rather bad content qualities and non-uniform temperatures. This would strongly change the form of the steady state behavior with respect to gas throughput. This cannot be handled by modelling. Such flow regimes are also difficult to scaleup and should be avoided in good design.

5. Sensitivity of the Steady State to Temperature Uniformities and the Kinetics of the Gasification Reactions

We noted before that not only are the reaction rate constants imperfectly known, but they may vary from coal to coal and the sensitivity to reactivity of the coal was presented. We also looked at the sensitivity of the model to the mixing regime of the fluidized bed. In the following, the analysis is extended to include the sensitivity to some other simpligying assumptions which were used to derive the model.

A basic simplifying assumption is that the oxygen in the combustion section is converted completely to CO_2. To check the effect of incomplete combustion on the steady state behavior of the bed, we investigate an alternate case in which the combustion reaction at the bottom results in a mixture of CO_2 and CO, in equal molar parts. For simplicity we assume that the rest of the reactor behaves as a stirred tank reactor.

The steady state performance of the bed under these conditions differs from our base case. To better understand the meaning of this deviation, we tried to compare the curves of

this case with the base case curves in which only CO_2 is formed. However, the comparison is done by adjusting the reactivity of the coal in the base case to give the closest overall fit between the two cases.

The results are given in Figure 8. As in Figure 5, the linear velocity, the holdup and the carbon content of the bed are kept constant while the output variables (temperature, heating value and cold gas efficiency) are plotted against the steam to oxygen ratio.

We note that the case in which CO and CO_2 are formed in equal molar quantities in the combustion section is very similar to our adjusted base case with a 30% increase in the coal reactivity.

Another simplifying assumption used in deriving our model was the temperature uniformity in the bed. Actually, near the air inlet the temperature is higher than in the rest of the bed. The temperatures in the hot region can be controlled, and the gradient can be minimized by a better design, but the phenomena will always occur. To investigate the effect of such nonuniformity of the temperature, we constructed a model in which the fluidized bed is divided into two zones (see Figure 9). Constant solid holdup is assumed in both sections. Fresh coal is fed into the upper zone. The solid is exchanged between the two sections but ash is withdrawn from the process, only from the upper zone. We arbitrarily chose some reasonable parameters for the model. The carbon content of the upper part was taken to be equal to the base case value (30%) and the ash withdrawal rate is adjusted accordingly. The gas feed (air + steam) enters

the lower zone. The combustion products from the lower zone are fed to the upper section. The bottom zone is hotter and contains lower coal concentration.

The results are shown in Figure 10. Again, the performance of this model is equivalent to the base case with increased reactivity. (The factor of three obtained is a coincidence.) Higher temperatures at the bottom contribute significant kinetic advantage as the conversion is increased without reducing the thermal efficiency. We would, therefore, expect in a large bed, higher activities than we could predict from small, well controlled temperature, pilot plant experiments.

Two stage processes (such as the proposed entrained gasifiers or the moving bed with its high bottom temperatures) have certain advantages in this sense. Those gasifiers have also some disadvantages, but a broad comparison between several types of gasifiers is beyond the scope of this paper.

In a fluidized bed, a high temperature zone near the air inlet could result in ash agglomeration. We would only benefit from it if the agglomerate can be removed as suggested in some designs. However, in order to operate in a nonagglomerating way, the temperature gradient has to be kept below a certain limit.

While the overall behavior of the two stage model and the base case model is similar, the higher temperature zone at the bottom introduces some problems with respect to both scaleup and modelling of the reactor, and an experimental investigation is required before their importance can be assessed. The excess temperature at the bottom could change both with scaleup and gas velocity, which makes predictions more difficult.

Another basic assumption of our model, namely, the fact that the shift reaction is fast and attains equilibrium throughout the bed, is investigated in Figure 11. For comparison we assume an extreme case in which the shift reaction (2c) is very slow and can be neglected. The performance of this case deviates from the base case, especially in the high steam partial pressure region (high steam/oxygen region). It can be explained by the fact that the shift reaction is an exothermic reaction. Lower temperatures are resulted when the reaction is neglected and, therefore, lower conversion, lower methane formation (due to the lower H_2 partial pressure), and lower total gas flow rate at the output.

The steep decrease in the heating value and in the cold gas efficiency is offset a bit by the fact that steam is not included in the net dry heating value calculation, (and more steam remains in the output gas in this case). At the range of low steam partial pressure the latter phenomenon is dominating, and there is also a narrow region in which a reverse shift reaction is taking place. Neglecting the shift reaction in that region contributes, therefore, to higher heating values as compared to the base case.

In Figure 12 we give the performance of the bed at a different activation energy of the gasification reactions (-50% of the base case value). In order to be able to compare this case with our base case, the exponential rate constant was adjusted to give the same reaction rate at T = 1705^{o}F (corresponding to a steam/oxygen ratio = 2.0 in the base case). The largest effect on the performance of the reactor is, of course, at the region

of high steam/air ratio where the steam partial pressure is high.

This simulates the effect of partial diffusion controlled reaction rates. We have neglected in our model, diffusion effects inside the particles, as well as boundary layer mass transfer effects. At the range of temperatures of interest below 1800°F and the small particles envisioned (about 1mm average), this is a reasonable assumption consistent with experimental evidence. Checking the performance of the model for deviations in activation energies serves to understand the effect of diffusion for the cases where it may apply.

At last we also show the effect of the devolitilization process. This is done by looking at the extreme case, where the feed consists of char instead of fresh coal. The char is gasified with air to release only negligible amounts of methane. The results are given in Figure 13.

The composition of the char in this case was assumed to be similar to the one obtained in our base case after completion of the devolitilization. The heating value and the cold gas efficiency attain lower values as compared to our base case, due to the fact that no methane is formed and also due to the fact that no humidity was assumed in the char. The maximum for the heating value lies to the left of the base case maximum.

6. Steady State Control

In any design where we have to operate the unit over a wide range of throughputs and feed properties, we have to provide the capability for such changes in the design while taking into account the strong constraints in its operating conditions.

There are two aspects to the control problems:

a) What are the steady state operating limits, and what are the penalties involved in operating at a throughput different from the initial design?

b) What happens during dynamic changes, or when adjusting from one steady state to another?

Let us first look at the steady state problem and the limitations it imposes. For a fluid bed at a constant pressure there are strong limitations as to how much the flow rate can be adjusted. We need a high gas velocity to provide the proper mixing. At turndown ratio of 2-3 is probably the most we can allow.

But even a reduction of the flowrate by a factor of 2 will cause significant changes. Higher conversion will be achieved due to increased gas contact time (or decreased space velocity). This would reduce temperature maybe more than can be afforded. To illustrate these changes we plot in Figure 14 for one design example, the effect of changing steam or air rate on the main output variables. In Figure 14 the ash withdrawal rate is a constant fraction of the coal feed and, therefore, coal conversion is kept constant for each operating point.

The results are given in form of isotherms (Figure 14a), curves of constant total heating value/hr (Figure 14b) and curves of constant heating value (Figure 14c), using total air flow and steam flow as the prime input variables. Total solid inventory is held constant, such that the ratio (W/Fg) and the space velocities are different for each operating point. The

base operating point is indicated at the cross of the two axes. Value of the air flow rate and the steam flow rate are given both in absolute value (lb mole/hr·ft^2) and as a ratio between the value at each operating point and the corresponding base case value.

From an operational point of view, termperature is an important constraint. Excess temperature will lead to agglomeration, and lower temperatures could lead to tar formation and reduced reactivity. If we want to keep a constant temperature, then reducing air rate requires an even stronger reduction of the steam to air ratio. Due to the lower space velocity, conversion will increase and the excess steam must be reduced to maintain a constant temperature. At very low space velocities the importance of this effect decreases as conversion is almost complete. While temperature is the most important constraint in terms of the gasifier operation, the total BTU of fuel delivered per hour is usually the important output in terms of the overall system. We note that in our case the steam flow has only a small effect on it and the total BTU output is mainly determined by the air rate. At very low steam rates the effect of the steam rate would be more significant, but such low rates are not advisable as the thermal efficiency would be low.

The heating value of the gas (on a dry basis) is much less affected by changes in either air or steam flow rate than any of the other variables as can be seen from Figure 14c.

In Figure 16, line b, we have plotted the total BTU per hour as a function of the total molar flow rate (steam + air) along the isotherm $\Delta T=0$ of Figure 14a. We note that if we require only 60% of the fuel, the total flow rate changes much more and becomes approximately 1/3 of the initial value.

This strongly limits our ability to reduce the total output of the gasifier and limits our turndown ratio more than one would expect. One way to counteract this would be to adjust the holdup during changes in demand. At the new steady state, following such a change in the solid holdup, the output variables would remain unchanged and the linear velocity would be proportional to the total power demand. But in a fluid bed this has a long response time which is undesirable.

In Figure 14 we kept coal conversion constant. This is difficult to do as it requires careful adjustment of ash removal rate. Adjusting the removal rate of hot solids from the bed is a slow process and also technically problematic. To investigate the effect of the ash removal mode of operation on the steady state control, we look at the extreme case where ash removal rate is kept constant, at any operating point, at its initial value. Results are given in Figures 15a-15c. For comparison we also replot in Figure 15a one isotherm from the constant conversion case. We note that the constant temperature line deviates even stronger from the 45° slope (constant steam to air ratio) than before.

The total BTU output versus total molar flow rate for this case is also given in Figure 16 (dashed line b) in comparison with the constant conversion case along the isotherm $\Delta T=0$. We note the molar flow rate decreases even more steeply than in the case of constant conversion. If we can relax our constraint and allow a reduction in bed temperature, the situation slightly improves, as can be seen from Figures 14a and 15a (allowing the shifting of the operating point from one isotherm to another), but the required reduction in total molar flow rate always exceeds the reduction in total BTU.

In Figure 16 we also give the steam to air ratio for both cases (line a) as a function of total BTU/hr output, again along the isotherm $\Delta T=0$. We note that the case of constant ash removal rate demands a much steeper reduction in the steam rate to keep the temperature constant.

The fact that the slope of the ΔT isotherm in Figure 15 (or 14) is steep, or in other words strong reduction in steam to air ratio is required to maintain a constant temperature if air rate is reduced, may cause additional implications. Significant reduction of the steam to air ratio would cause local excess temperatures in the zone near the air inlet. In development of such gasifiers, the amount by which steam flow can be reduced is an important parameter that requires investigation. Furthermore, the results of Figures 14 and 15 indicate that we might have to balance the need to vary the output rate of fuel versus the need to get high efficiency at maximum throughput. We

have to choose a design condition which is less than optimal, to allow for sufficient turndown ratios. A higher initial steam to air rate would reduce efficiency at maximum flow rate but allows better swing capability.

In a similar vein, if we use a colder feed temperature of steam or air at maximum throughput, we would have larger freedom in maintaining the temperature during turndown by heating the feed.

To illustrate what happens to the efficiency during turndown, we plot in Figure 17 (line a) η_{net} as a function of the throughput keeping the temperature constant (along the isotherms $\Delta T=0$ of Figures 14 and 15). For a given solid inventory it decreases with increasing throughput if temperature and coal conversion are kept constant. Steady state efficiency of the gasifier is therefore not adversely affected by turndown.

If we cannot adjust the ash removal rate, coal conversion would drop (X_c would increase - dashed line b). We note that η_{net} in this case strongly decreases during periods of reduced throughput. This means that load changes will lead to temporary losses in efficiency due to lower coal conversion in such a gasifier.

At constant pressure there are strong limitations to reducing the total throughput. One way of overcoming these limitations would be to reduce the pressure during periods of reduced throughput. This complicates the overall control scheme of the system but has significant advantages for the

gasifier itself. The minimum throughput required for good fluidization decreases with decreasing pressure. In turbulent fluidization the important flow parameter is ρu^2, where ρ is the density of the gas and u the linear velocity. For a given mass flow G, ρu^2 is proportional to G^2/ρ, which is inversely proportional to pressure. Reducing pressure therefore increases the linear velocity and ρu^2, and thereby allowing a slightly larger turndown ratio. Decreasing pressure has another potentially beneficial effect. If, for example, the conversion of steam and CO_2 is first order in pressure, then the conversion would stay constant if pressure reduction follows a decrease in the throughput. This would then allow us to maintain a constant steam to air ratio at constant temperature, eliminating some of the interactions discussed previously. However, one would not expect the steam gasification reaction to be first order at pressures of 300 psi, but rather to be a Langmuir type expression which can be approximated by an overall pressure dependence of a fractional order. To illustrate this effect we replot in Figure 18 the isotherms of Figure 14 for different pressure dependencies. The coal conversion is kept constant and the pressure at each point is adjusted to give a constant linear velocity.

We note that for the first order pressure dependence the isotherm for $\Delta T=0$ has a 45° slope. However, if the pressure dependence is half order or less, the slope is very close to that of the constant pressure case. The same is true if we assumed that the rate expression is given by

a Langmuir type rate equation (see Table 3). We have no exact data for the pressure effect. Our constants for the Langmuir type reaction expression are derived from batch experiments data (May et al, 1958, Lewis et al, 1949). In these experiments no combustion exists and H_2 (or CO) gradients along the bed were low. In a real gasifier the particle continuously passes from the combustion zone to the gasification zone, which could totally change the absorption desorption equilibrium and give increased reaction rates at higher pressures. In that case we would expect a relation closer to the case of a first order rate dependence on pressure.

While we can get a rather good idea about the control problem at constant pressure based on available data, we had no data for the variable pressure case. Simulation using different rate expression can only indicate what the problems are.

Based on our present knowledge reducing pressure has one clear beneficial effect. It allows higher linear velocities at reduced throughputs. The effect on conversion and temperature is less clear though it could be predicted to be at least not detrimental.

In total, we would conclude that the turndown ratio of such a gasifier is rather limited and that a value of three would be optimistic. One could consider using several gasifiers in parallel. To do this one would have to experimentally investigate the problems associated with startup or with keeping a gasifier hot with no throughput.

7. Dynamic Behavior of the Gasifier

Having looked at the steady state characteristics and control of our model we can now investigate its dynamic behavior. For this analysis we assume that the model is subjected to step inputs in the air flow rate (which is the main forcing function in the process), and the steam flow rate (which is the main control variable). The approximate transfer functions and their properties can be identified by the open loop responses to those inputs.

Complete open loop response cannot be computed as the solid inventory would increase without limitation if the flow rate is reduced significantly. We, therefore, assume at first that the solid inventory is kept constant by adjusting the coal feed via a feedback loop. For simplicity we assume that the feedback loop acts without any lag. The effect of a lag in the solid inventory control loop is investigated separately. The withdrawal rate is assumed to be kept constant at its initial value. This is a realistic assumption for a relatively fast response due to the large time lag involved in controlling hot solid flow.

The responses to the various inputs are initiated at a base steady state, the parameters of which are given in Table 5. The parameters were chosen to give a steady state temperature of about 1700^{o}F. This is a reasonable compromise between both the cold gas efficiency and the net efficiency as was discussed earlier.

In order to identify the nature of the process transfer functions, the physical process constraints (such as temperature and velocity) and their impact on the process gross behavior, were neglected. While it is permissible to do so for our purpose, those constraints should be taken into account in the design of a control system for the process, as the process would have to be controlled such that it stays within those constraints at all times.

The responses of the model to steps in the inlet air and steam flow rates are given in Figures 19 and 20 respectively. The response is given for a $\pm$ 1% change as well as for a $\pm$ 10% and $\pm$50% step in the (air or steam) flow rate and suitably scaled on the same curve. The output variables plotted are the temperature, the heating value of the dry gas, the total energy produced (BTU content of the dry gas x output flow rate), the hydrogen content of the gas and the coal feed rate required to keep the solid inventory constant. Temperature deviations are given in ^{o}F, whereas all other variations are given in percentage change from their initial steady state values. The hydrogen concentration is added here, as it is relatively easily measured and can be considered as a potentially measured variable for feedback control.

The first problem to be discussed is the nonlinearity of the response and the dependency of its magnitude and its form on the step input magnitude. We note from Figure 19 (response to step inputs in the air + low rate) that the

system model is fairly linear. This is surprising as the process contains some strong nonlinearities. Both the magnitude and the form do not change drastically when steps of 1% and 50% are applied. However, the magnitude becomes more asymetric following step inputs of ± 50% compared to the symmetry of small step responses. There are also some deviations in the response time constants for large step inputs.

The temperature bahaves monotonously. Its value does not exceed the final steady state, and the response is therefore always overdamped. Due to the assumption that ash is withdrawn at a constant rate, carbon conversion changes during the response to a step change in the input. However, this is a slow process (with a time constant of an order of magnitude of 1 hour, as calculated in Appendix 2), compared to the thermal holdup (with a time constant of an approximately 1 minute as shown in Figure 19). This is why the temperature as well as other output variables achieves a "semi" steady state within a few minutes during which the carbon concentration is almost constant. Only after a slow drift, the process finally reaches the new steady state.

The responses of both the heating value and the hydrogen content contain large initial overshoot followed by a slight undershoot.

The undershoot is caused due to the large difference between the two process time constants as was previously

discussed. The large overshoot can be explained as follows: If the air rate is reduced, the steam to air ratio increases. Initially the steam is decomposed at a faster rate, due to the increased gas resident time, and a large jump in the heating value is followed. For a constant temperature, the heating value would remain at the same high level. But the heat soaked by the accelerated endothermic reactions forces the bed to cool down. The cooling is a slow process due to the large thermal inertia of the solid bed, and it takes a while till the heating value is reduced toward a new steady state.

It can be illustrated also (see Figure 21) by comparing the steady states achieved after changes in the air flow in both an isothermal reactor (in which the temperature remains at the same initial level) and an adiabatic reactor. The heating value variations in the isothermal reactor are much larger than those obtained in the adiabatic reactor.

By examining the total BTU/hr response, we note again (as previously discussed in the steady state control analysis) that changes in the total output energy are smaller than the corresponding changes in the air flow rate. Another interesting fact is that the large overshoot in the heating value of the gas may cause an initial inverse response in the total BTU production. (In Figure 22f, the initial response is magnified to illustrate this point. Refer to the solid line for the present discussion.)

Both the magnitude and the duration of the inverse response are functions of the step input magnitude and the location of the operating point (as will be discussed later). In some cases the inverse response can be eliminated or its magnitude and duration can be minimized but its potential existence is bothersome. The total BTU production is the prime output variable and an inverse response makes control more difficult.

The responses to changes in the steam feed rate is of a similar form to the response to air feed rate changes (see Figure 20), though for some of the variables the response has an opposite sign as can be expected from the steady state control analysis. This is true for the bed temperature, the heating value and the hydrogen content. The increase in the gas resident time in this case, following a negative step in the steam feed rate, is compensated by the fact that less steam is being supplied to the bed. The direction of the initial response of the heating value is equal to the direction of the step input and, as a result, the inverse response in the total BTU/hr does not exist.

We note also that the similarity between the response of the heating value and the hydrogen content is poor in this case, and, as in the air flow rate step response, the hydrogen content initial overshoot is larger than the heating value overshoot. This is a disadvantage if hydrogen content measurement is chosen to represent changes in the gas heating value.

However, the overall response to steam rate steps is more linear than the response to air rate steps in the sense that it is more symmetric and less dependent on the magnitude of the input step.

Another aspect of the nonlinearity in such a system is the dependence of the response on the location of the operating point. To investigate this aspect we show in Figures 22 and 23, curves equivalent to those given in Figures 19 and 20, for different initial steady states. Three different steam to air ratios were chosen while the total feed rate was adjusted to the same linear velocity, in all cases.

The response to a -50% step in the air flow rate (Figure 22) lacks the inverse response of the total BTU/hr for low steam to air ratios. However, it exhibits a much more pronounced inverse response for a high steam to air ratio (see also Figure 22f, in which the initial response is magnified). This is due to the larger overshoot in the heating value for the high steam to air ratio case. The heating value undershoot in this case is also deeper. Similar phenomena occur in the response to a -50% in the steam flow rate, from different locations (Figure 23). In this case the initial overshoot in the heating value, the hydrogen content and the total BTU/hr is larger for high steam to air ratios.

We note, therefore, that the nearly linear behavior disappears for very large changes in the inputs initiated at different locations. The transfer function's nature varies with changes in the operating point location. From the steady state behavior given in Figure 5, we would expect that at very high steam to air ratios the response could be inverted, but it is unlikely that such conditions would be chosen for design of an air blown gasifier.

For completeness we give, in Figure 24, the response to overall flow rate steps, keeping the steam to air ratio constant. The curves are quite similar to the air case, though the deviations in the temperature and the overshoots are lower. It could be predicted from the steady state control analysis. We indicated there that in order to minimize temperature variations, the steam rates should be changed in the same direction as the air rate changes. However, in order to achieve constant temperature, the steam rate changes should be larger than the corresponding air rate changes.

To summarize, our main results with respect to the dynamic behavior of the fluidized bed model are given in Figures 14-24. It should give a good idea about the potential overall behavior and controllability of such a gasifier.

In the following we show the sensitivity of these results to the model assumptions and the dynamic behavior changes under different conditions.

First, the assumption of gas plug flow in the bed is investigated. The response of the base case in which plug flow was assumed is compared with the response of a complete gas mixing model (see Figure 25).

The responses are very similar, though the complete mixing case response contains lower overshoots and undershoots. From the control point of view, this is a distinctive advantage, in spite of the fact that stirred tank model adheres lower overall efficiencies at the steady state.

As previously stated, the sensitivity to the mixing phenomena could become more pronounced than indicated in Figure 25 for significantly reduced flow rates region. In this region the whole fluidization's nature could be changed. The most significant effect could be at the reactor's bottom, where access temperature zones could occur due to the fast combustion reactions.

Furthermore, the nature of the fluidization which has much stronger effects on conversion than backmixing, could largely be affected. We have no reliable ways to predict the exact sensitivity of a model to this kind of model variations, except the fact that it could further limit the turndown ratio.

Another assumption had to do with the coal feed rate and the solid inventory control in the bed. We assumed that the solid inventory is maintained constant by rapid manipulations of the coal feed rate. Coal feeders do not

operate that smoothly or respond as fast as we assumed, particularly if high pressure is involved. One advantage of the fluid bed over the entrained bed is that it is less affected by solid rate variations. However, non-uniform solid feed rates and lags do have a pronounced effect on the dynamic behavior. Devolatilization is a fast process. If the coal feed rate is maintained at its initial value followed a step in the air input due to lags in the solid inventory control loop, the output total energy is affected temporarily. This effect is illustrated in Figure 26 where more realistic coal feed control loop is used. As can be seen, the overshoot in the heating value and the inverse response in the total BTU/hr as compared to our base case, are magnified. In practice, those effects could become even larger.

Another assumption is investigated in Figure 27, where the base case is compared to the case where the coal feed is replaced by char. The main overall behavior is similar for the two cases. However, the main difference is that the inverse response in the total BTU/hr is eliminated.

In Figure 28 the response to a step in the air flow rate for a lower activation energy of the gasification reactions is compared to the base case response. The temperature dependence is stronger while the final reduction in the total heating value is lower than the corresponding phenomenon in the base case. The steady state control is more difficult but there is a very small difference in the overall dynamic behavior.

In Figure 29 we repeat the same comparison for a different coal reactivity with rather similar results. We may conclude here that our general results are quite robust, and give a good indication of the type of control problems one would meet in the design of such a gasifier. It is also providing a sound basis for comparison with other gasifiers.

The above discussion dealt with the forms of the process transfer functions using an open loop analysis. The real response would be a closed loop one, and will, therefore, depend on the control system. Closed loop control design and evaluation is outside the scope of this work. Two closed loop cases, however, are presented in the following in order to complete our steady state control discussion.

In Figure 30, the response to a -50% step in the air flow rate is given for the case where the bed temperature is controlled by a PI controller, which manipulates the steam to air ratio. There was no attempt to reach an "optimal" tuning of the controller. However, a realistic tuning was assumed, for which the reset time of the integral mode was taken approximately equal to the open loop time constant. The proportional gain was maximized while avoiding the possibility of reaching zero steam rate during the transient, and while limiting the initial inverse response in the total BTU/hr to the same order of magnitude as in the open loop response.

Variations in the controller gains would be required when model variations and lags in the solid inventory control are taken into account. This could lead to a larger transient deviations in the temperature as well as in other variables. More careful interactive tuning is therefore required in practice.

In Figure 31 we deal with the responses of the system to air rate steps when the pressure is reduced to keep a constant linear velocity. For a first order kinetics the deviations of the various variables become much smaller than the corresponding variations in the open loop response. There is no inverse response in the total BTU/hr, and the overshoot in the heating value is minimized. In fact, as previously point out, an additional fast adjustment of the steam in this case would ensure almost constant values for all variables. The Langmuir type dependency of the gasification reaction rates is approximated for this case by a ½ order dependency on pressure (zero order dependency would be equivalent to our base case). The advantage of the constant linear velocity control for a ½ order dependency is significantly reduced. Purely from the control of the gasifier point of view, the reduced pressure scheme has some advantages toward better turndown ratio. Unfortunately, presently available data are insufficient to evaluate these advantages. Other advantages of the scheme such as better mixing at lower flow rates are not apparent in our results and cannot be evaluated, as those factors were not included in our model.

8. Discussion and Conclusions

In the preceding chapters we presented a simplified model of a coal gasifier and evaluated its implication for control in presence of large fluctuations of throughput. We evaluated both the controllability in terms of steady state control and the dynamic response. The results should be useful to provide guidelines for the development of such gasifiers and we will here try to summerize the implications.

All fluid bed gasifiers share one problem The range of steady state operation is limited due to the requirements of high turbulent mixing for fluidization. In the fluid bed gasifier this requirement is even more stringent as we require intense mixing in the bottom zone to prevent excess temperatures. Our results show that the range could be even more limited than dictated by pure fluid dynamics. If the gasifier does not operate at very high conversion of CO_2 and steam, then reduced flowrate will increase the conversion and increase the total BTU production consistent with a given flowrate. The temperature constraints on the system further enhances the control problem. This effect depends on the choice of the steady state operating point and should be taken into account in the design of the gasifier.

The short time dynamic behavior is dominated by the thermal inertia of the system. The total fuel production which is the main input to the turbine can exhibit a short time inverse response, an interesting but unpleasant feature which merits attention. Its duration is of the order of

twenty seconds to several minutes and it could be attenuated by using the volume of the scrubber as a hold-up. Specific control schemes were outside the scope of the thesis but those basic features of a fluid bed gasifier should be thoroughly evaluated in future design. Modelling of the type presented in the thesis can only indicate what type of behavior we can expect. The exact magnitude of these phenomena has to be evaluated experimentally.

There is a second feature that dominates the control behavior. The ash content of the bed changes slowly and its change depends on our ability to adjust the ash removal rate. This is hard to accurately control and will introduce slow drifts in process variables. It will also effect the efficiency at lower flowrates. This behavior should be taken into account in the design of a control system. Its timescale and dependence of other variables is discussed in the thesis.

There is one point we want to stress. Our model is really only valid for small pertubations despite the fact that we took the kinetic nonlinearities into account in modelling the dynamic behavior. The reason is that for large pertubations in the flow, the mixing processes change. If, for example, the mixing in the combustion zone is not intense enough, the model given in Figure 9 might be a more correct representation. Mixing between the combustion and the gasification zones will depend on the overall flowrate, which introduce additional constraints. This indicates that proper

design of the mixing zone at the bottom is of primary importance for good controllability.

Our intent here was not to supply a dynamic model for detailed controller design, but rather to provide a frame work for identification experiments and preliminary evaluation of alternative control strategies.

Appendix 1

Disappearance of Oxygen

Following Field (1967) the rate of the oxygen carbon reaction $C + \frac{1}{2}O_2 \rightarrow CO$ can be described by:

$$r = \frac{P_{O_2}}{\frac{1}{K_{diff}} + \frac{1}{K_s}} = K_{eqv.} \cdot P \cdot X_{O_2} \qquad \text{(A1-1)}$$

where K_s is the surface reaction rate coefficient and K_{diff} is the diffusion rate coefficient.

K_s is given by:

$$K_s = 8710 \cdot \mathrm{Exp}\left(-\frac{35000}{R \cdot T(^{\circ}K)}\right) \frac{g\ c}{cm^2 \cdot sec \cdot atm} \qquad \text{(A1-2)}$$

$$\text{at } 1700^{\circ}F \quad K_s = 3.7 \cdot 10^{-3} \frac{g\ c}{cm^2 \cdot sec \cdot atm} \qquad \text{(A1-3)}$$

for particle size of dp=0.1cm, at 1700°F and P=25 atm:

$$K_{diff} = 4.4 \cdot 10^{-3} \frac{g\ c}{cm^2 \cdot sec \cdot atm} \qquad \text{(A1-4)}$$

so that

$$K_{eqv.} = 2 \cdot 10^{-3} \frac{g\ c}{cm^2 \cdot sec \cdot atm} \qquad \text{(A1-5)}$$

to convert the reaction rate coefficient to be given per unit volume we multiply by $(\frac{6}{dp})$ $(\frac{cm^2}{cm^3})$ and for dp=0.1cm we get:

$$K_{eqv.} = 118.5 \frac{g\ c}{cm^3(solid) \cdot sec \cdot atm} = 228.4 \frac{lb\ mole\ of\ O_2}{ft^3(solid) \cdot hr \cdot atm} \qquad \text{(A1-6)}$$

Assuming constant volumetric flow rate within the combustion section we get:

$$Fg \cdot \frac{dX_{O_2}}{dz} = -K_{eqv.} \cdot P \cdot X_{O_2} \cdot (1-\varepsilon) \qquad \text{(A1-7)}$$

$$X_{O_2}(z) = X_{O_2(in)} \cdot \text{Exp}\left(-\frac{K_{eqv.} \cdot P \cdot (1-\varepsilon)}{Fg} z\right) \qquad \text{(A1-8)}$$

Using the base case values: ε=0.6, Fg-165 $\frac{\text{lb mole}}{\text{ft}^2 \cdot \text{hr}}$ and $X_{O_2 in}$=.21

We get that at z = .5 ft, $X_{O_2} \approx 10^{-3}$

Appendix 2

Time Constant of X_c

The total mass balance and the carbon balance equations are given in Table 4 (equations (T4-6)). Using the notation of Table 4 and assuming constant ash withdrawal rate and constant solid inventory during the transient response, we get from (T4-6) that:

$$FC = \frac{FW+CG}{1-\beta} \qquad (A2\text{-}1)$$

substituting back into the carbon balance equation we get that:

$$W\cdot\frac{dX_c}{dt} + FW\cdot X_c = CG\cdot\left(\frac{Y_c-\lambda}{1-\beta} - 1\right) + FW\cdot\frac{Y_c-\lambda}{1-\beta} \qquad (A2\text{-}2)$$

While the value of the second term in (A2-2) on the right hand side is constant due to the constant ash withdrawal rate assumption, the first term on the right changes with X_c, from 104.3 to 124.2 for X_c between 0.3 and 0.7.

If we approximate the first term on the right by:

$$\delta = K\cdot X_c \qquad (A2\text{-}3)$$

the value of K can be found from:

$$K = \frac{\Delta\delta}{\Delta X_c} = \frac{124.2-104.3}{0.3 - 0.7} \cong -50 \qquad (A2\text{-}4)$$

The time constant of equation (A2-2) can be found now to be:

$$\tau_{X_c} = \frac{W_{s\cdot s}}{FW_{s\cdot s} - K} = \frac{275}{217+50} \cong 1.03 \text{ hr}$$

Appendix 3

Particle Size Distribution Model

When a chemical reaction kinetics of a particulate systems depends on particle size, a particle size distribution model should be added to the kinetic model to account for particle size distribution variations during transient responses.

The model described below applies when the gasification reactions occur on the surface of the coal particles and their rates depend, therefore, on the overall area available for reaction. This model can also be applied to any other similar process in which the kinetics can be described by a shrinking core model when the ash layer resistance can be neglected. Our model is based on the mathematical frame developed by Hulburt, Katz, and Shinner (Hulburt and Katz (1964), Katz and Shinnar (1969)), and applied later to the processes of polymerization, crystallization, and other processes (Sherwin, et al (1969), Glasser, et al (1973), Liss, et al (1976)).

We denote:

r - Characteristic radius of a particle.

t - Time

$f(r,t)$ - Particle size distribution in the fluidized bed. Thus, $f(r,t)dr$ is the number of particles in the bed having radii in the range $(r,r+dr)$ at time t.

$f_o(r,t)$ - Normalized particle distribution of the feed. Thus, $f_o(r,t)$ is the fraction of the total number of particles in the feed, having radii in the range $(r,r+dr)$ at time t.

$G(r,t)$ - Particle's shrinking rate.

$F_c(t)$ - Total number of particles entering the bed per unit time.

$\bar{A}$ - Steady state value of variable A.

μ_n - n-th moment of $f(r,t)$.

η_n - n-th moment of $f_o(r,t)$.

Note that $f(r,t)$ is not normalized and that the integral $\int_o^\infty f(r,t)dr$ is not unity but rather the total number of particles in the bed at time t, whereas the integral $\int_o^\infty f_o(r,t)dr$ is equal to unity.

The mass balance within the interval (r,r+dr) with the appropriate boundary and initial condition becomes:

$$\frac{\partial f(r,t)}{\partial r} = \frac{\partial}{\partial r}\left(G(r,t)\cdot f(r,t)\right) = F_c(t)\ f_o(r,t)$$

$$\text{B.C.} \quad f(r,t) = o \text{ for } r<0 \qquad \text{(A3-1)}$$

$$f(f,t) = 0 \text{ for } r>r_{max}$$

$$\text{I.C.} \quad f(r,o) = \overline{f(r)}$$

The first term on the left corresponds to the accumulation of particles in the interval. The second term on the left corresponds to the net number of particles shrinking away from the interval and the term on the right corresponds to the number of particles entering the interval from the feed.

$G(r,t)$-the shrinking rate, $F_c(t)$-the coal particles' feed rate and $f_o(r,t)$-the feed distribution, are the forcing functions for this equation. $G(r,t)$ is a function of the gasifier inputs and the kinetics in the bed. When the coal feed rate is feedback controlled to keep a constant solid inventory in the

bed, it is also a function of the gasification rate and, therefore, a function of G(r,t). Otherwise, it is an independent forcing function.

The first boundary condition for r<o corresponds to the assumption that particles die at size zero. This term could alternately be included in the right hand side as an output of size zero or any other size.

If we further assume that the shrinking rate -G(r,t) is not a function of r, or in other words, if we neglect the effect of the ash layer resistance (and other phenomena which may effect the shrinking rate as the reaction surface progresses into the particle), we can simplify equation (A3-1) and get:

$$\frac{\partial f(r,t)}{\partial t} - G(t)\ \frac{\partial f(r,t)}{\partial r} = F_c(t)\ f_o(r,t) \qquad \text{(A3-2)}$$

the steady state equation then becomes:

$$-\bar{G}\ \frac{\overline{\partial f(r)}}{\partial} = \overline{F_c}\ \overline{f_o(r)} \qquad \text{(A3-3)}$$

The above equations can be connected to the kinetic model using the moment equations which can be derived by substituting the moments of the distribution functions into (A3-2) and (A3-3).

The moments of the distribution functions and their physical significance are given below:

$$\mu_n(t) = \int_o^\infty r^n f(r,t)\ dr \quad \text{n-th moment of } f(r,t) \qquad \text{(A3-4)}$$

Thus:

$$\mu_o(t) = \int_o^\infty f(r,t)\, dr = \text{total number of particles}$$

$$\mu_1(t) = \int_o^\infty r\, f(r,t) = \text{total "radius" in the bed}$$

$$3K\,\mu_2(t) = 3K \int_o^\infty r^2\, f(r,t)\, dr = \text{total surface in the bed} \qquad \text{(A3-5)}$$

$$K\,\mu_3(t) = K \int_o^\infty r^3\, f(r,t)\, dr = \text{total volume of solid in the bed}$$

etc. . .

where K is the particle shape factor ($\frac{4}{3}\pi$ for a spherical particle).

A similar set can be defined for the feed distribution moments $\eta_n(t)$. The only difference in this case is that $f_o(r,t)$ is normalized and in order to get the absolute number, one has to multiply by $F_c(t)$.

Multiplying equation (A3-2) by r^n and integrating with respect to r from r=o to r = ∞ (or r_{max}) we get a set of moment equations:

$$\begin{aligned}
\dot{\mu}_o(t) &= F_c(t)\,\eta_o(t) - G(t)\, f(o,t) \\
\dot{\mu}_1(t) &= F_c(t)\,\eta_1(t) - G(t)\,\mu_o(t) \\
\dot{\mu}_2(t) &= F_c(t)\,\eta_2(t) - 2\,G(t)\,\mu_1(t) \\
\dot{\mu}_3(t) &= F_c(t)\,\eta_3(t) - 3\,G(t)\,\mu_2(t) \\
&\cdot \\
&\cdot \\
&\cdot
\end{aligned} \qquad \text{(A3-6)}$$

The solution of the steady state equation (A3-3) depends on $\overline{f_o(r)}$ - the steady state inlet distribution. For a single size feed, $f_o(r)$ is given by:

the term on the right hand side of (A3-2) was replaced by the second boundary condition of (A3-12). The two representations are equivalent.

By taking the Laplace Transform of (A3-12) we get:

$$s\,\hat{f}(r,s) - f(r,0) - G_2\,\frac{df(r,s)}{dr} = 0$$

$$\text{B.C. } \hat{f}(r,s) = 0 \text{ for } r<o,\ r>r_o \qquad \text{(A3-13)}$$

$$\hat{f}(r_o,s) = \frac{1}{s}\,\frac{F_c}{G_2}$$

in which $\hat{f}(r,s)$ is the Laplace Transform of $f(r,t)$. The homogenous equation and its solution are:

$$\left.\begin{aligned} &\frac{d\hat{f}(r,s)}{dr} - \frac{s}{G_2}\,\hat{f}(r,s) = 0 \\ &\hat{f}_H(r,s) = G_1 \cdot \text{Exp}\left(-\frac{s}{G_2}\cdot r\right) \end{aligned}\right\} \qquad \text{(A3-14)}$$

The particular solution for the overall equation is given by:

$$f_p(r,s) = \frac{1}{s}f(r,o) = \frac{1}{s}\cdot\frac{F_c}{G_1} \qquad \text{(A3-15)}$$

the overall solution is therefore:

$$\hat{f}(r,s)=\hat{f}_H(r,s)+\hat{f}_p(r,s)=C_1\cdot\text{Exp}\left(-\frac{s}{G_2}\cdot r\right)+\frac{1}{s}\,\frac{F_c}{G_1} \qquad \text{(A3-16)}$$

To find C_1 we use the boundary condition at r_o and we get:

$$C_1 = \frac{F_c}{G_1}\,\frac{1}{s}\left(\frac{G_1}{G_2} - 1\right)\text{Exp}\left(-\frac{s}{G_2}\cdot r_o\right) \qquad \text{(A3-17)}$$

Thus

$$\hat{f}(r,s)=\frac{1}{s}\,\frac{F_c}{G_1}\left\{1-\left(\frac{G_1}{G_2}-1\right)\cdot\text{Exp}\ \frac{s}{G_2}(r_o-r)\right\} \qquad \text{(A3-18)}$$

and

$$f(r,t) = \frac{F_c}{G_1} + \frac{F_c}{G_1}\left(\frac{G_1}{G_2} - 1\right)\cdot U\left(t-\frac{r_o-r}{G_2}\right) \qquad \text{(A3-19)}$$

An interesting fact can be noted from the above results even before solving the unsteady state equation. If the bed solid inventory is controlled by supplying coal in an amount equal to the amount gasified per unit time, the ratio $\overline{F_c}/\overline{G}$ remains constant even during the transient response (followed a change in the input). Thus, the distribution f(r,t) and all of its moments remain constant and equal to their values at the steady state.

The solution of the unsteady state, nonlinear, partial differential equation (A3-2) can be found analytically using the Laplace Transform technique when G(r,t) is a step function. We give here the solution for two cases:

a) $G(r,t) = U(t)$

b) $G(r,t) = G_o(t)\ G_1(t) = G_o \cdot U(t) \cdot (1+ar)$

For both cases we assume that the inlet distribution at all times is given by equation (A3-7) (constant single size distribution), and that F_c remains constant.

For case a), equation (A3-2) can be written as:

$$\frac{\partial f(r,t)}{\partial t} - G_2 \frac{\partial f(r,t)}{\partial r} = 0$$

$$\text{B.C. } f(r,t) = 0 \text{ for } r<o,\ r>r_o \qquad \text{(A3-12)}$$

$$f(r_o,t) = \frac{F_c}{G_2}$$

$$\text{I.C. } f(r,o) = \overline{f(r)} = \frac{F_c}{G_1}\ U(r) - U(r-r_o)$$

in which G_1 and G_2 are the values of G(t) at the initial steady state and after the step respectively. For mathematical reasons

$$\overline{f_o(r)} = \delta(r-r_o) \tag{A3-7}$$

and the solution of (A3-3) is then given by:

$$\overline{f(r)} = \frac{\overline{F_c}}{\overline{G}} \; U(r) - U(r-r_o) \tag{A3-8}$$

where δ is the dirac delta function at $r=r_o$ and $U(r-r_o)$ is the unit step function at $r=r_o$. The steady state moments of $\overline{f(r)}$ are given by:

$$\begin{aligned}
\overline{\mu_o} &= \frac{\overline{F_c}}{\overline{G}} \, r_o \\
\overline{\mu_1} &= \frac{\overline{F_c}}{\overline{G}} \, \frac{r_o^2}{2} \\
\overline{\mu_2} &= \frac{\overline{F_c}}{\overline{G}} \, \frac{r_o^3}{3} \\
\overline{\mu_3} &= \frac{\overline{F_c}}{\overline{G}} \, \frac{r_o^4}{4} \\
&\vdots
\end{aligned} \tag{A3-9}$$

for a uniform feed distribution:

$$\overline{f_o(r)} = \frac{1}{r_o} \; U(r) - U(r-r_o) \tag{A3-10}$$

and

$$\overline{f(r)} = \frac{\overline{F_c}}{\overline{G}} \left[1 - \frac{r}{r_o} \; U(r) \right] \tag{A3-11}$$

The steady state solutions for the above two cases are given in figures A3-1 and A3-2.

The value of f(o,t) is needed in order to solve the moment equations (A3-6). It can be obtained by substituting r=o in (A3-19). We get that

$$f(o,t) = \frac{F_c}{G_1}\left[1+\left(\frac{G_1}{G_2}-1\right)\cdot U\left(t-\frac{r_o}{G_2}\right)\right] \qquad \text{(A3-20)}$$

the result obtained in equation (A3-21) could be predicted and it is somewhat obvious. We get that the perturbation in the number of particles at size r=o is resulted from the net perturbation at size $r=r_o$, $\frac{r_o}{G_2}$ units of time before. This is true only for the case where G(t) is not a function of r. Otherwise, the solution contains an integral with respect to r. The value of the integral can be calculated for case b and the solution is:

$$f(r,t) = \frac{F_c}{G_1 \cdot G_1(r)}\cdot\left[1+\left(\frac{G_1}{G_2}-1\right)\cdot U\left(t-\frac{1}{G_2\cdot a}\ln\frac{1+ar_o}{1+ar}\right)\right] \qquad \text{(A3-21)}$$

in which G_1 and G_2 are the values of G(r,t) at size r=o before and after the step respectively.

The solutions obtained in equations (A3-20) and (A3-21) are shown schematically in Figures A3-3 and A3-4.

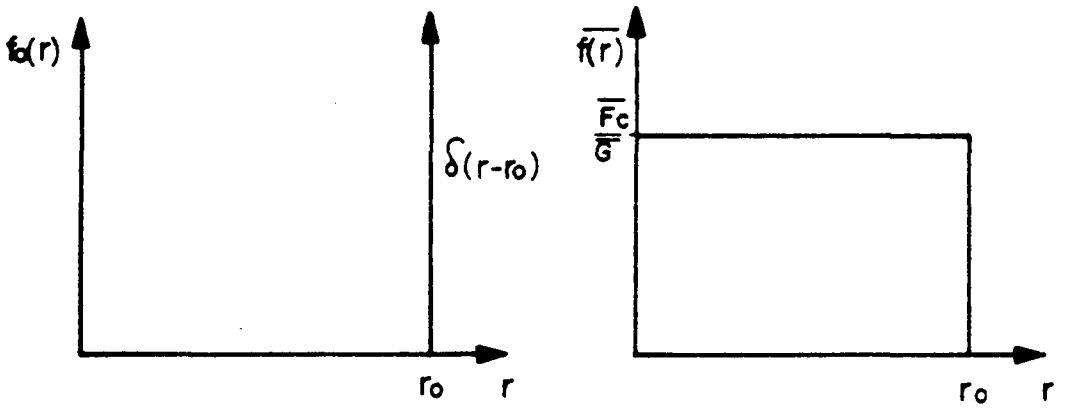

Figure A3-1: Steady State Distribution of f(r) and fo(r) for a Single Size Inlet Distribution

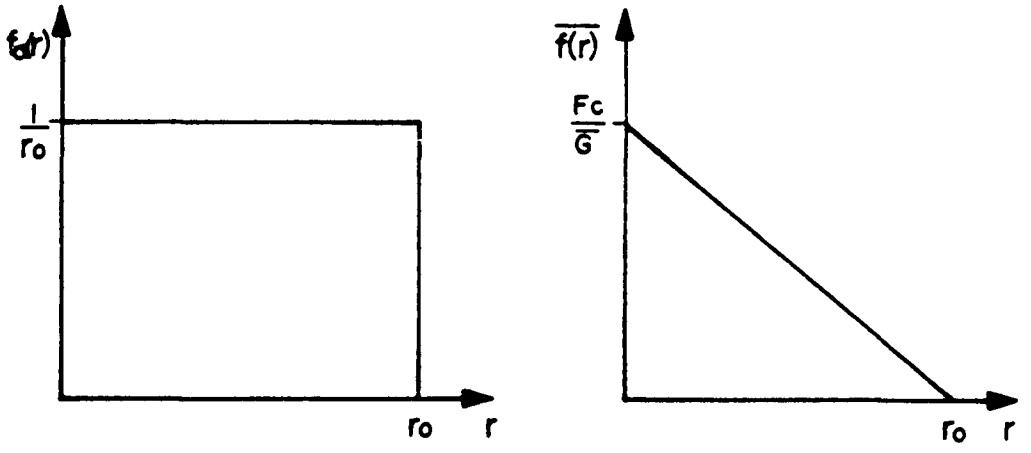

Figure A3-2: Steady State Distribution of f(r) and fo(r) for a Uniform Inlet Distribution

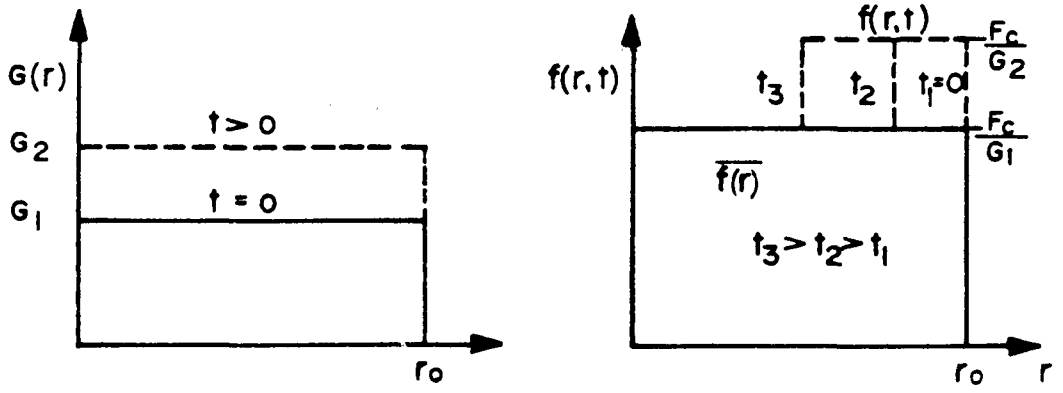

Figure A3-3: Response of the Particle Size Distribution f(r,t) to a step in G(r) - Case a

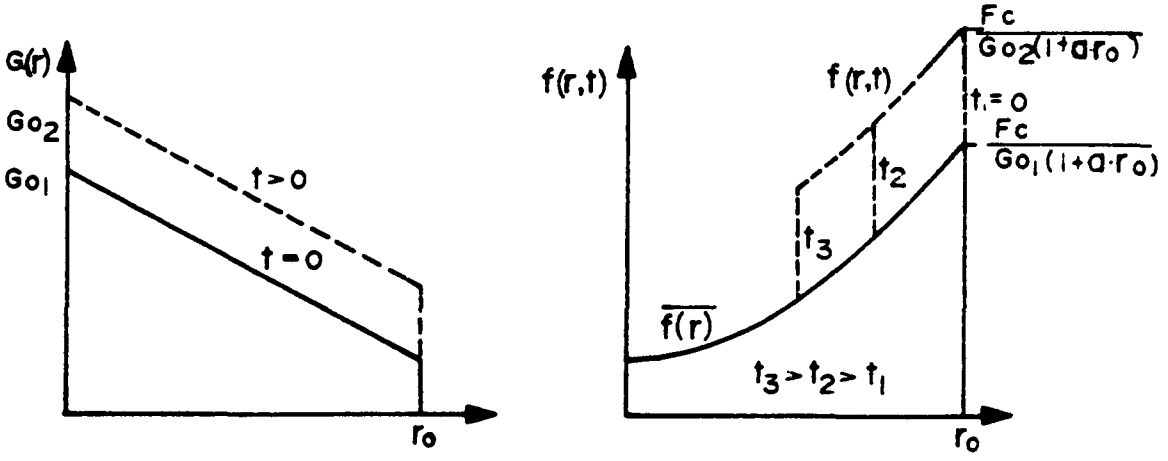

Figure A3-4: Response of the Particle Size Distribution f(r,t) to a step in G(r) - Case b

Nomenclature

BTU	net dry heating value
C_p	heat capacity
CG	carbon gasified per unit time
CG_{dev}	carbon devolatilized per unit time
DH_2	devolitilization coefficient (Eq. T2-1)
Fg	molar flow rate
FC	coal feed rate
FW	ash withdrawal rate
H_{loss}	heat loss
$K_{eqv.}$,K	reaction rate coefficient
K_s	surface reaction coefficient
$K_{diff.}$	diffusion coefficient
$K_{eq.}$	reaction equilibrium coefficient
P	pressure
P_A	partial pressure of A
Q_s	latent heat
r	reaction rate
SOR	steam to oxygen molar ratio
T	temperature
t	time
U	linear velocity
V	bed volume
VM	volatile matter devolitilized per unit time
W	bed solid inventory
X_A	molar fraction of A
X_C	carbon concentration in the bed
Y_A	weight percentage of A in the coal

Nomenclature (continued)

Greek Symbols

α	devolitilization coefficient (Eq. T2-1)
β	devolitilization coefficient (Eq. T2-3)
λ	devolitilization coefficient (Eq. T2-4)
ΔH_i	heat of reaction i
η	cold gas efficiency
η_{net}	net thermal efficiency
ε	bed voidage
ϕ	$\frac{FC}{FW}$

Bibliography

Anthony D.B., Howard J.B., A.Ch.E.J., Vol. 22, No. 4 (1976).

Avedsian M.M., Davidson J.F., Trans. Int. Chem. Engrs., Vol. 51 (1973).

Batchhelder H.R., Busche R.M., I&EC., Vol. 45, No. 9 (1953).

Blockwood J.D., Ingeme A.J., Aust. J. Chem., Vol. 13 (1960).

Blockwood J.D., McGory F., Aust. J. Chem., Vol. 11 (1958).

Caram H.A., Amundson N.R., I&EC, Fund., Vol. 16, No. 2 (1977).

Dutta S., Wen C.Y., Belt R.J., I&EC, Proc. Des. Dev., Vol. 16, No. 1 (1977).

Ergun S., J. Phys. Chem., Vol. 60 (1956).

Field M.A., Gill D.W., Morgan B.B., Hawk P.G.W., "Combustion of Pulverized Coal", BCURA, England (1967).

Gadsbay J., Long F.J., Sleightholm P., Sykes K.W., Proc. Roy. Soc., Vol. 193 (1948).

Gibson M.A., Euker C.A., A.I.Ch.E. Symp. on Laboratory Reactors (1975).

Glasser D., Katz S., Shinner R., I&EC, Fund., Vol. 12, No. 2 (1973).

Gorolon A.L., Amundson N.R., Chem. Eng. Sci., Vol. 31 (1976).

Hougen O.A., Watson K.M., "Chemical Process Principles", J. Wiley (1957).

Hulbert H., Katz S., Chem. Eng. Sci., Vol. 191 (1964).

Johnson J.L., Adr. Chem. Ser., No. 131 (1974).

Johnson J.L., Amer. Chem. Soc. Symp. on Coal Gasification, 173rd Nat. Meet. (1977).

Kato K., Wen C.Y., Chem. Eng. Sci., Vol. 24 (1969).

Katz S., Shinner R., I&EC, Vol. 61, No. 4 (1969).

Kestenbaum A., Shinner R., Thau, F.E., I&EC, Proc. Des. Dev., Vol. 15, No. 1 (1976).

Bibliography (continued)

Krambeck F.J., Katz S., Shinner R., Chem. Eng. Sci., Vol. 24 (1969).

Lewis W.K., Gillard E.R., McBride G.T., I&EC, Vol. 41, No. 6 (1949).

Liss B., Shinner R., A.I.Ch.E. Symp. Ser., Vol.72, No. 153 (1976).

Lowry H.H. (Editor), "Chemistry and Industry", J.Wiley (1950).

Lowry H.H. (Editor), "Chemistry of Coal Utilization", J.Wiley (1963).

Luss D., Amundson N.R., A.I.Ch.E. J., Vol. 15, No. 2 (1969).

May W.G., Mueller R.H., Sweetser S.B., I&EC, Vol. 9, No. 9 (1958).

Mayers M.A., Amer. Chem. Soc. J., Vol. 56 (1934).

Palmor Z., Shinnar R., to be published in I&EC, Proc. Des. Dev. (1978).

Sherwin M.B., Shinner R., Katz S., Chem. Eng. Prog. Symp. Ser., Vol. 65, No. 95 (1969).

Silverstein J., Shinnar R., presented at the A.I.Ch.E. meeting N.Y. (Nov. 1977).

Squires A.M., Trans. Inst. Chem. Engrs., Vol. 39, No. 1 (1961).

Wen C.Y., Bailic R.C., Lin C.Y., O'Brien W.S., Adv. Chem. Ser., No. 131 (1974).

Zielke C.W., Gorin E., I&EC, Vol. 49, No. 3 (1957).

Table 1. Coal Analysis

Type	Illinois No. 6
Approximate analysis	
Moisture	4.2 wt%
Ash	9.6
Fixed carbon	52.0
Volatile matter	34.2
	100%
Ultimate analysis	
Carbon	77.26 wt%
Hydrogen	5.92
Oxygen	11.14
Nitrogen	1.39
Sulfur	4.29
	100%
Heating value as recovered	
H.H.V	12,235 $\frac{BTU}{lb}$
L.H.V	11,709 $\frac{BTU}{lb}$

Table 2. Devolatilization Equations

a) Definitions:

$$\alpha = \frac{\text{lb C to form } C_{H_4}}{\text{lb C in the feed}} \qquad \text{(T2-1)}$$

$\alpha = 0.1 + 0.015 \cdot P_{H_2}$ (correlated from Gibson and Euker 1975)

$$D_{H_2} = \frac{\text{lb } H_2 \text{ remaining in the char}}{\text{lb coal}} \qquad \text{(T2-2)}$$

$D_{H_2} = 100 \cdot 10^{(1.37-0.00165T^{\circ}C)}$ (from Lowry 1950)

$$\delta = \frac{\text{lb volatile matter which excapes during the process}}{\text{lb coal}} \qquad \text{(T2-3)}$$

$$\lambda = \frac{\text{lb C consumer during the process}}{\text{lb coal}} \qquad \text{(T2-4)}$$

Y_C, Y_{O_2}, Y_{H_2}, Y_S, Y_{N_2}, Y_{H_2O}, Y_{ash} - Weight percentage (T2-5)

in $(\frac{\text{lb}}{\text{lb coal}})$, of C, O_2, H_2, S, N_2, H_2O, and Ash, respectively

b) Model parameters

The amounts which devolatilized $(\frac{\text{lb}}{\text{lb coal}})$ during the process are given by

$$\left.\begin{aligned}
CH_4 &= Y_C \cdot \alpha \cdot (16/12) \\
CO &= Y_{O_2} \cdot 0.375 \cdot (56/32) \\
CO_2 &= Y_{O_2} \cdot 0.375 \cdot (44/32) \\
H_2O &= Y_{O_2} \cdot 0.25 \cdot (36/32) + Y_{H_2O} \\
H_2S &= Y_s \cdot (34/32) \\
N_2 &= Y_{N_2} \\
H_2 &= Y_{H_2} - Y_C \cdot \alpha \cdot (4/12) - 0.25 \cdot Y_{O_2} \cdot (1+0.375 \cdot (12/32)) \\
&\quad + Y_{H_2} - DH_2
\end{aligned}\right\} \qquad \text{(T2-6)}$$

Table 2 (continued)

$$\lambda = Y_C \cdot \alpha + (24/32) + 12/32) \cdot 0.375 \cdot Y_{O_2} \left(\frac{lb}{lb\ coal}\right) \quad (T2\text{-}7)$$

$$\beta = Y_S + Y_{H_2O} + Y_C \alpha + Y_{H_2} + Y_{N_2} + Y_{O_2} \cdot (1+(24/32)\cdot 0.375 + (12/32) \cdot 0.375) - DH_2 \left(\frac{lb}{lb\ coal}\right) \quad (T2\text{-}8)$$

Table 3 - Kinetic and Thermodynamic Data

a) $C + H_2O \rightarrow CO + H_2$ Reaction Rate

Reference	Reaction Rate Expression	Reaction Rate Constants	Experiment Conditions	Parameters For Fig. 2
a) Mayers (1934)	$r = K \cdot P_{H_2O}$	$\log_{10} K = (.51097 - \frac{13822.}{T^{o}(R)})$ $\frac{\text{mole}}{\text{ft.}^2 \text{ sec. atm.}}$	1) P = 1 atm. 2) P_{H_2O} = 1 atm. 3) carbon rod	P = 5 atm.
b) May et al (1958)	$r = \frac{K_1 \cdot P_{H_2O}}{1+K_2 \cdot P_{H_2}}$	$\log_{10} K_1 = (9.4214 - \frac{21058.5}{T^{o}(R)})$ $\frac{\text{mole}}{\text{mole hr. atm.}}$ $\log_{10} K_2 = (2.1706 - \frac{3840.9}{T(^{o}R)})$ $\frac{1}{\text{atm.}}$	1) P = 1-10 atm. 2) P_{H_2O} = 1-10 atm. (with N_2 and H_2) 3) Fluidized bed part size 24/60 mesh 4) High, low temp. coke	P = 20 atm.
c) Johnson (1974)	$r = f_L \cdot K_T \cdot (1-X_c^{0.66}) \cdot \exp(-\alpha X_c^2)$ X_c = base carbon conversion K_T = total gasif. rate constant f_L = relative reactivity factor $\alpha = f(P_{H_2O}, P_{H_2}, P_{CO})$	$K = \frac{\exp(9.02 - \frac{31705.}{T(^{o}R)}) \cdot (1 - \frac{P_{CO} \cdot P_{H_2}}{P_{H_2O} \cdot K_{eq}})}{\left[1+\exp(-22.216 + \frac{44787.}{T(^{o}R)}) \cdot P\right]^2}$ $\frac{1}{\text{min.}}$ $\beta = \frac{1}{P_{H_2O}} \cdot (1+16. \cdot P_{H_2} + 43.5 \cdot P_{CO})$	1) P = 1-70 atm. 2) Various mixtures of H_2 and H_2O 3) Suspended particles in a fluid bed 4) Pittsburgh No. 8 coal char	$\alpha = 1$ $X_c = 0$ $f_L = 1$ P = 20 atm.

Table 3 (Continued)

d) Zielke and Gorin (1957)		reaction rates were taken from plotted results given in the paper	1) P = 1-30 atm. 2) Various mixtures of H_2 and H_2O 3) Fluidized bed particle size - 65-150 mesh 4) Low temp. coke	$\frac{H_2}{H_2O} = \frac{0.25}{0.75}$ P = 30 atm. $X_c = 0$
e) Gibson and Euker (1975)	$r = K P_{H_2O}$	$Kill = 412. \exp\left(-\frac{21137.4}{T(^oK)}\right)$ $\frac{mole}{mole\ s.\ atm.}$ $Kwyom = 613 \cdot \exp\left(-\frac{17614.5}{T(^oK)}\right)$ "	1) P = 1-7 atm 2) P_{H_2O} = 1-7 atm. with N_2 3) Fluidized bed 4) Illinois aol Wyoming coals char	P = 5 atm.
f) Blackwood & Mc Gory (1958)	$r = \frac{K_1 \cdot P_{H_2O}}{1+K_2 \cdot P_{H_2} + K_3 \cdot P_{H_2O}}$	$\log_{10} K_1 = (11.3058 - \frac{25706.54}{T(^oR)})$ $\frac{mole}{mole\ min.\ atm.}$ $\log_{10} K_2 = (3.8383 - \frac{9348.17}{T(^oR)})$ $\frac{1}{atm.}$ $K_3 = 35.$ $\frac{1}{atm.}$	1) P = 1-5 atm. 2) Various mixtures of H_2 and H_2O 3) Suspended sample 4) Coconut char	P = 20 atm.
g) Ergun (1956)	$r = \frac{K_1 C_t}{(1 + \frac{P_{H_2}}{P_{H_2O} K_{eq}})}$	reaction rates were taken from plotted results given in the paper	1) P = 1 atm. 2) P_{H_2O} = 0-1 atm. with He 3) Fluidized bed partic. size - 8-140 mesh 4) Met. coke	P = 5 atm.

Table 3 (Continued)

b) $C + CO_2 \rightarrow 2CO$ Reaction Rate

Reference	Reaction Rate Expression	Reaction Rate Constants	Experiment Conditions	Parameters For Fig. 2
a) Mayers (1934)	$r = K \cdot P_{H_2O}$	$\log_{10} K = (0.7294 - \frac{15226.}{T(^oR)})$ $\frac{mole}{ft.^2 \cdot atm.}$	1) P = 1 atm. 2) P_{CO_2} = 1 atm. 3) Carbon rod	P = 5 atm.
b) Lewis et al (1949)	$r = \frac{K_1 \cdot P_{CO_2}}{1+K_2 \cdot P_{CO}+K_3 \cdot P_{CO_2}}$	$\log_{10} K_1 = (5.995 - \frac{19036.}{T(^oR)})$ $\frac{mole}{mole\ min.\ atm.}$ $\log_{10} K_2 = (-1.892 + \frac{5964.14}{T(^oR)})$ $\frac{1}{atm.}$ $\log_{10} K_3 = (-0.6315 + \frac{2400.}{T(^oR)})$ $\frac{1}{atm.}$	1) P = 1 atm. 2) P_{CO_2} = 0-1 atm. with CO_2 and N_2 3) Fluidized bed partic. size - -60/+200 mesh 4) coke	P = 20 atm.
c) Blackwood & Ingeme (1960)	$r = \frac{K_1 \cdot P_{CO_2}+K_2 \cdot P_{CO_2}^2}{1+K_3 \cdot P_{CO}+K_4 \cdot P_{CO_2}}$	values of K_i's are tablulated in the paper	1) P = 1-40 atm. 2) Fixed bed 3) Charcoal	P = 20 atm.
d) Dutta et al (1977)	$r = \eta \cdot a \cdot K_1 \cdot P_{CO_2} \cdot (1-X_c)$ η = interparticle diffusion factor a = fraction of conversion X_c = fraction of carbon conversion	reaction rates were taken from plotted results (extrapolated to $X_c = 0$)	1) P = 1 atm. 2) P_{CO_2} = 1 atm. 3) Fluidized bed particle size - 60/100 mesh 4) Ill. No. 6 coal char and other chars	P = 5 atm.

Table 3 (Continued)

e) Ergun (1956)	$r = \frac{K \cdot C_t}{\left(\frac{P_{CO}}{1 + P_{O_2} \cdot K_{eq}}\right)}$ C_t - concentration of free sites	reaction rates were taken from plotted results given in the paper	1) P = 1 atm. 2) P_{CO_2} = 0-1 atm. with He 3) Fluidized bed particle size - 8/140 mesh 4) Met. coke	P = 5 atm.
f) Gadsby et al (1948)	$r_{CO_2} = \frac{K_1 \cdot P_{CO_2}}{1 + K_2 \cdot P_{CO} + K_3 \cdot P_{CO_2}}$	$K_1 = 6.3 \cdot 10^{8} \cdot \exp\left(-\frac{29592.3}{T(^{o}K)}\right)$ $\frac{\text{mole}}{\text{lb. min. atm.}}$ $K_2 = 1.26 \cdot 10^{-8} \cdot \exp\left(\frac{22899.8}{T(^{o}K)}\right)$ $\frac{1}{\text{atm.}}$ $K_3 = 3.16 \cdot 10^{6} \cdot \exp\left(-\frac{15149.5}{T(^{o}K)}\right)$ $\frac{1}{\text{atm.}}$	1) P = 1 atm. 2) P_{CO_2} = 0-1 atm. with CO 3) Fixed bed 4) Charcoal	P = 5 atm.

Table 3 (continued)

c) Combustion Reactions

Reference	Reaction	Reaction Rate Expression	Reaction Rate Constant
Hougen and Watson (1946)	$2CO + O_2 \rightarrow CO_2$	$r = K \cdot P_{CO_2}^{2} \cdot P_{O_2}$	$\log_{10} K = (-\frac{9179.7}{T(^{o}K)} + 10.7462) \frac{mole}{ft^3\ hr\ atm^3}$
Field (1967)	$C + \frac{1}{2}O_2 \rightarrow CO$	$r = \frac{P_{O_2}}{(\frac{1}{K_{diff}} + \frac{1}{K_s})}$	$\log_{10} K_s = 8710. \cdot \exp(-\frac{35000}{R \cdot T(^{o}K)}) \frac{g\ c}{cm^2 s\ atm}$ $K_{diff} = 0.12$ (-11-)

Table 3 (continued)

d) Equilibrium Constant, Heat of Reaction (Lowry, 1963)

Reaction	K_{eq} (partial pressures units)	Standard Heat of Reaction at 298.16°K Kcal/gmole
$C + H_2O \rightarrow CO + H_2$	$EXP(17.2982 - \frac{29414.}{T(^oR)})$	31.382
$C + CO_2 \rightarrow 2CO$	$EXP(20.9882 - \frac{36602.92}{T(^oR)})$	41.2204
$CO + H_2O \rightarrow CO_2 + H_2$	$EXP(-13.2898 + \frac{9517.7}{T(^oR)} + 1.1021 \ln T(^oR))$	-9.838
$C + \frac{1}{2}O_2 \rightarrow CO$	at $1200^oK = 3.1462 \times 10^9$	-26.4157
$C + O_2 \rightarrow CO_2$	at $1200^oK = 1.7376 \times 10^{17}$	-94.0518

Table 3 (continued)

e) Molar Heat Capacities of Gases (Hougen et al, Part I, 1954)

$cp = a + bT + CT^2 + dT^3$ ($T = {}^{o}K$) Temperature Range 273-1800^{o}K

Gas	a	b x 10^2	c x 10^5	d x 10^9
Air	6.713	0.04697	0.1147	-0.4696
Nitrogen	6.903	-0.03753	0.1930	-0.6861
Oxygen	6.085	0.3631	-0.1709	0.3133
Hydrogen	6.952	-0.04576	0.09563	-0.2079
Carbon Monoxide	6.726	0.04001	0.1283	-0.5307
Carbon Dioxide	5.316	1.4285	-0.8362	1.784
Water Vapor	7.700	0.04594	0.2521	-0.8587
Hydrogen Sulfide	7.070	0.3128	0.1364	-0.7867
Methane	4.750	1.200	0.3030	-2.630

Table 4. Model Equations

a) Reactions

The combustion reaction

$$CH_a + (1 + \frac{a}{4} O_2) \rightarrow CO_2 + \frac{a}{2} H_2O$$

can be divided into three reactions as follows

1) $2C + O_2 \rightarrow 2CO$ }

2) $2CO + O_2 \rightarrow 2CO_2$ }

3) $2H_2 + O_2 \rightarrow 2H_2O$ }

The gasification reactions are: (T4-1)

4) $C + H_2O \rightarrow CO + H_2$ }

5) $C + CO_2 \rightarrow 2CO$ }

6) $CO + H_2O \rightarrow CO_2 + H_2$ (shift reaction) }

b) Reaction rates $\left(\frac{\text{lb moles}}{\text{ft}^3 \text{ bed hr}}\right)$

$$r_1 = K_1(T) \cdot (P_{CO}^2 \cdot P_{O_2}) \quad \}$$

$$r_2 = K_2(T) \cdot P_{O_2} \cdot P_{CO}^2 \cdot (1-\varepsilon) \quad \}$$

$$r_3 = K_3(T) \cdot P_{H_2} \cdot P_{O_2} \cdot (1-\varepsilon) \quad \} \qquad \text{(T4-2)}$$

$$r_4 = K_4(T) \cdot \left(P_{H_2O} - \frac{P_{H_2O} \cdot P_{CO}}{k_{eq.\ 4}}\right) \cdot \frac{W \cdot X_c}{V} \quad \}$$

$$r_5 = K_5(T) \cdot \left(P_{CO_2} - \frac{P_{CO}^2}{K_{eq.\ 5}}\right) \cdot \frac{W \cdot X_c}{V} \quad \}$$

shift reaction was assumed to reach equilibrium throughout the bed.

Table 4 (continued)

c) Mass balance equation for a plug flow reactor

The bed was divided into 100 equal sections of length dz. At each section the following equations can be written:

$$\left.\begin{aligned}
\frac{d}{dz}(Fg \cdot X_{O2}) &= -r_1 - r_2 - r_3 \\
\frac{d}{dz}(Fg \cdot X_{CO}) &= 2r_1 - 2r_2 + r_4 + 2r_5 \\
\frac{d}{dz}(Fg \cdot X_{CO_2}) &= 2r_2 - r_5 \\
\frac{d}{dz}(Fg \cdot X_{H_2}) &= -2r_3 + r_4 \\
\frac{d}{dz}(Fg \cdot X_{H_2O}) &= 2r_3 - r_4 \\
\frac{d}{dz}(Fg) &= +r_1 - r_2 - r_3 + r_4 + r_5
\end{aligned}\right\} \qquad \text{(T4-3)}$$

The shift dx in the mole fraction of the gas components according to the shift reaction was calculated at each section dz. by:

$$K_{eq.6} = \left(\frac{X_{CO_2} \cdot X_{H_2}}{X_{CO} \cdot X_{H_2O}}\right)^{*} = \frac{(X_{CO_2} + dx)\ (X_{H_2} + dx)}{(X_{CO} - dx)\ (X_{H_2O} - dx)} \qquad \text{(T4-4)}$$

where (*) denotes the final state when the shift is completed.

Table 4 (continued)

d) Mass balance equations for stirred tank model

$$\left.\begin{aligned} Fg_{ex} \cdot X_{CO_{ex}} &= V \cdot (r_4 + 2r_5) \\ Fg_{ex} \cdot X_{CO_{2ex}} - Fg_{in} \cdot X_{CO_{2in}} &= -V \cdot r_5 \\ Fg_{ex} \cdot X_{CO_{2ex}} &= V \cdot r_4 \\ Fg_{ex} X_{H_2O_{ex}} - Fg_{in} \cdot X_{H_2O\ in} &= -V \cdot r_4 \\ Fg_{ex} - Fg_{in} &= r_4 + r_5 \end{aligned}\right\} \quad \text{(T4-5)}$$

X_{H_2Oin}, X_{CO_2in} and Fg_{in} were calculated by assuming complete combustion of the oxygen to CO_2 and H_2O.

The shift in the relative mole fraction of the gas components was calculated by equation (T4-4) for the whole bed.

e) Total bed mass balance equations:

solid balance:

$$\frac{dW}{dt} = FC-CG-VM-FW \quad \text{(T4-6)}$$

carbon balance:

$$\frac{d(W \cdot X_C)}{dt} = FC \cdot Y_c - CG - CG_{dev} - FW \cdot X_C \quad \text{(T4-6)}$$

denoting:

$$\left.\begin{aligned} FW &= \emptyset \cdot FC \\ CG_{dev} &= \lambda \cdot FC \\ VM &= \beta \cdot FC \end{aligned}\right\} \quad \text{(T4-7)}$$

Table 4 (continued)

we get for constant solid inventory in the bed:

$$F_C = \frac{CG}{1-\beta-\phi} \qquad \text{(T4-8)}$$

for a given $\phi = FW/FC$ the carbon concentration at the steady state is given by:

$$X_c = 1 - \frac{1-\beta-\lambda-Y_c}{\phi} \qquad \text{(T4-9)}$$

or for a given carbon concentration the ratio $\phi = FW/FC$: at the steady state is given by:

$$\phi = \frac{1-\beta+\lambda-Y_c}{1-X_c} \qquad \text{(T4-10)}$$

f) The energy equation:

$$\frac{d(W \cdot C_p \cdot T)}{dt} = \left[\sum_i Fg_{in} \cdot X_{iin} \int_{T_{Ref}}^{T_{in}} (Cp_i(T)\,dt) + Q_s \cdot (Fg_{in} \cdot X_{H_2Oin})\right]$$

$$-\left[\sum_i Fg_{out} \cdot X_{iout} \cdot \int_{T_{Ref}}^{T_{out}} (Cp_i(T)\,dt) + Q_s \cdot (Fg_{out} \cdot X_{H_2Oout}) + \right.$$

$$\left. \sum_j Y_j \Delta H_j + FW \cdot C_{pash} \cdot (T_{out} - T_{Ref}) + H_{Loss}\right] \qquad \text{(T4-11)}$$

Table 5

Base Steady State Parameters

a. Inputs and Process Parameters

$Fg = 165$ lb mole/hr ft^2	total input gas flow rate
SOR = 2.0	steam/oxygen mole ratio
P = 25 atm	total pressure
$W = 275$ lb/ft^2	solid inventory
$X_C = 0.3$	carbon concentration

b. Outputs

BTU = 171.2 (BTU/SCF)	dry net heating value
$T = 1705.5^{\circ}F$	temperature
FC = 1483.1 lb/hr·ft^2	coal feed
$\emptyset = 0.147$	ash/coal ratio
$Fg_{out} = 233$ lb mole/hr·ft^2	output flow rate
$X_{CO} = 0.191$	output mole fraction
$X_{CO_2} = 0.082$	output mole fraction
$X_{H_2O} = 0.116$	output mole fraction
$X_{H_2} = 0.150$	output mole fraction
$X_{N_2} = 0.397$	output mole fraction
$X_{CH_4} = 0.056$	output mole fraction
$X_{H_2S} = 0.007$	output mole fraction

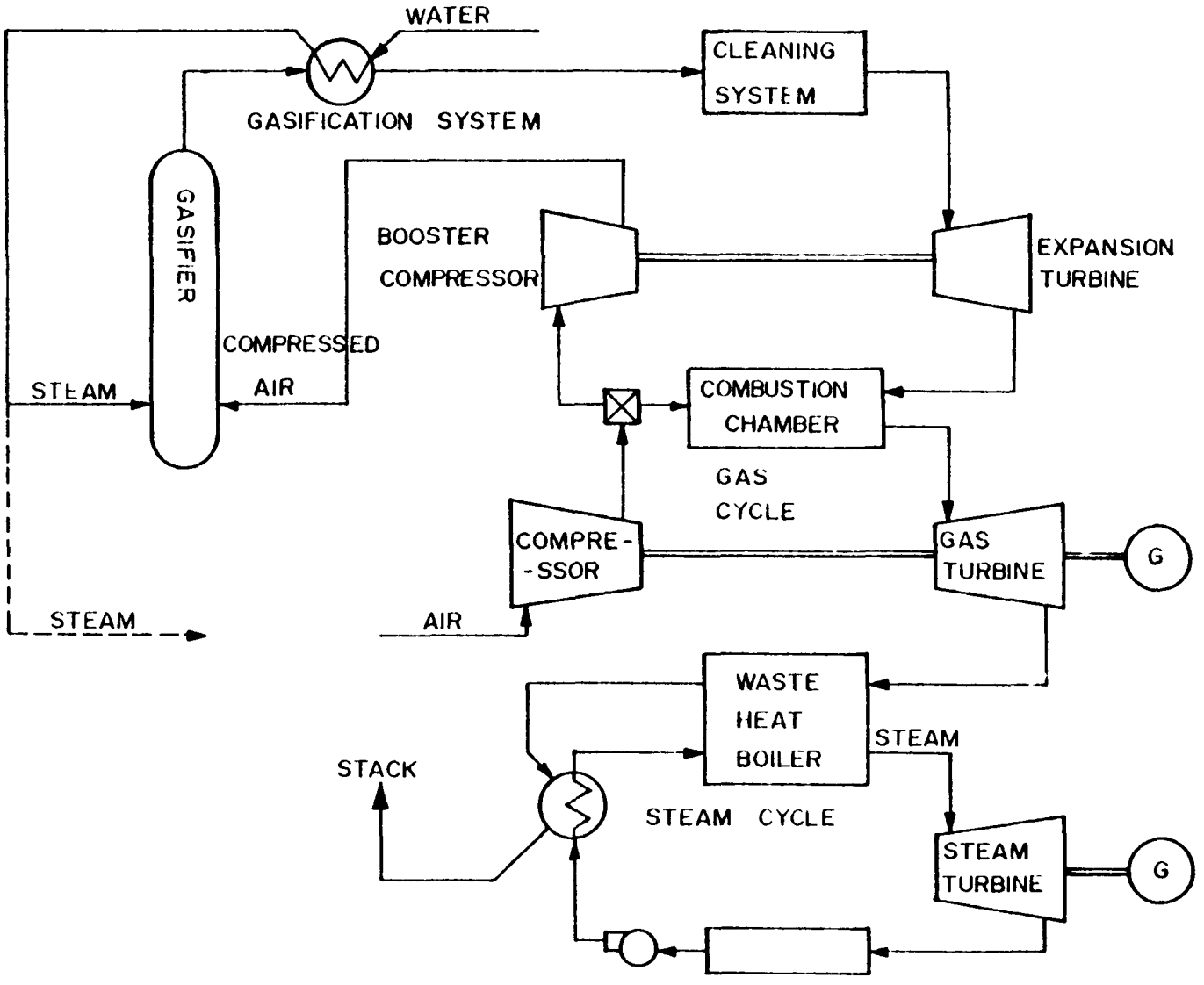

Figure 1: Combined Cycle for use with a Fluidized Bed Gasification System

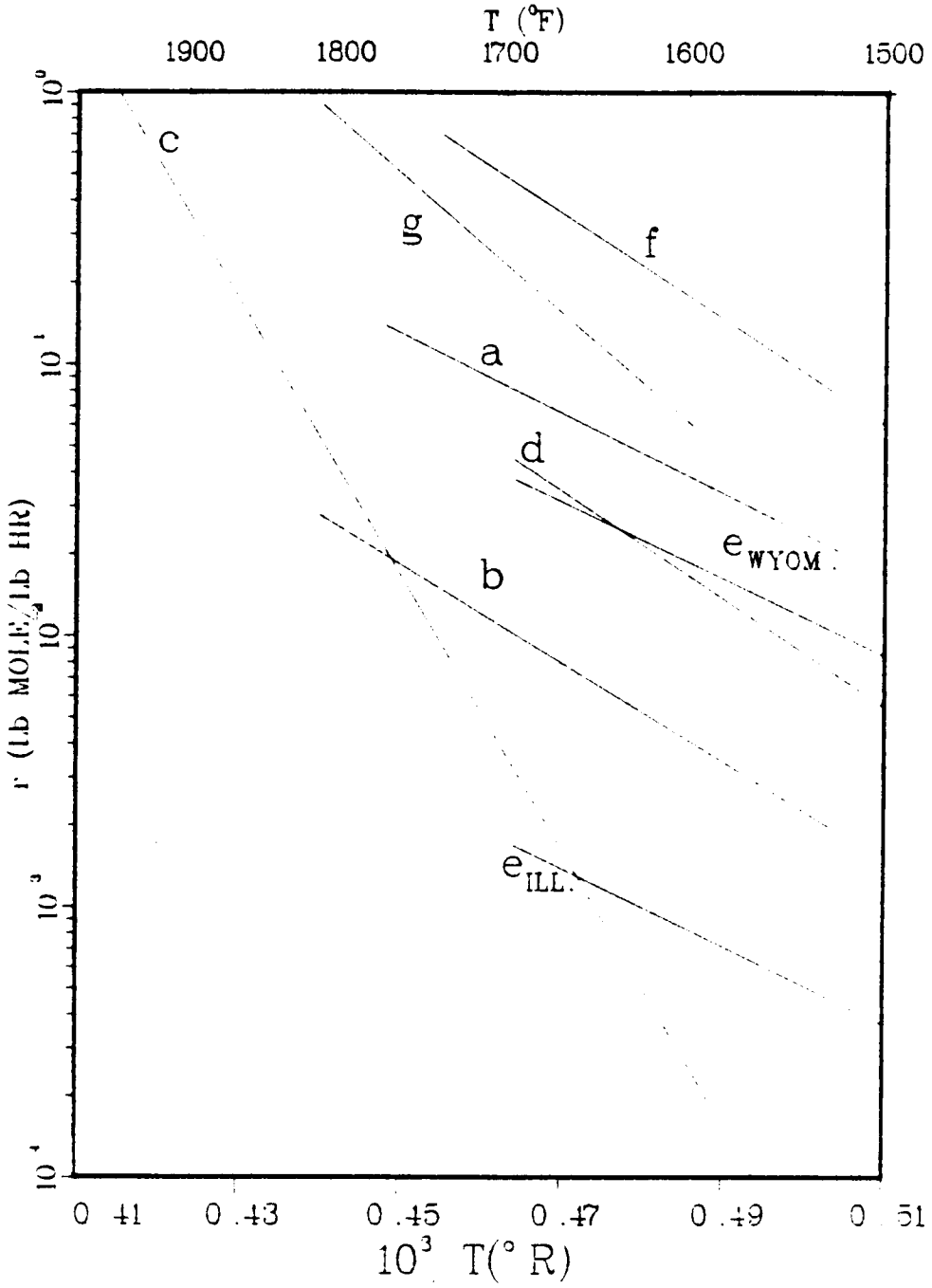

Figure 2a: Reaction Rate of the Steam - Carbon Reaction (for notation see Table 3)

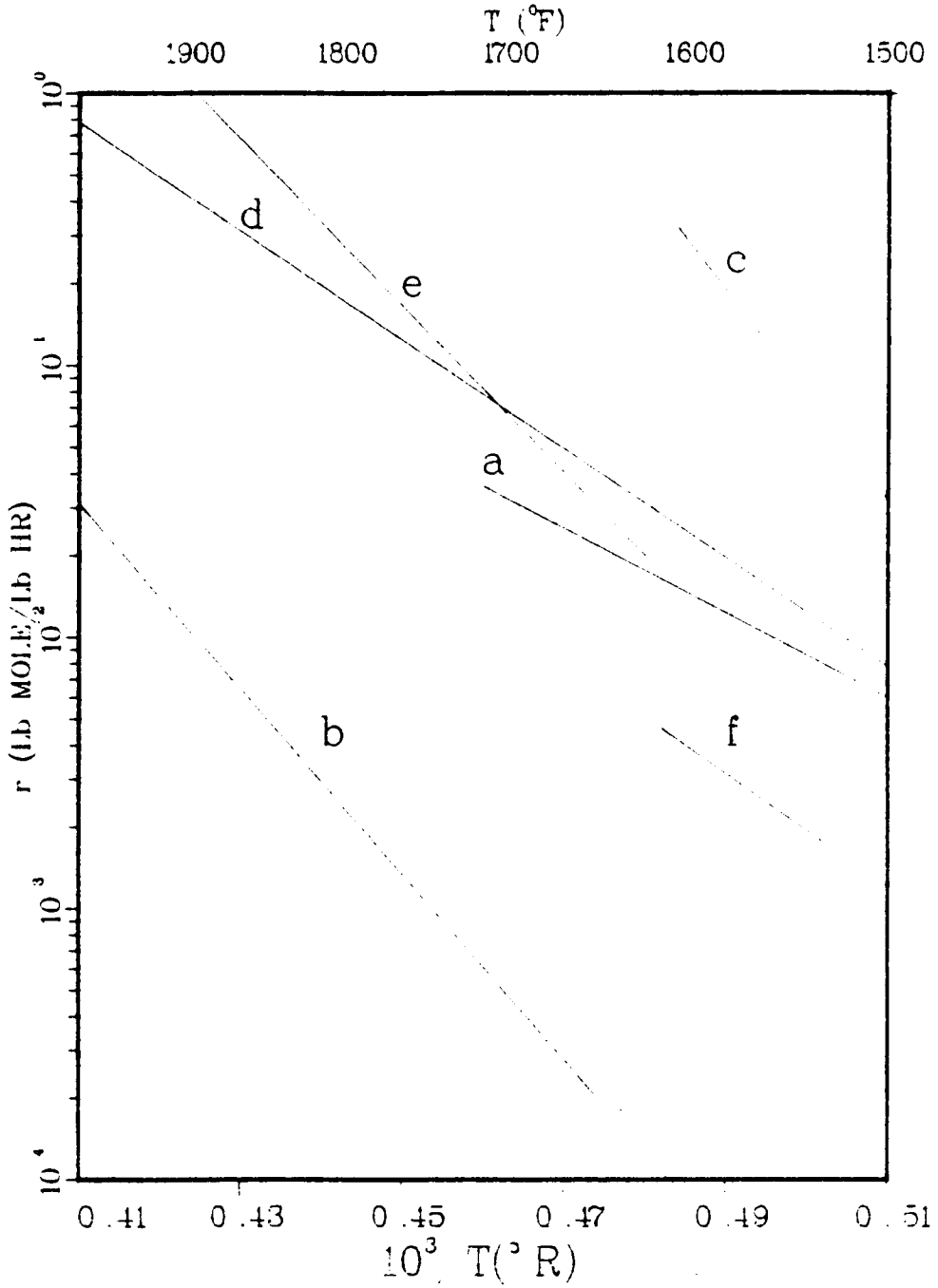

Figure 2b: Reaction Rate of the Carbon - Carbon Dioxide Reaction (for notation see Table 3)

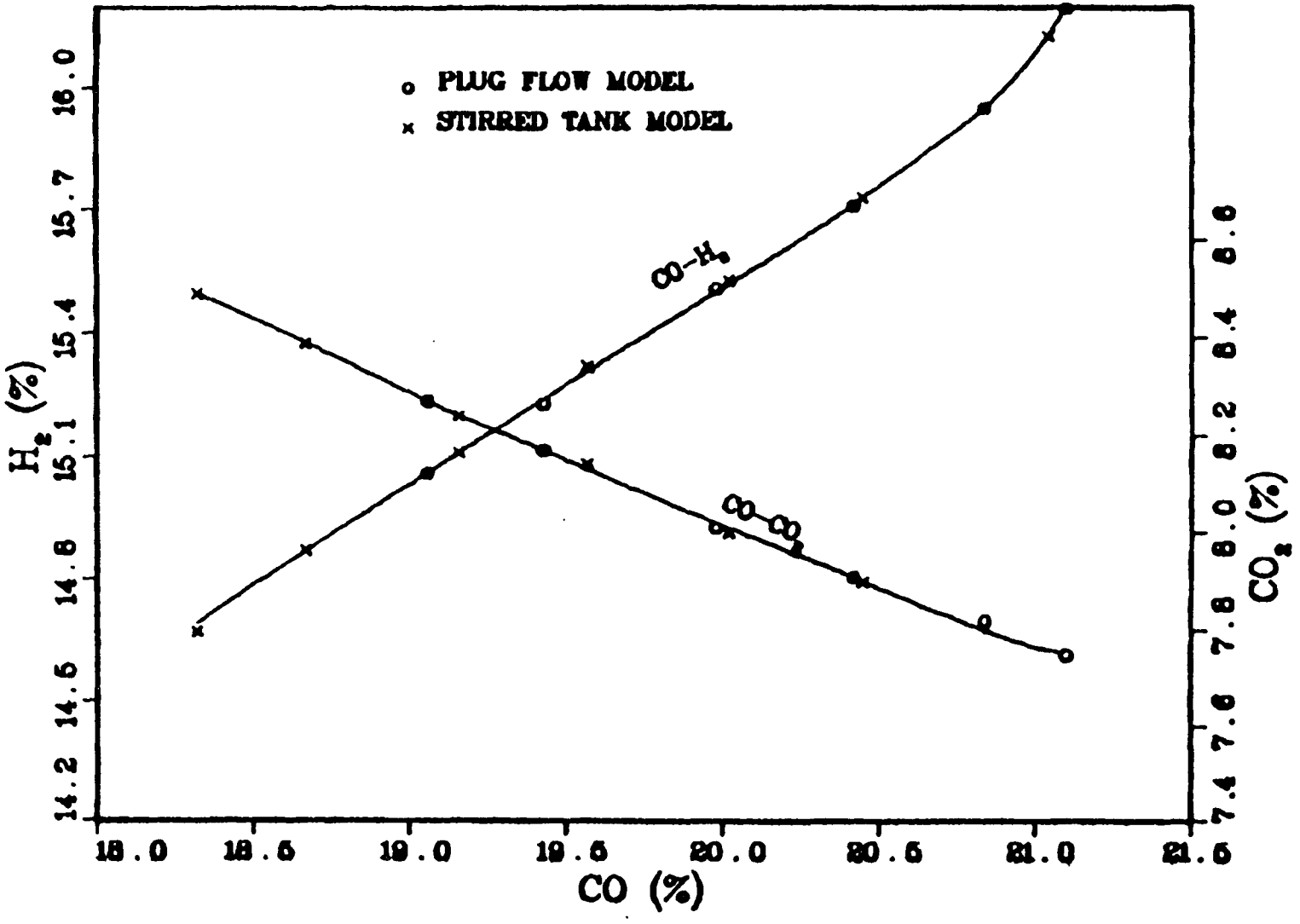

Figure 3a: Composition Space for a Plug Flow and a Stirred Tank Models

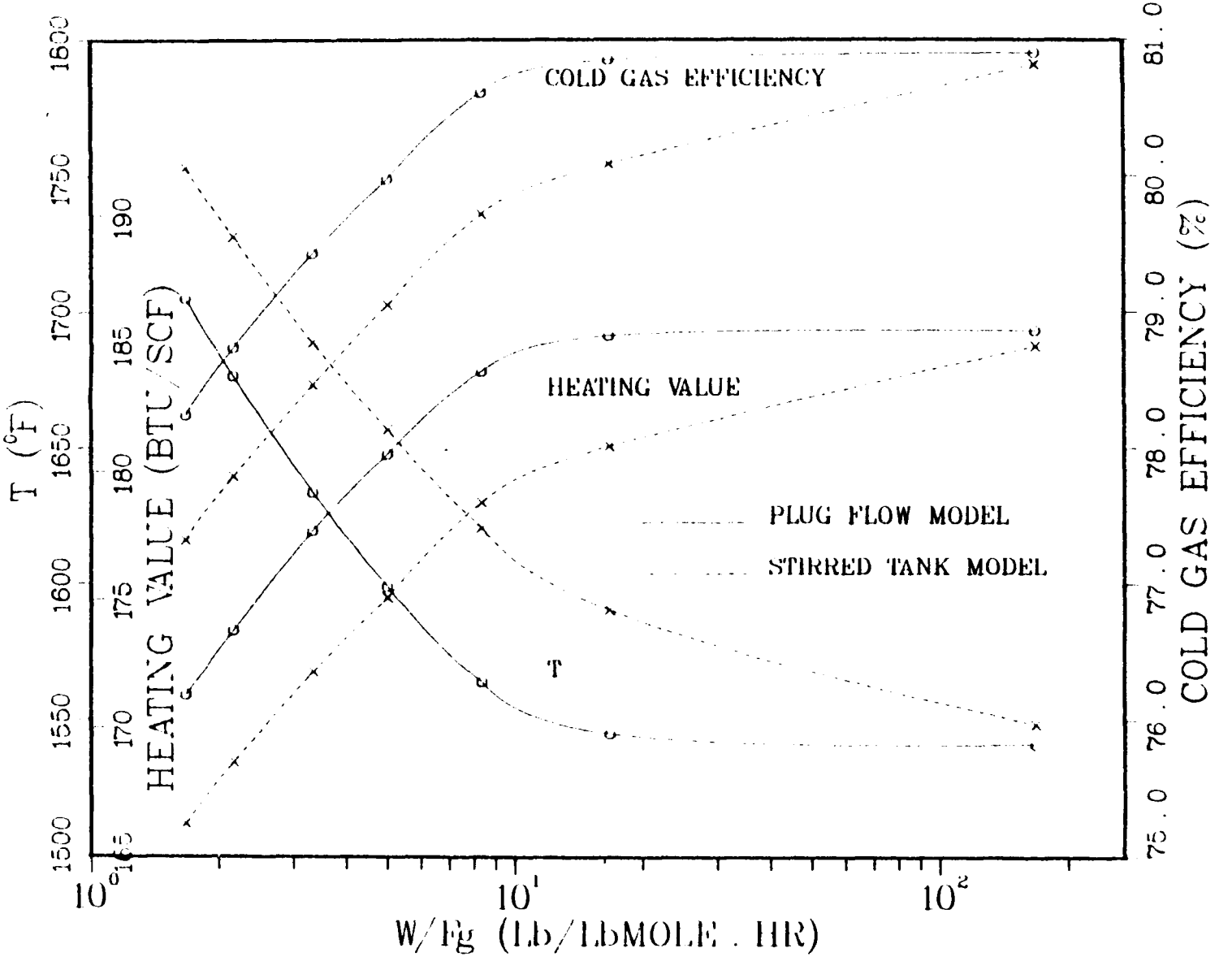

Figure 3b: Output Variables versus Inverse Space Velocity for a Plug Flow and a Stirred Tank Models

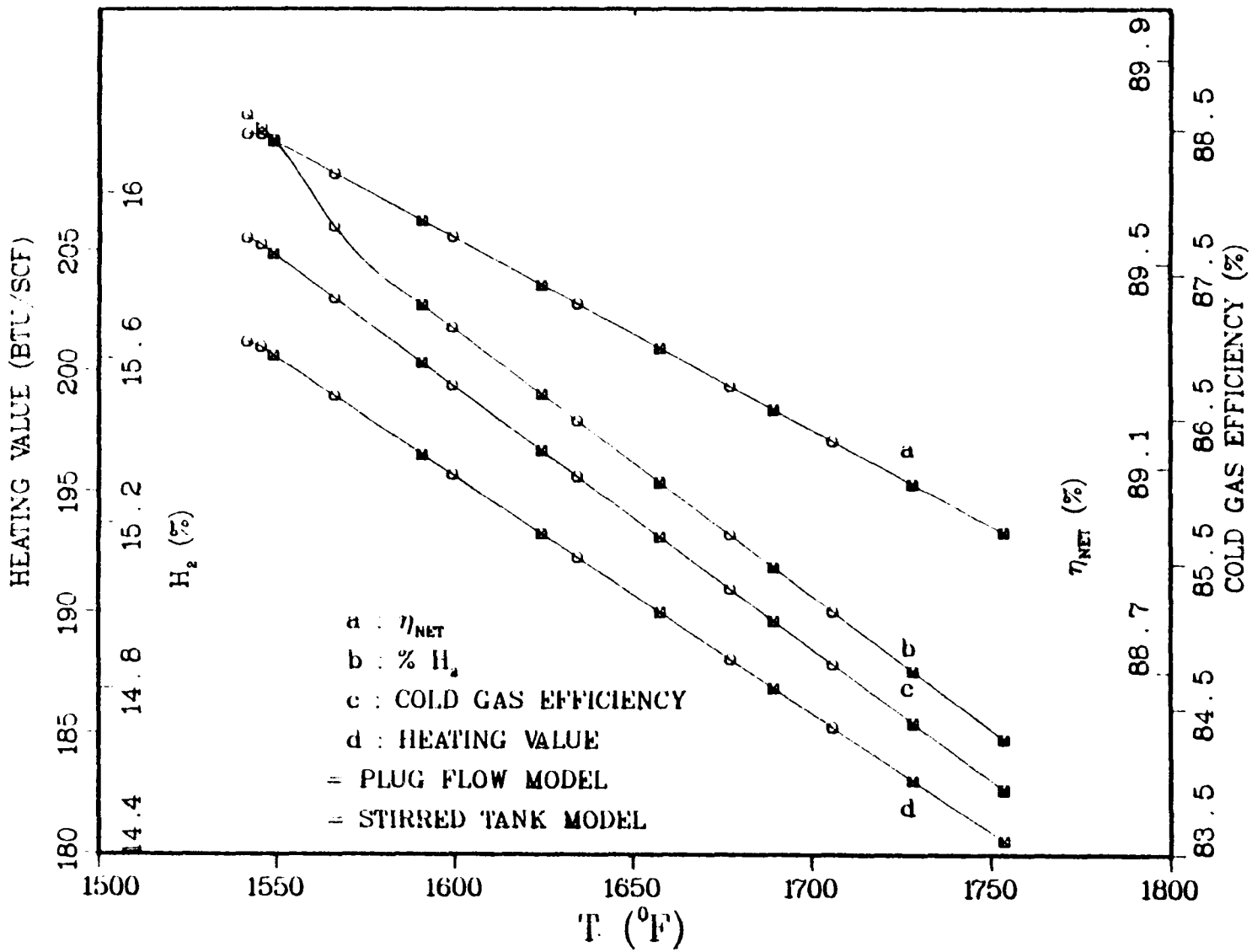

Figure 3c: Output Variables versus Temperature for a Plug Flow and a Stirred Tank Models

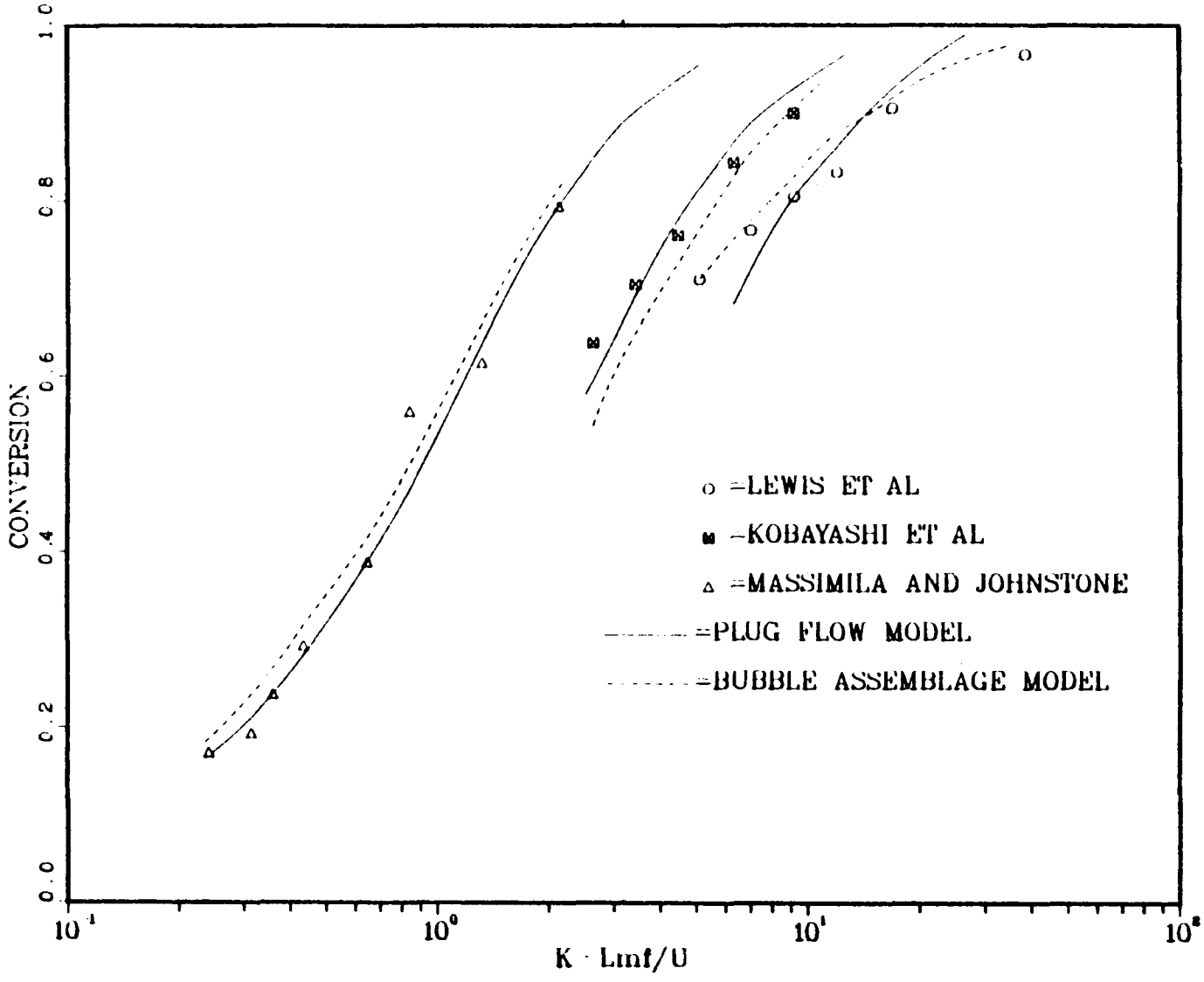

Figure 4: Comparison Between Experimental Results and Calculated Conversions of a Modified Plug Flow Model and a Bubble Assemblage Model (Kato and Wen, 1969)

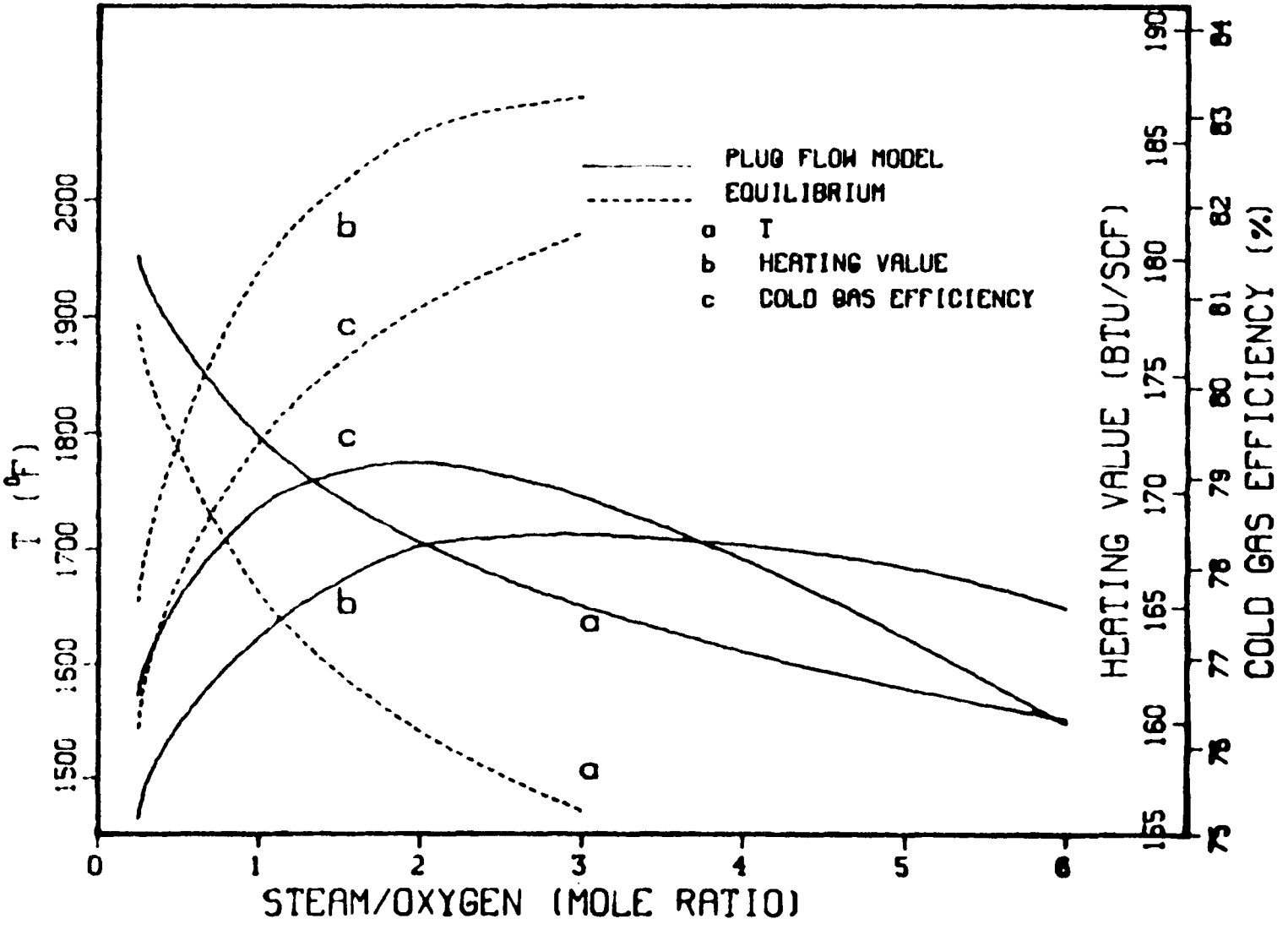

Figure 5a: Steady State Characteristics of a Plug Flow and Equilibrium Models. Output Variables versus Steam to Oxygen Ratio.

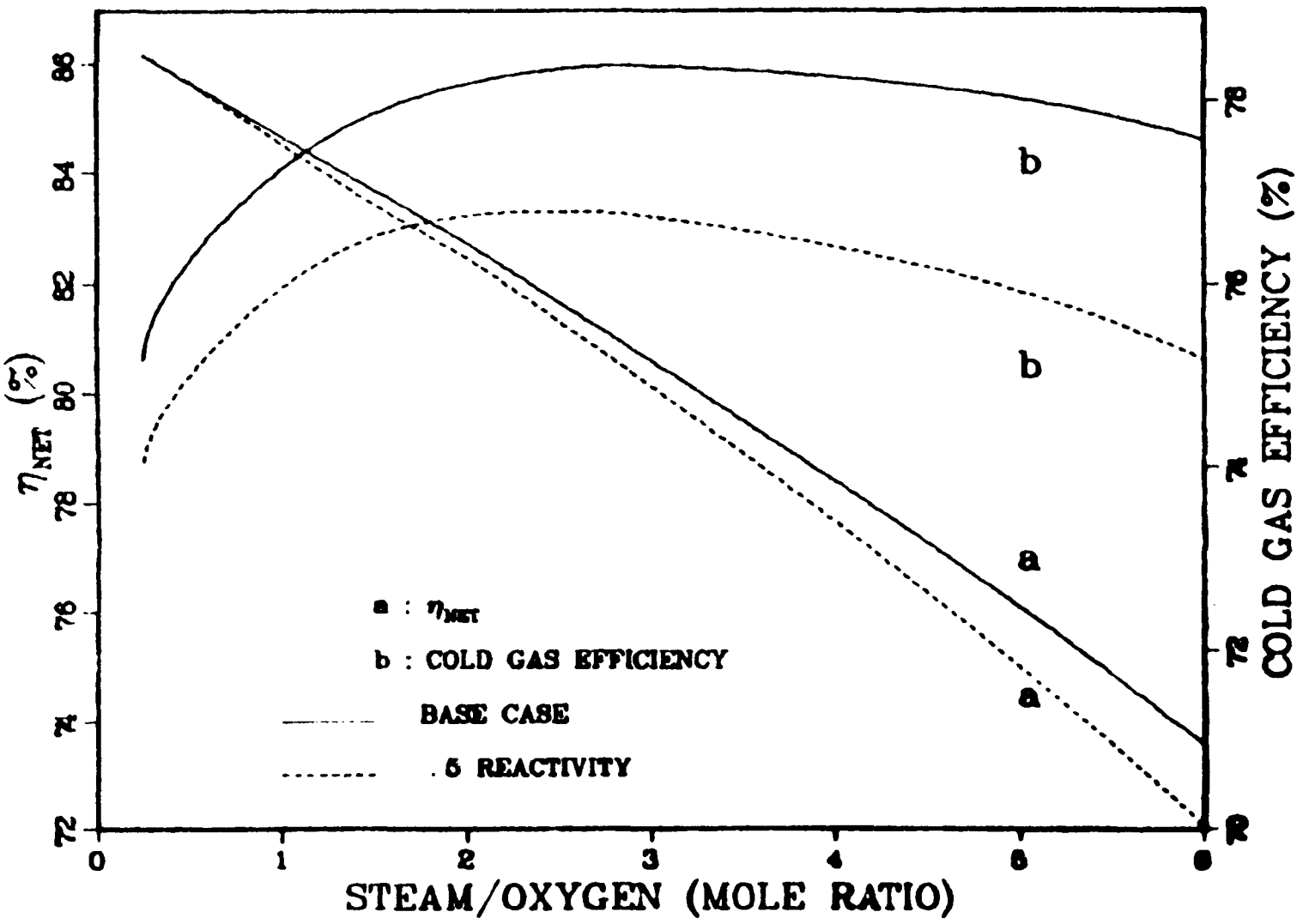

Figure 5b: Steady State Efficiencies of a Plug Flow Model (Base Case versus 50% Reactivity Case)

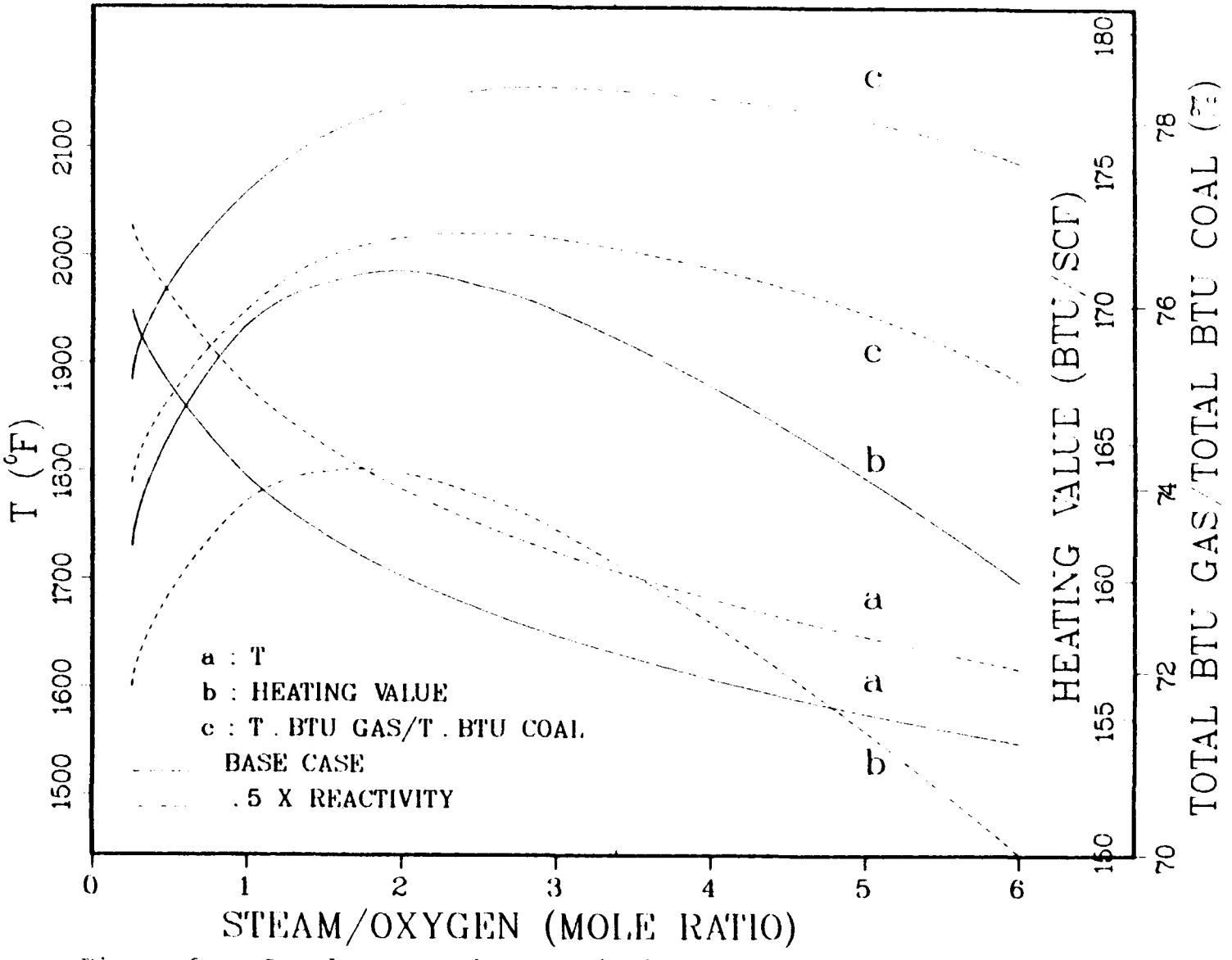

Figure 6a: Steady State Characteristics of a Plug Flow Model (Base Case versus 50% Reactivity Case)

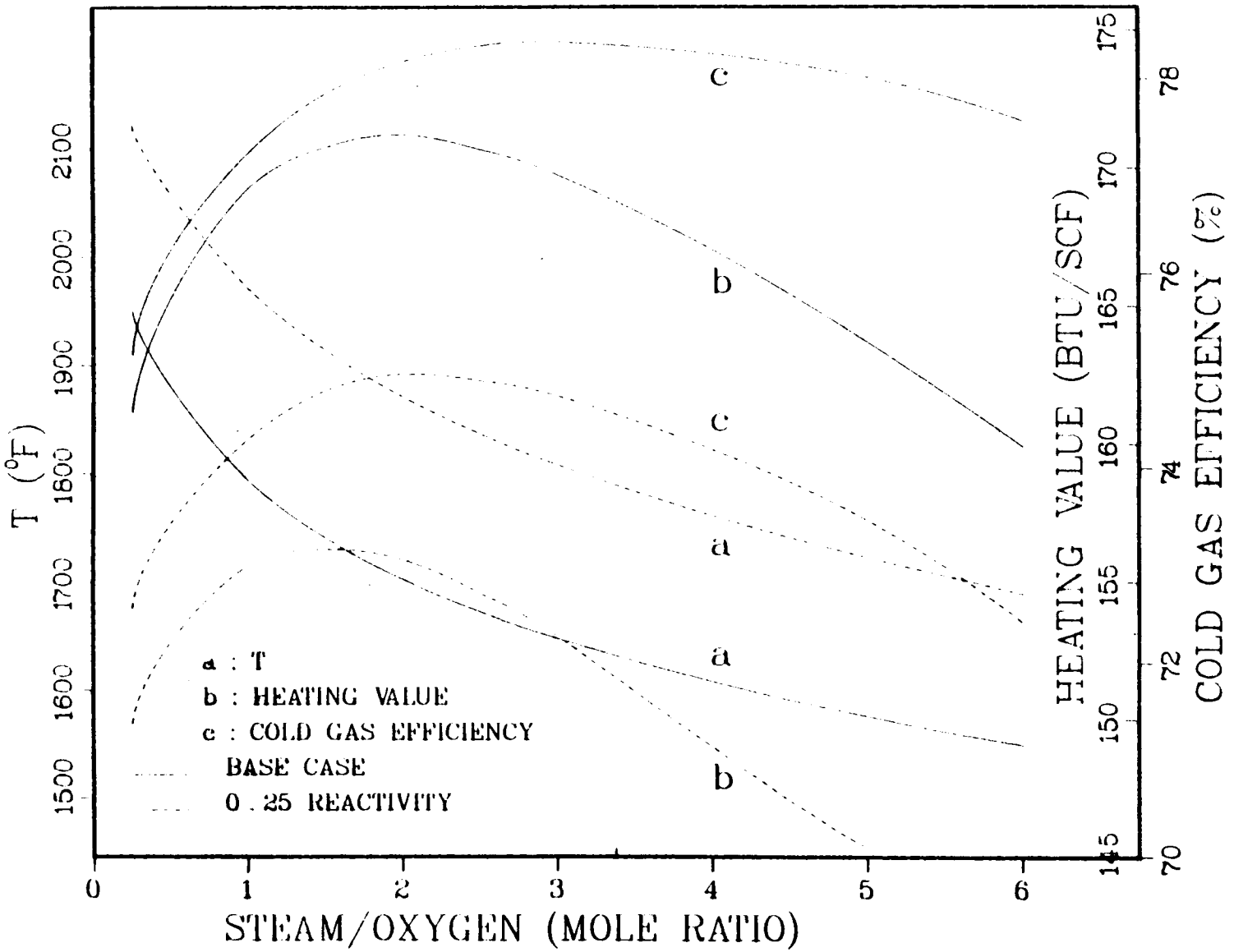

Figure 6b: Steady State Characteristics of a Plug Flow Model (Base Case versus 25% Reactivity Case)

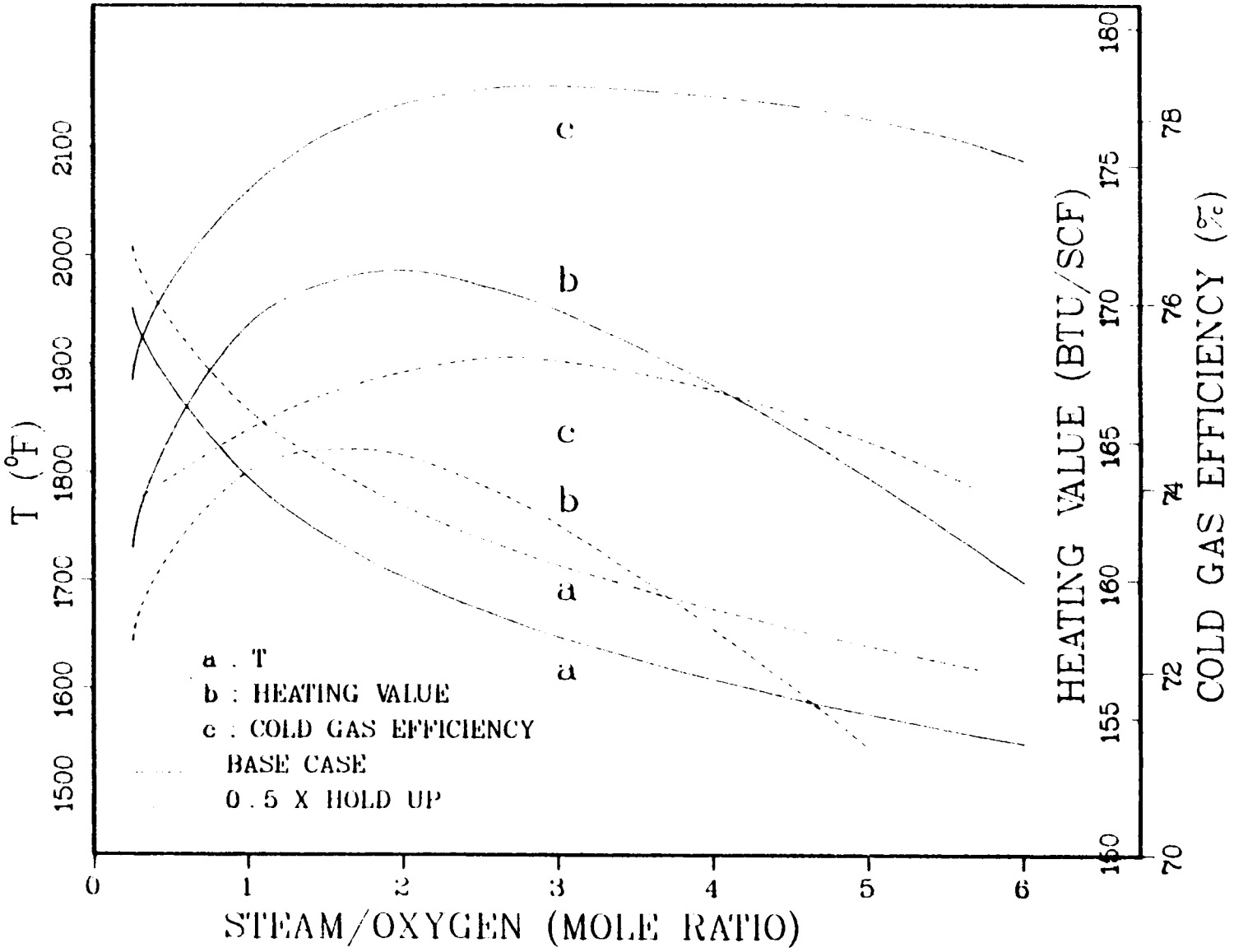

Figure 6c: Steady State Characteristics of a Plug Flow Model (Base Case versus 50% Hold-Up Case)

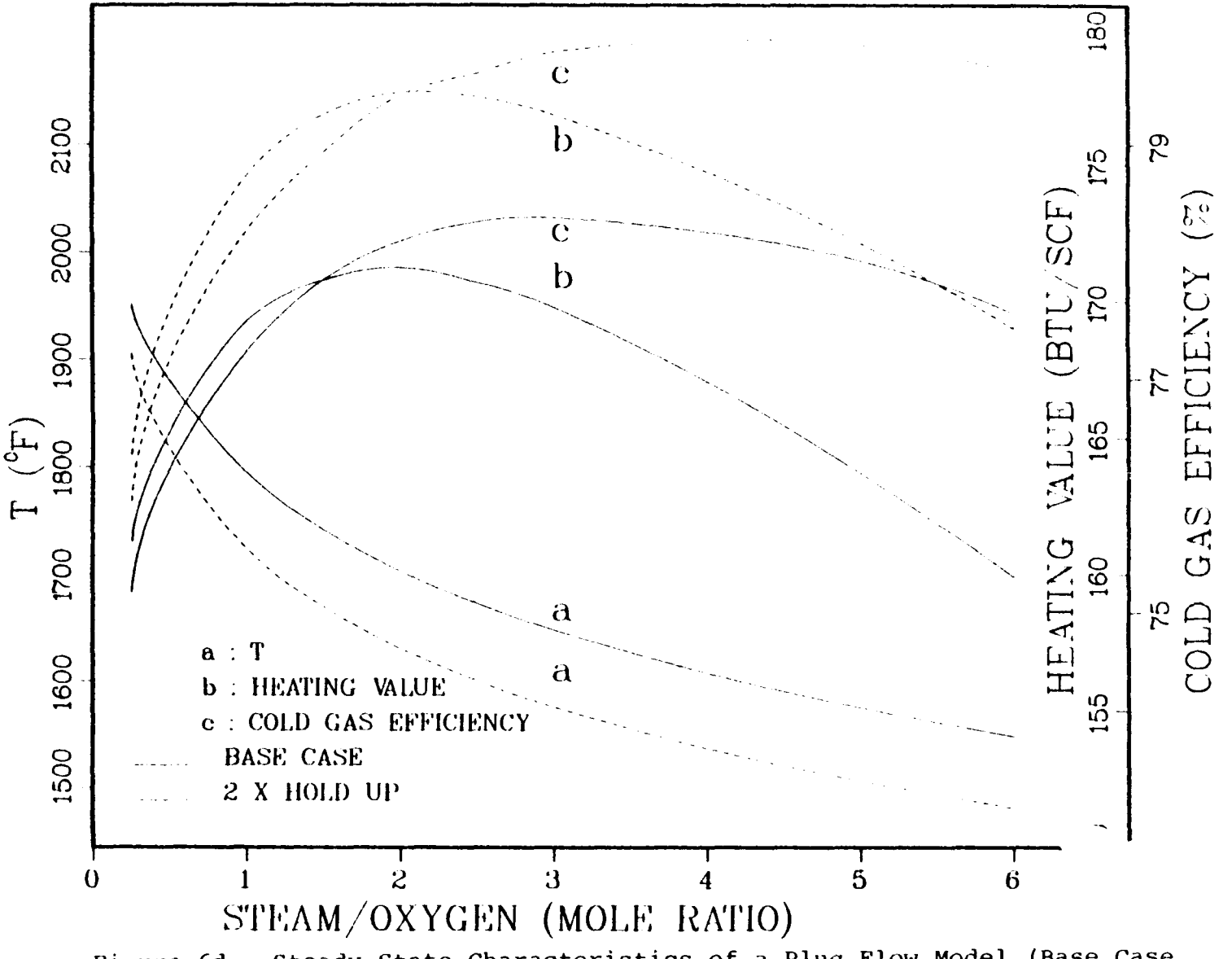

Figure 6d: Steady State Characteristics of a Plug Flow Model (Base Case versus 200% Hold-Up Case)

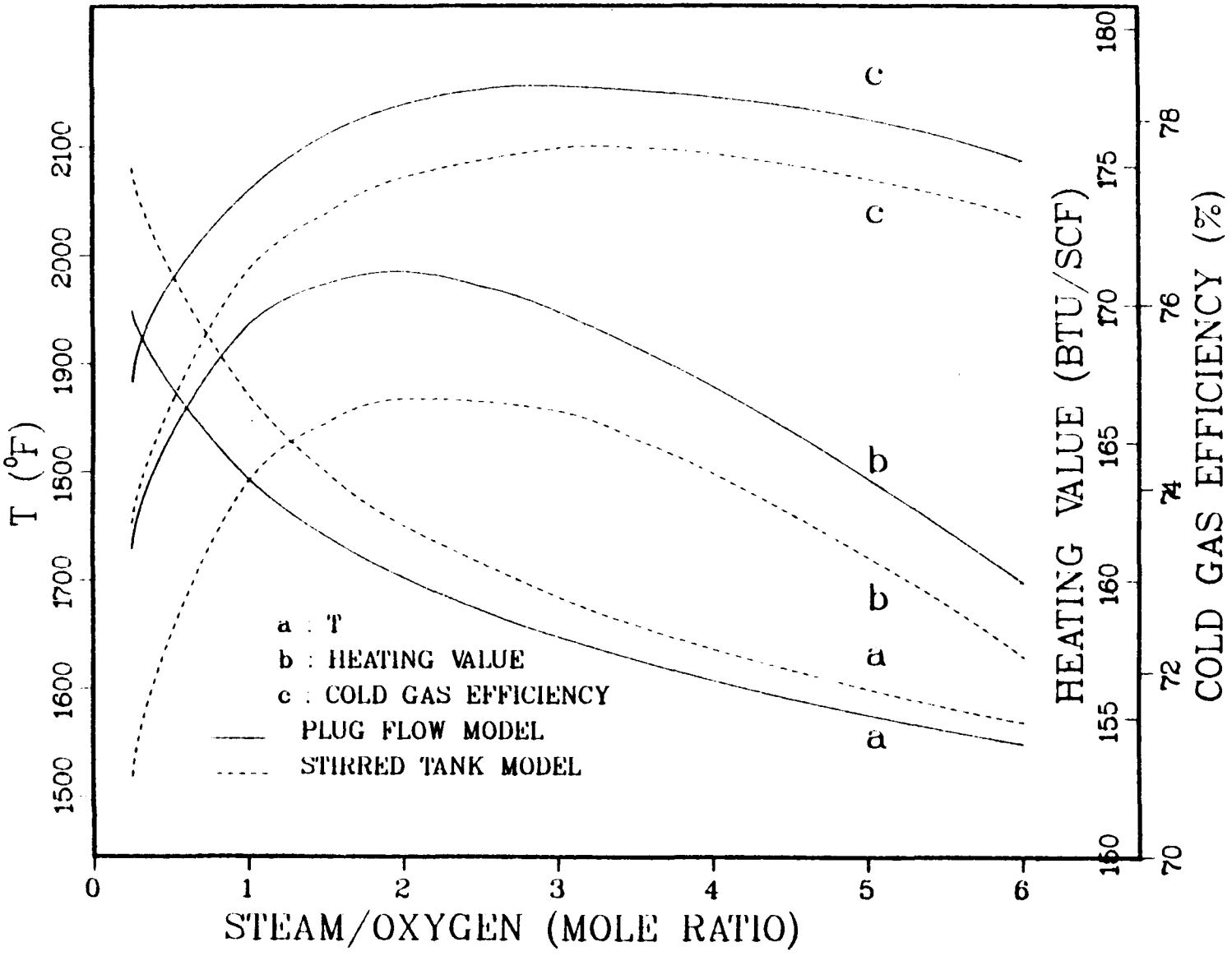

Figure 7: Steady State Characteristics. A Plug Flow Model versus a Stirred Tank Model

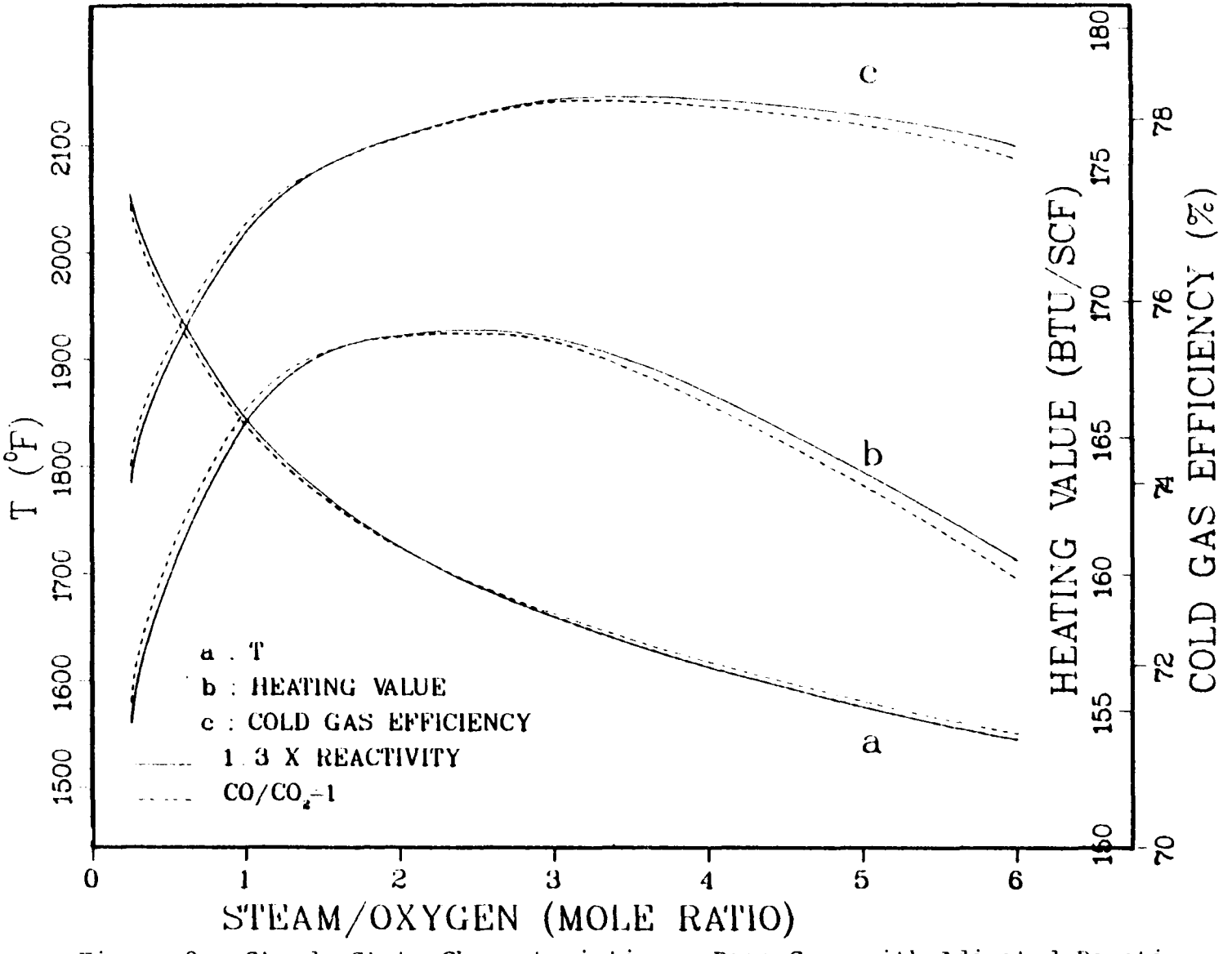

Figure 8: Steady State Characteristics. Base Case with Adjusted Reactivity versus Partial Combustion Case ($(CO_2)/(CO) = 1$).

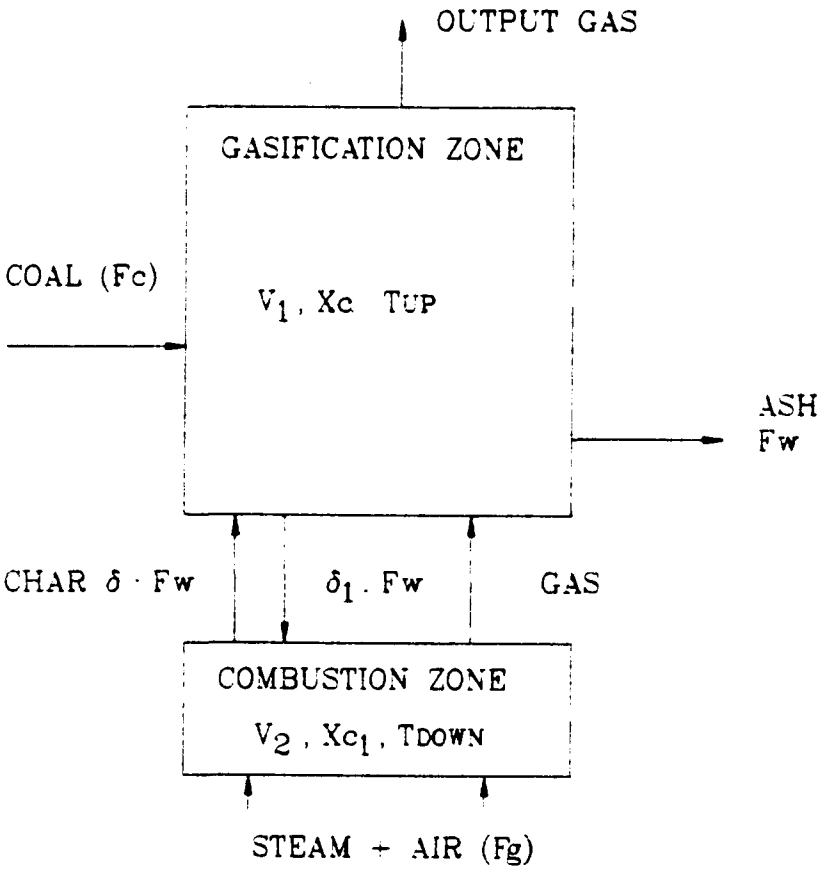

INPUTS AND PROCESS PARAMETERS

V_1=0 . 1 V
V_2=0 . 9 V
δ=13 .
Xc=0 . 3
Fg=165 (Lb mole/ hr ft^2)

OUTPUTS

TUP=1649 ($^\circ$F)
TDOWN=2293 ($^\circ$F)
Xc_1=0 . 12
δ_1=10 . 3
Fc=1590 (Lb/ hr ft^2)
Φ=(Fw/ Fc)=0 . 148
BTU=191 . 5

Figure 9: Schematic Diagram of a Two Sections Stirred Tank Model

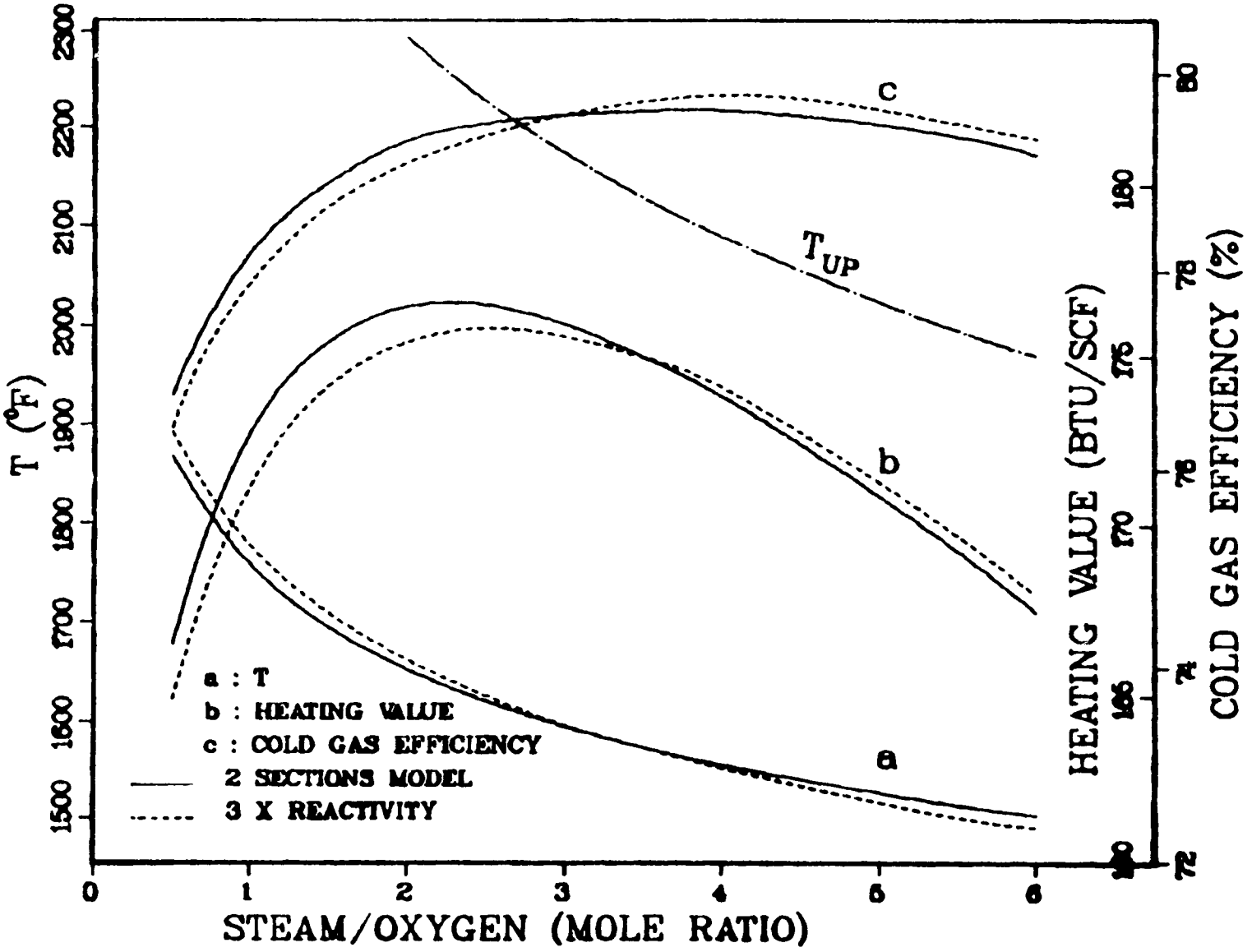

Figure 10: Steady State Characteristics. Base Case with Adjusted Reactivity versus Two Sections Model

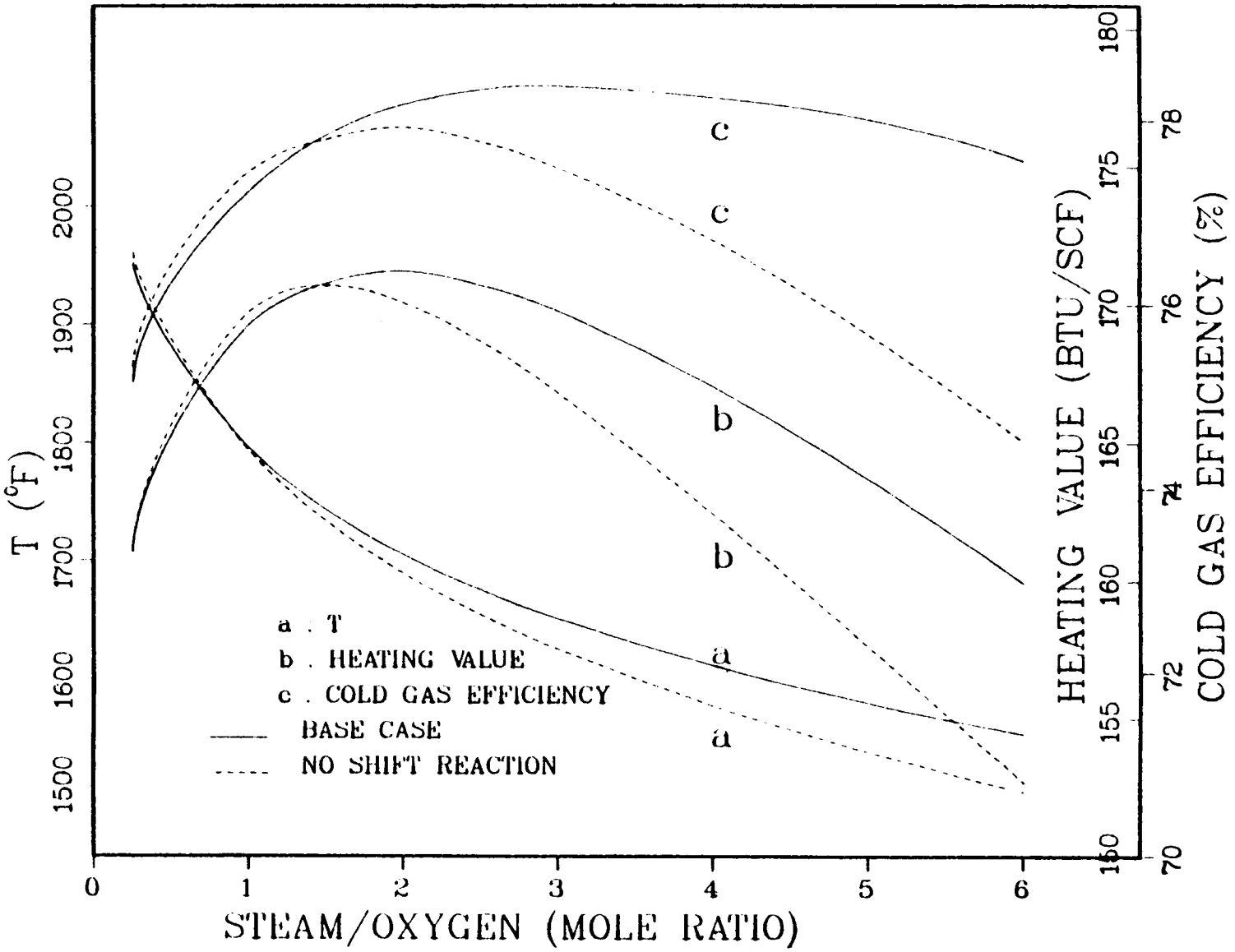

Figure 11: Steady State Characteristics. Base Case versus the Case where Shift Reaction is Neglected

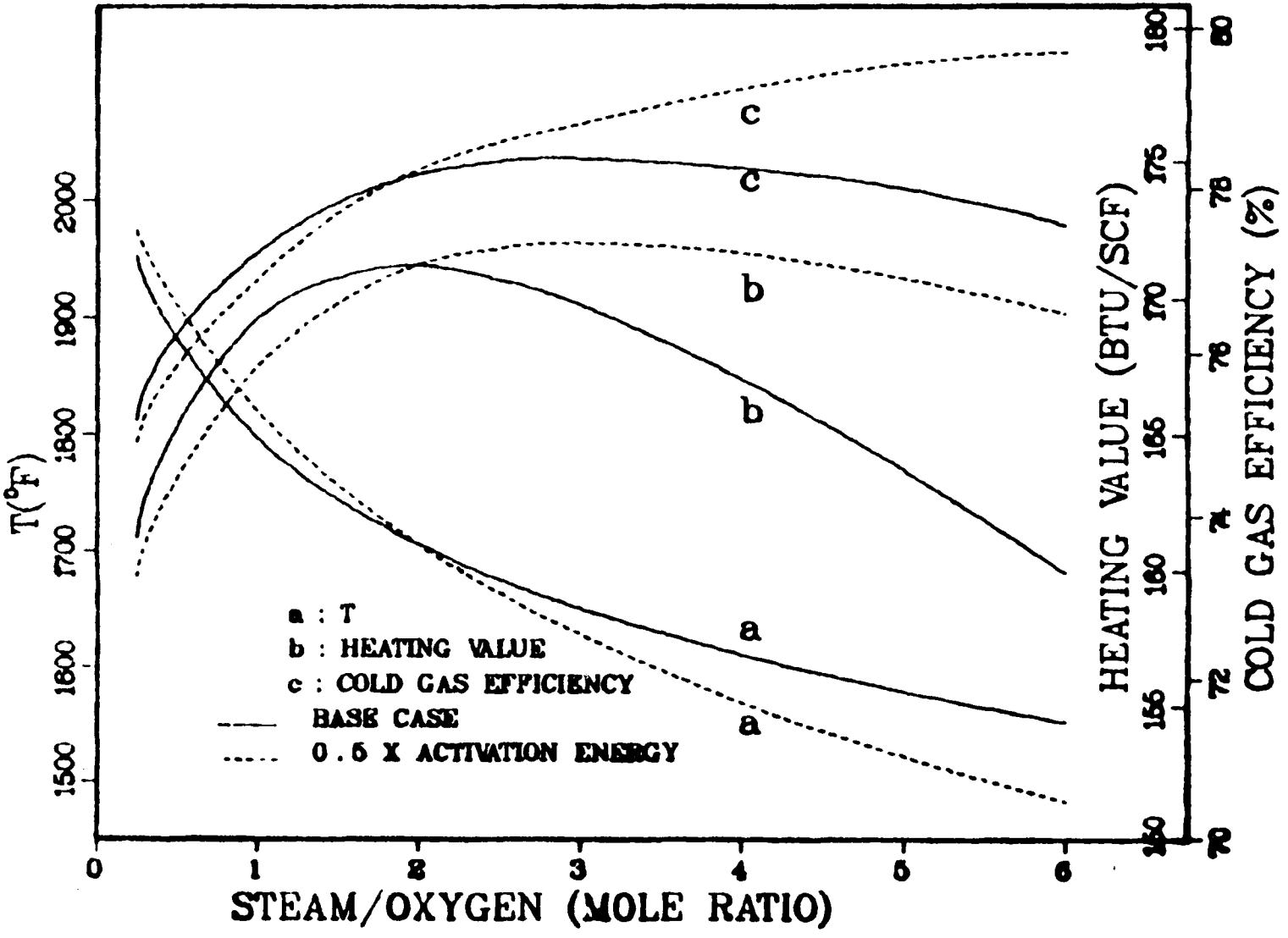

Figure 12: Steady State Characteristics of a Plug Flow Model (Base Case versus 50% Activation Energy Case)

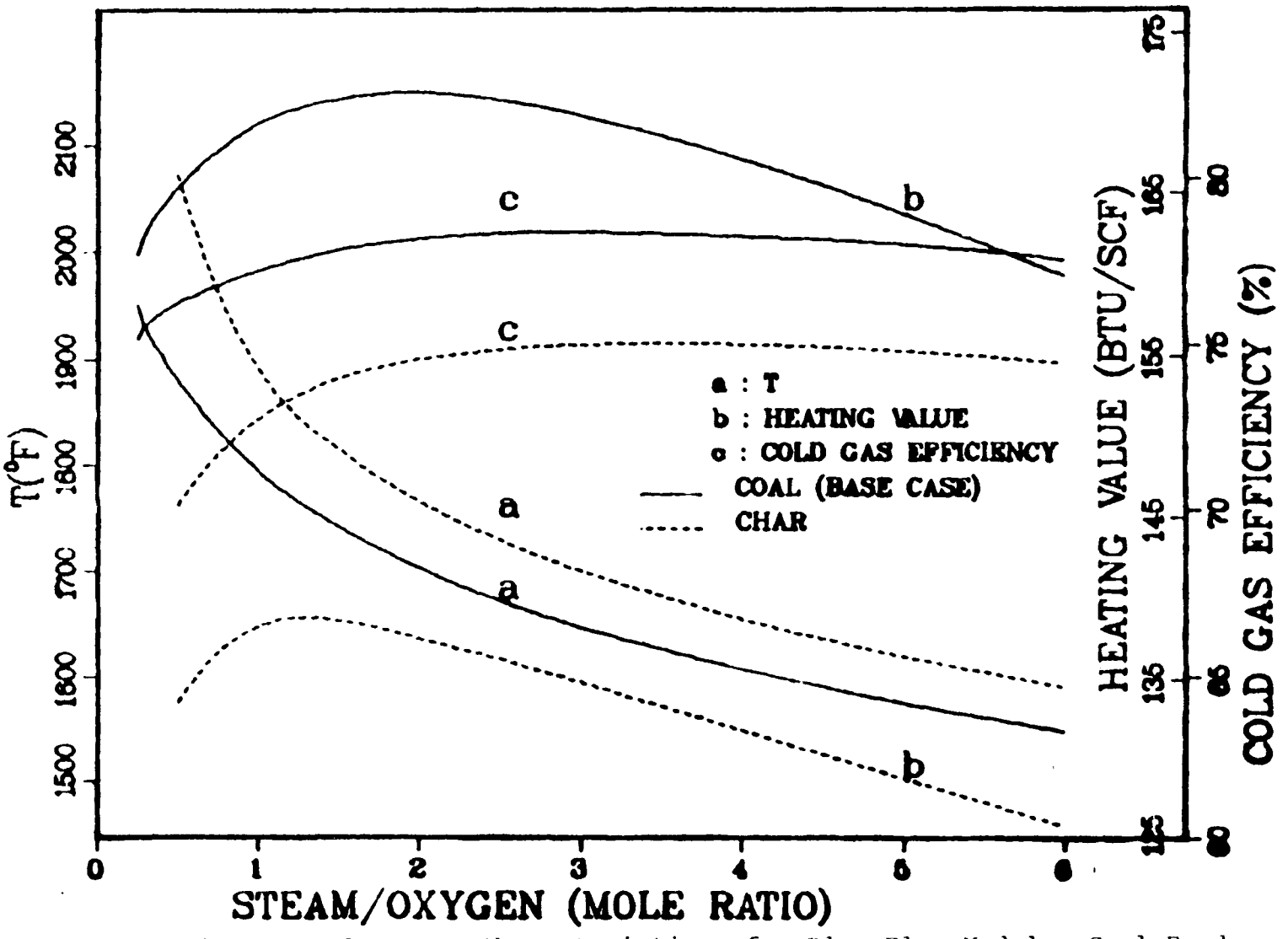

Figure 13: Steady State Characteristics of a Plug Flow Model. Coal Feed (Base Case) versus Char Feed Case

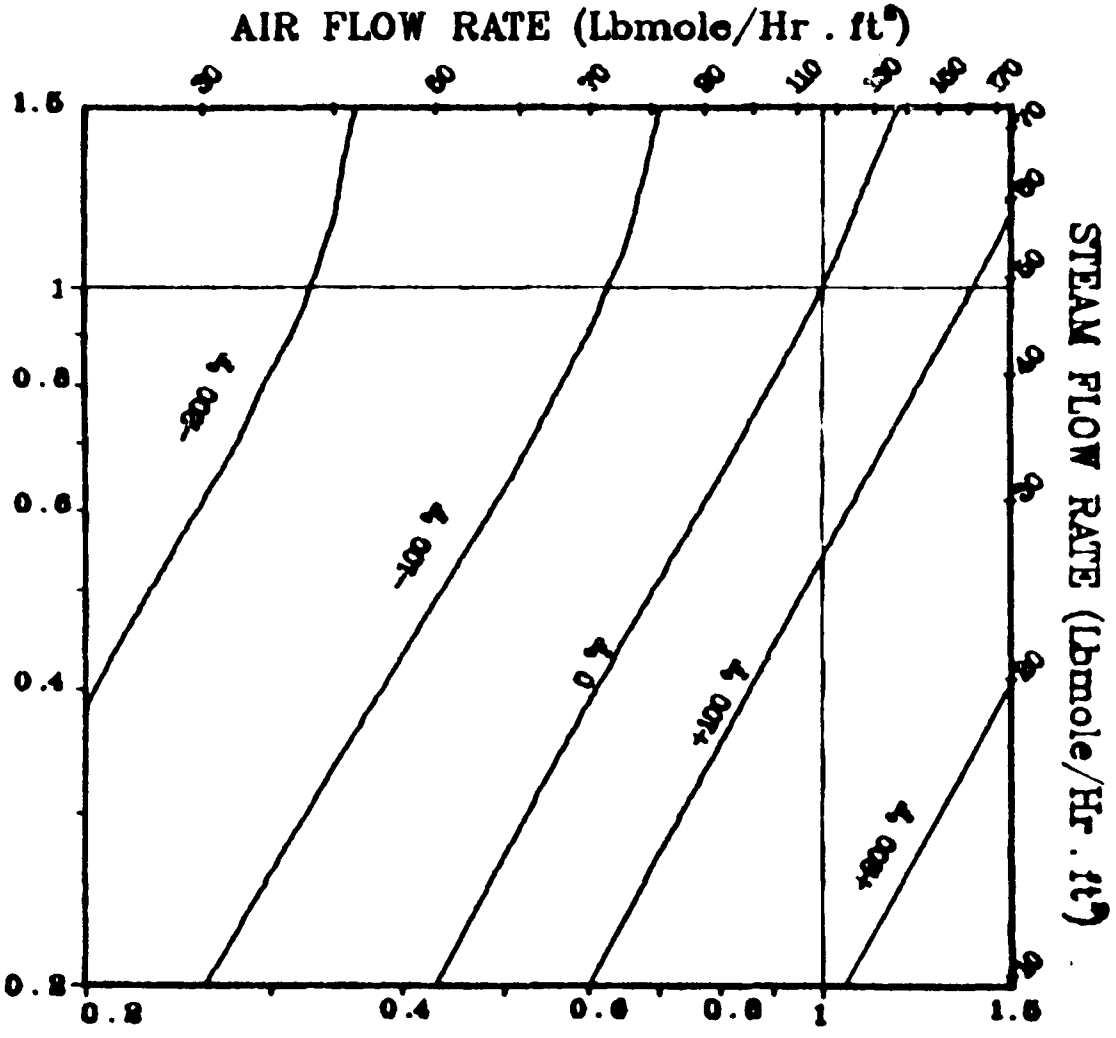

Figure 14a: Isotherms of the Steady State Control Map (Constant X_c)

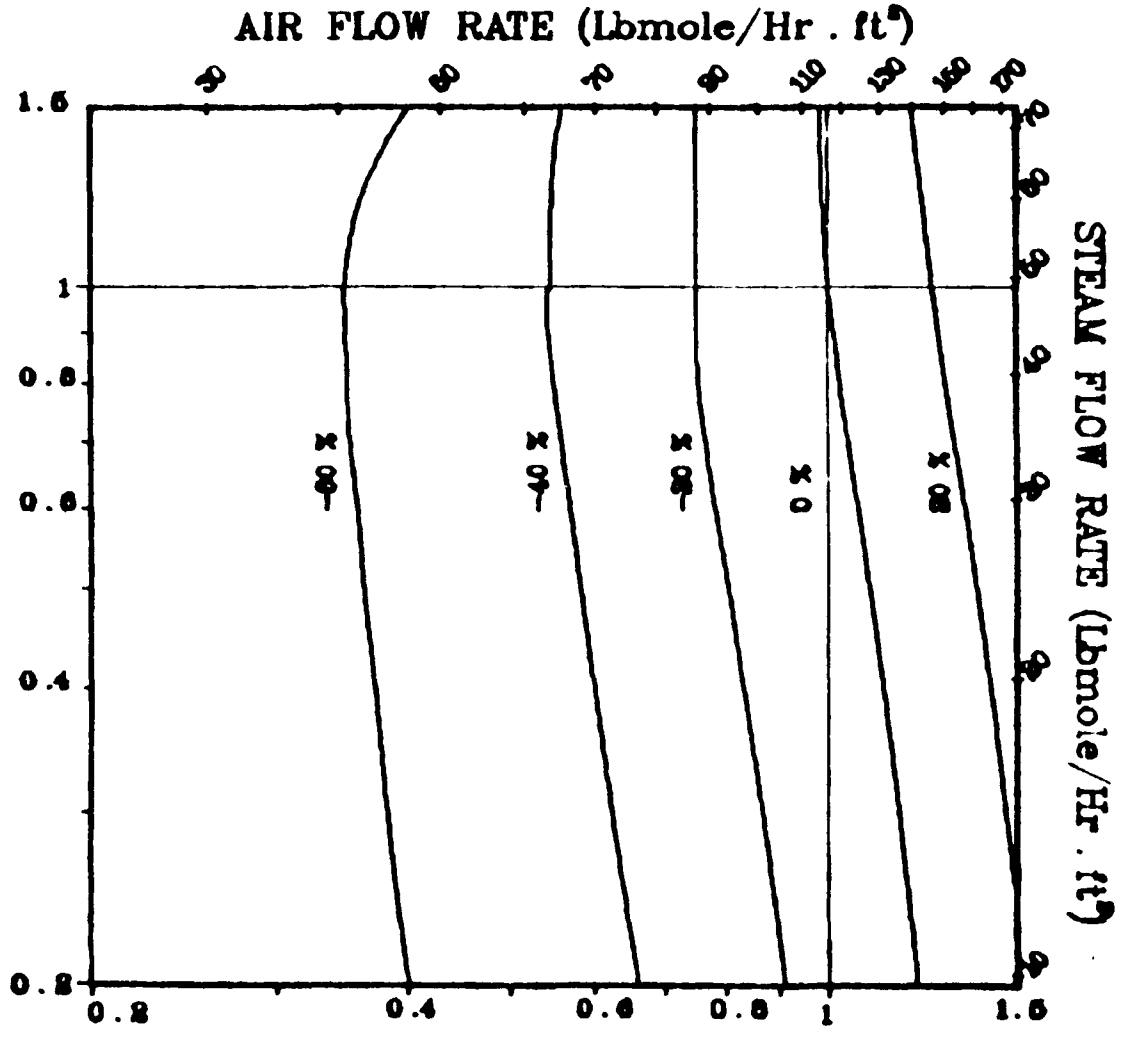

Figure 14b: Iso Total BTU/Hr. Lines of the Steady State Control Map (Constant X_c)

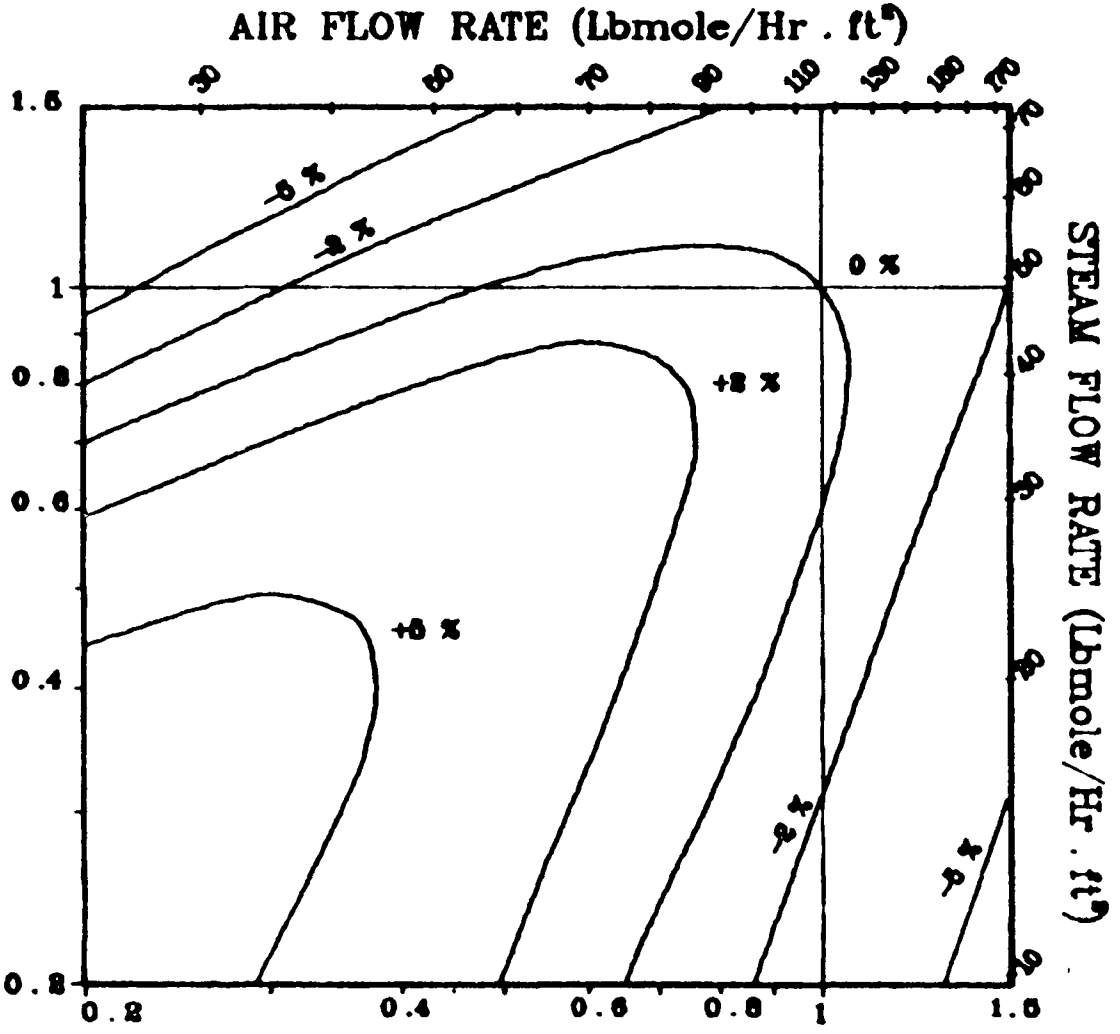

Figure 14c: Iso Heating Value Lines of the Steady State Map (Constant X_c)

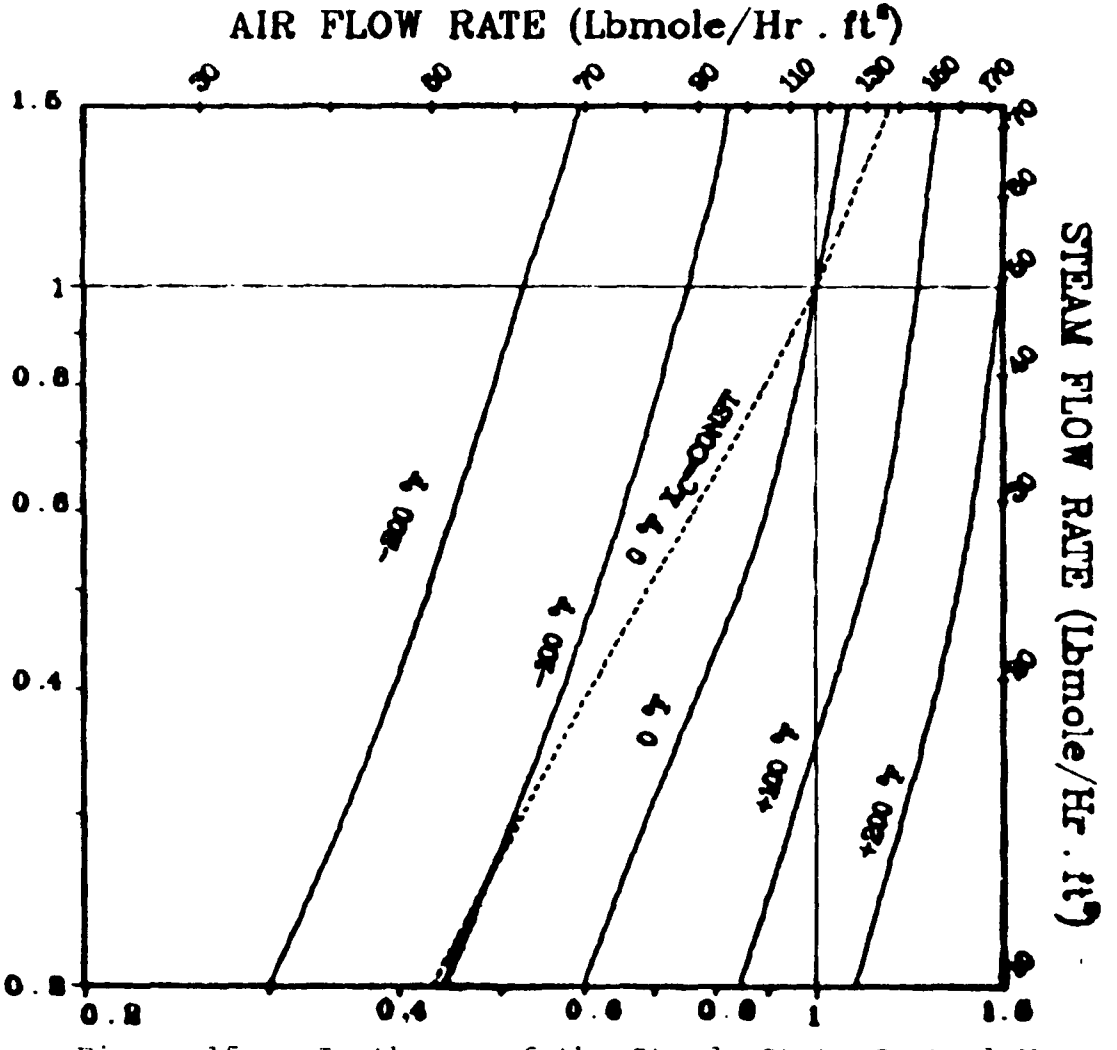

Figure 15a: Isotherms of the Steady State Control Map
(Constant Ash Withdrawal Rate)

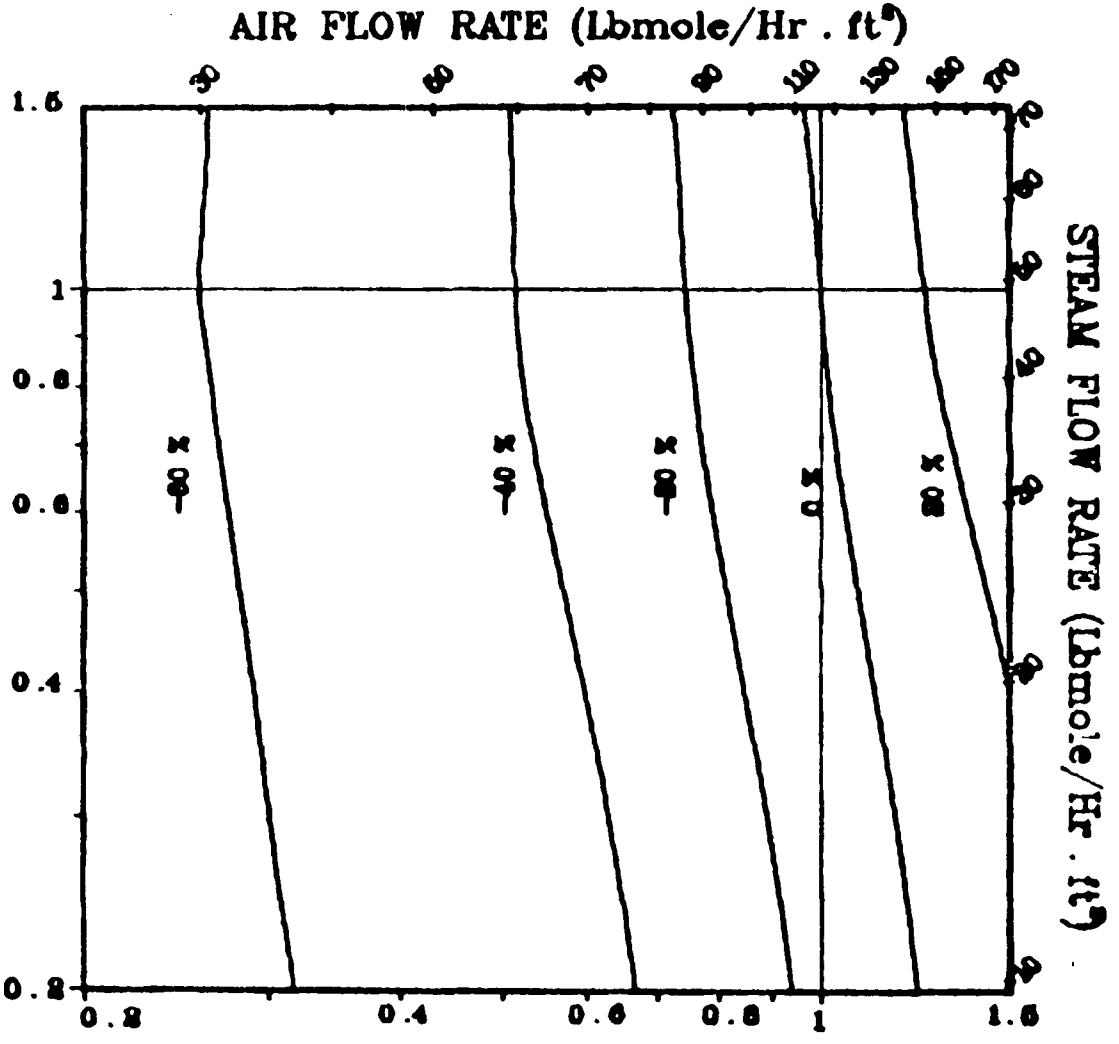

Figure 15b: Iso Total BTU/Hr. Lines of the Steady State Control Map (Constant Ash Withdrawal Rate)

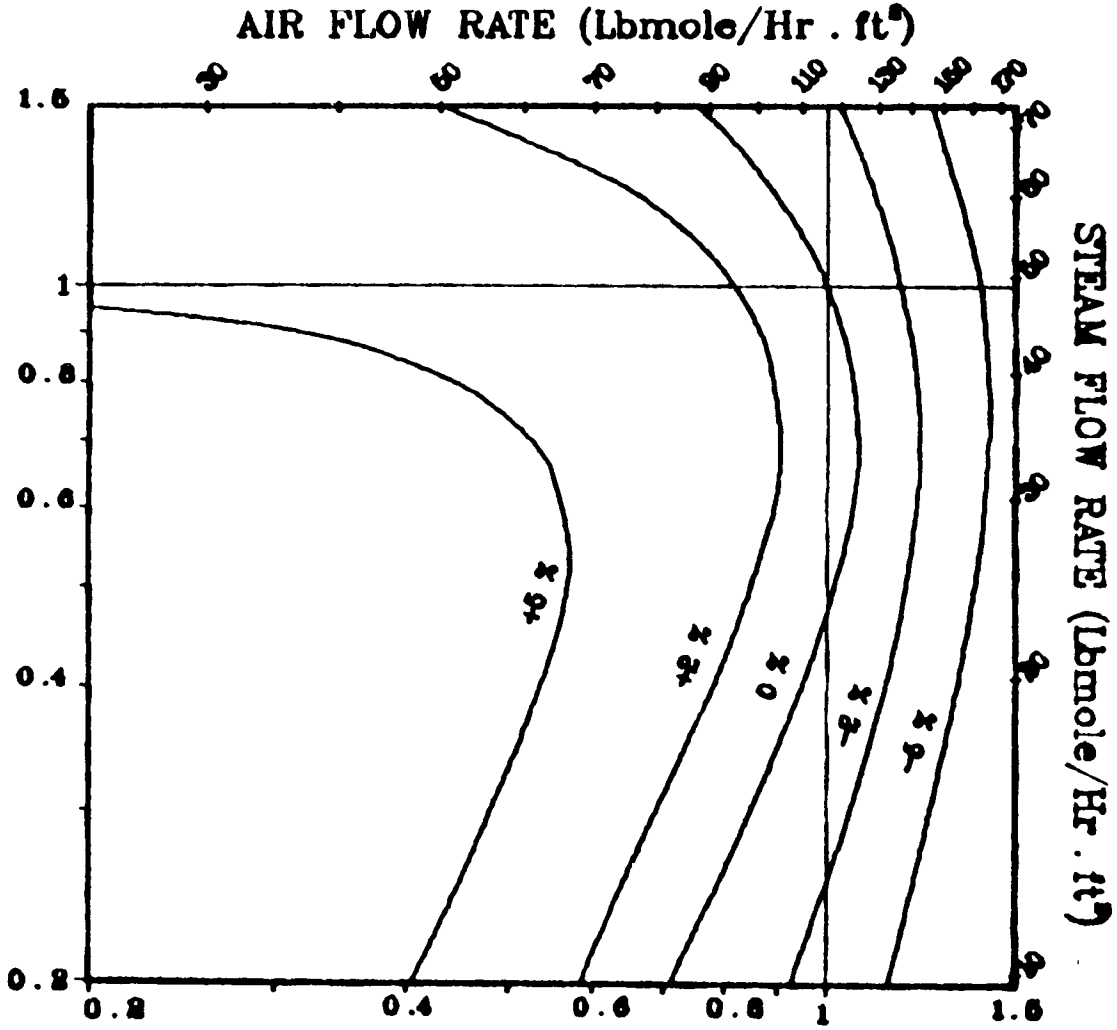

Figure 15c: ISO Heating Value lines of the Steady State Control Map (Constant Ash Withdrawal Rate)

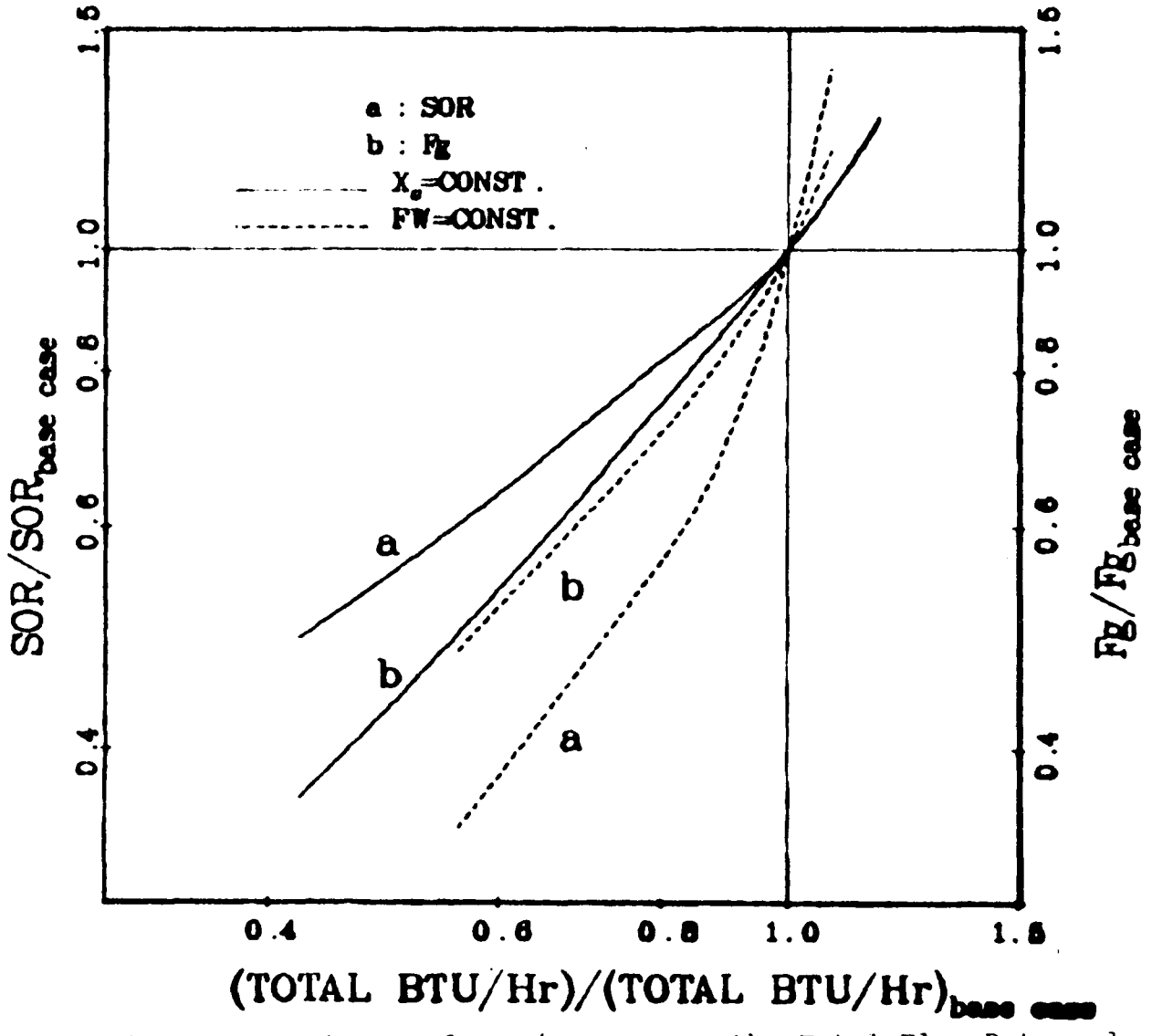

Figure 16: The Total BTU/Hr. versus the Total Flow Rate and the Steam/Air Ratio Along the Isotherm $\Delta T = 0$ of Figures 14a, 15a

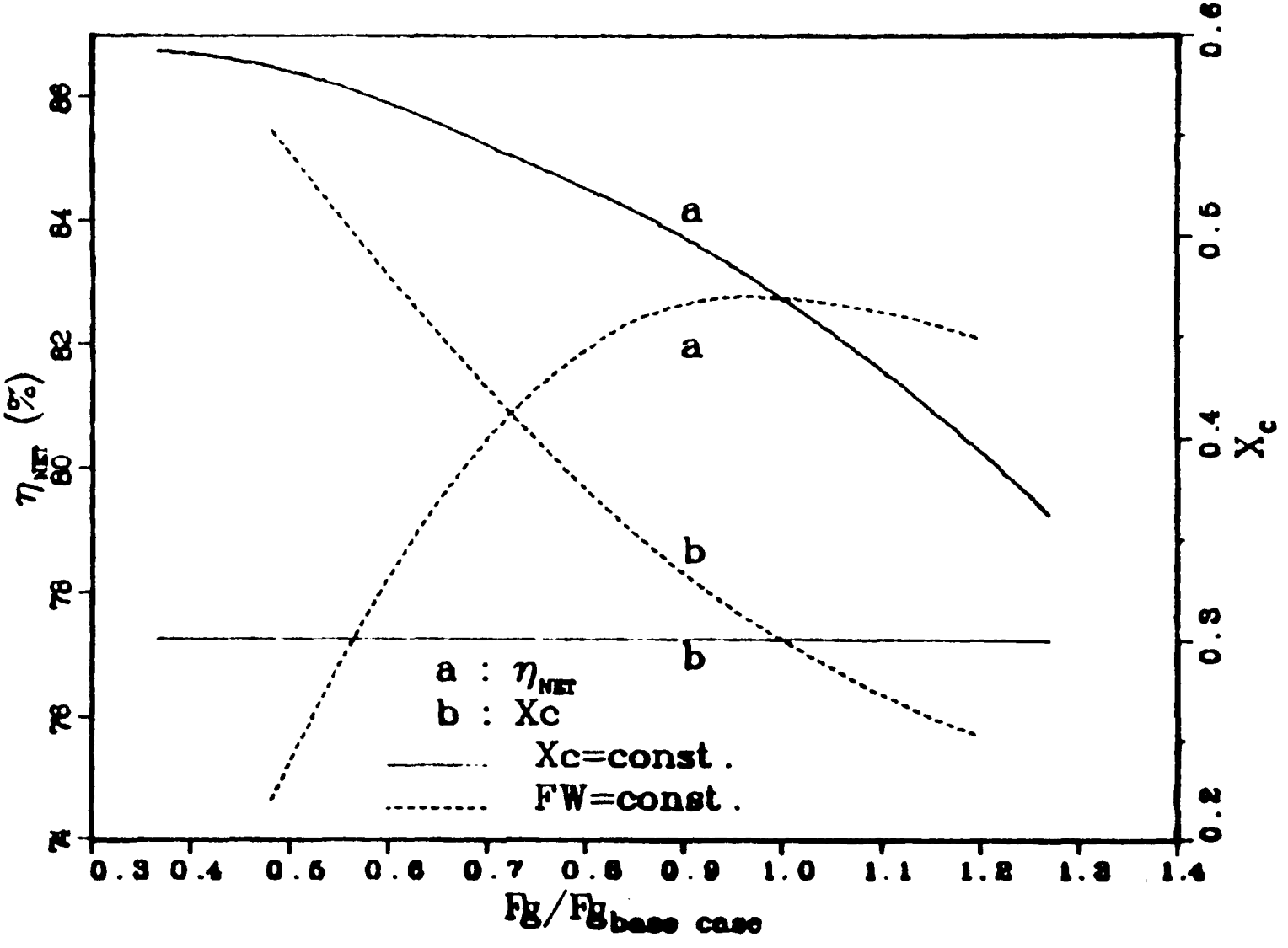

Figure 17: The Carbon Concentration and the Net Efficiency versus the Total Flow Rate Along the Isotherm $\Delta T = 0$ of Figures 14a, 15a

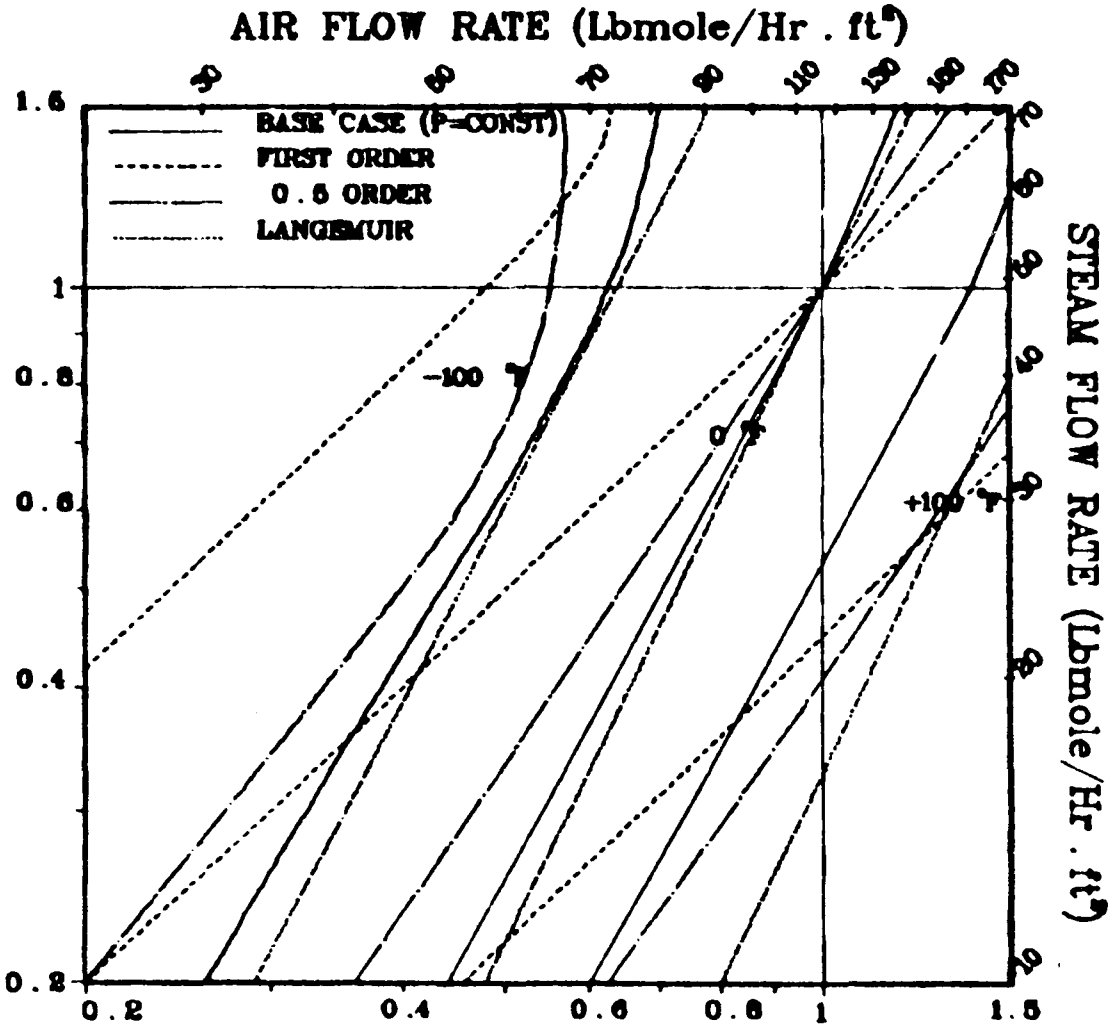

Figure 18: Isotherms of the Steady State Map. Different Pressure Dependencies (Constant X_c)

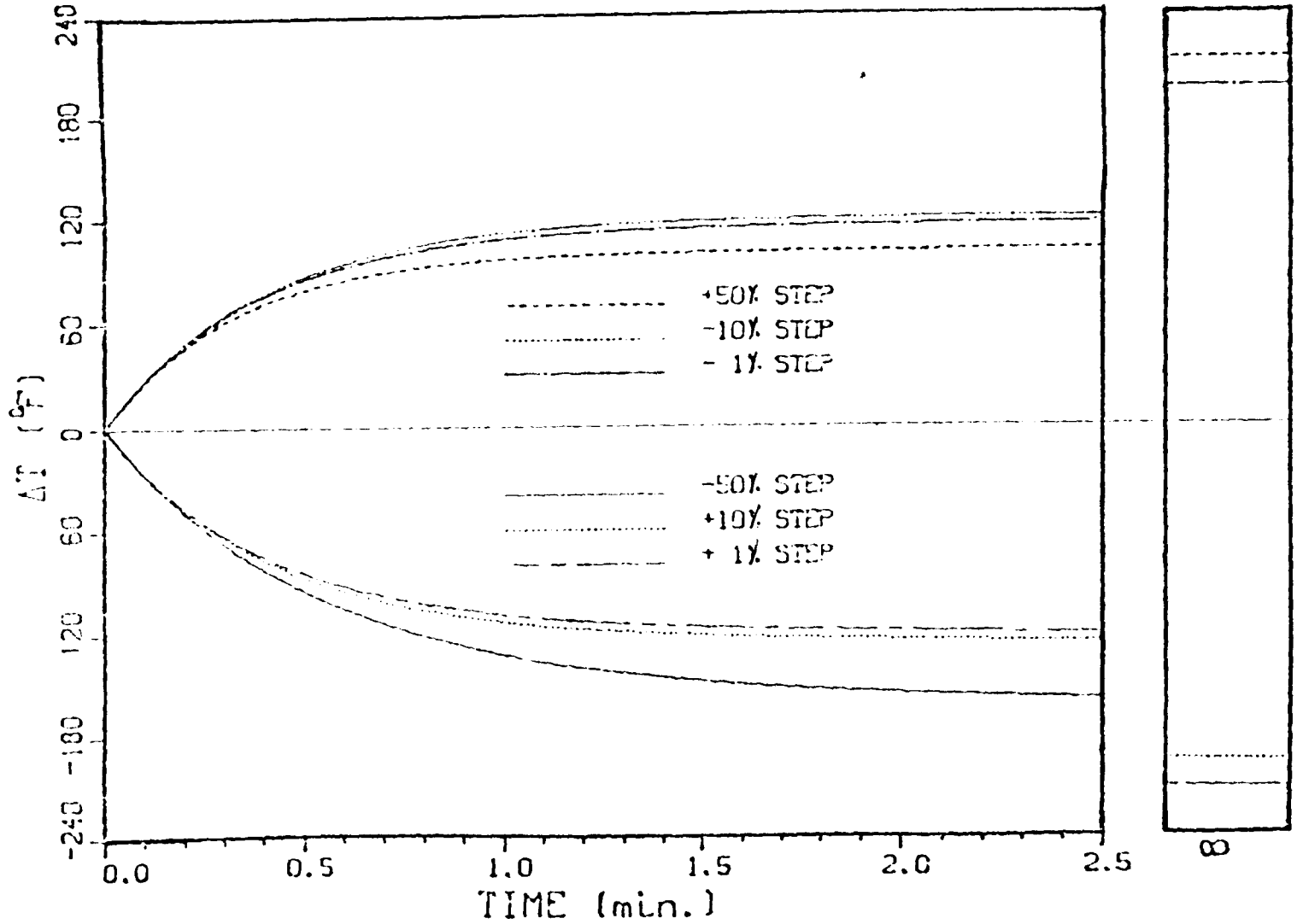

Figure 19a: Open Loop Response of the Temperature to Step Inputs in the Air Flow Rate

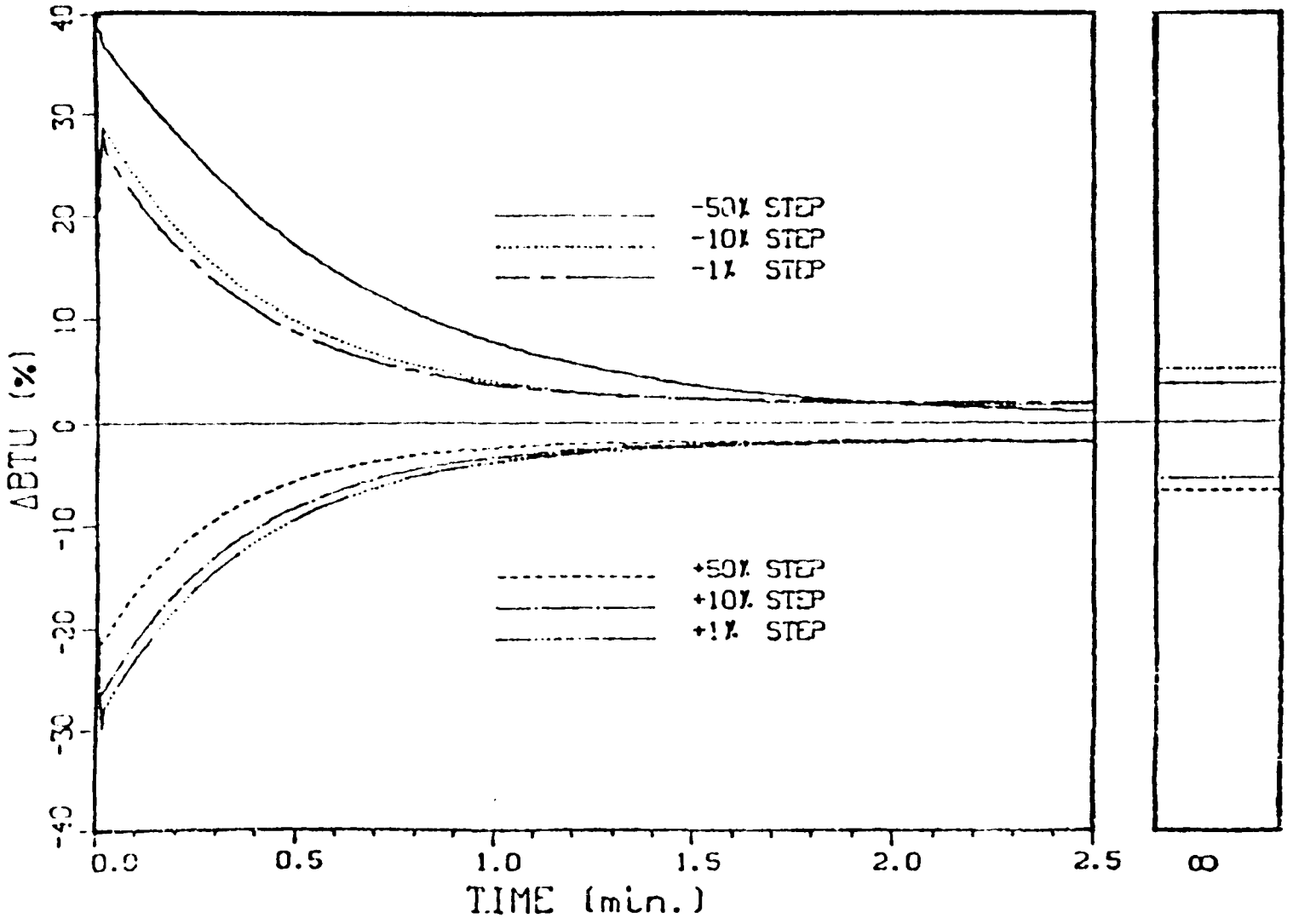

Figure 19b: Open Loop Response of the Heating Value to Step Inputs in the Air Flow Rate

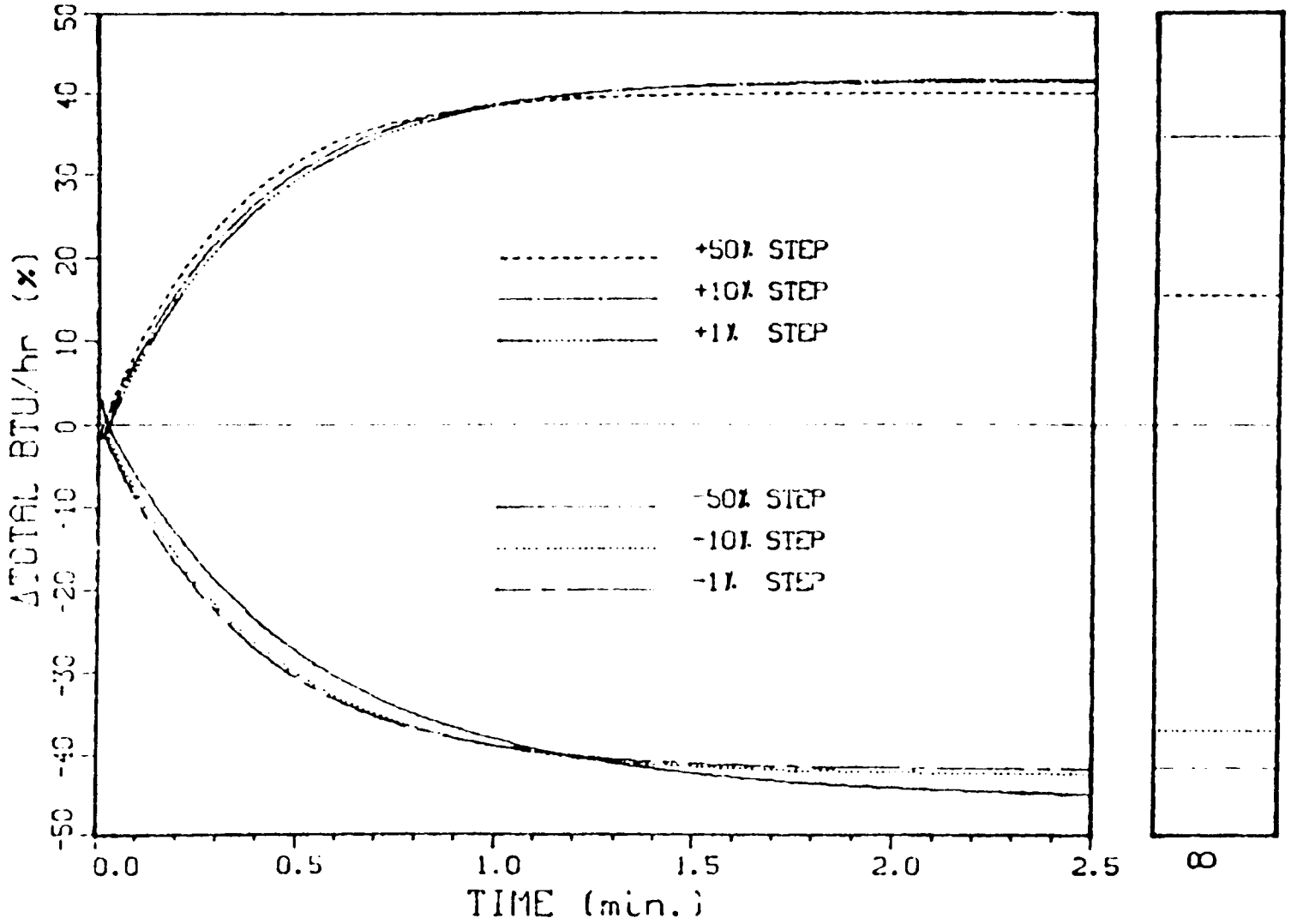

Figure 19c: Open Loop Response of the Total BTU/Hr. to Step Inputs in the Air Flow Rates

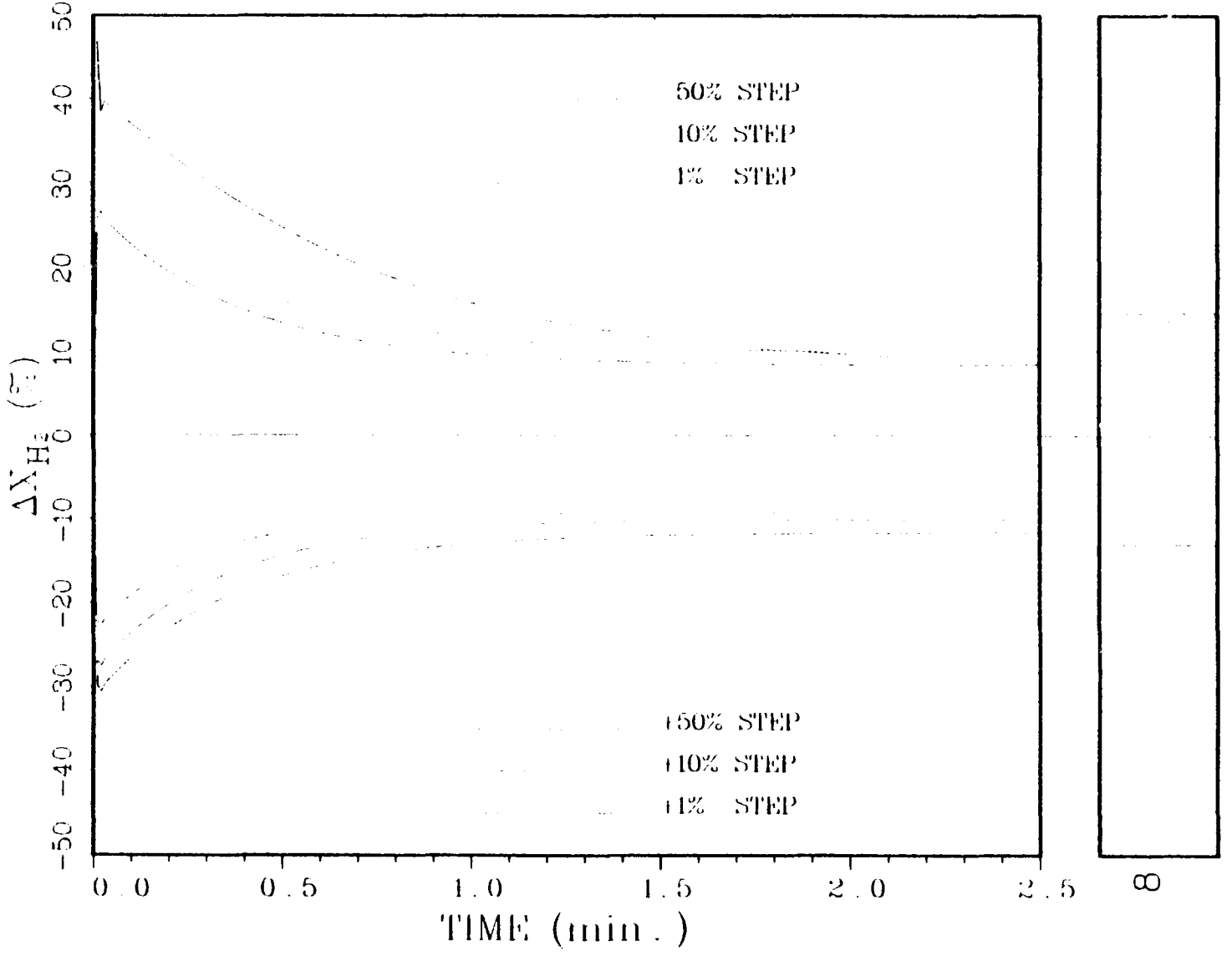

Figure 19d: Open Loop Response of the Hydrogen Content to Step Inputs in the Air Flow Rate

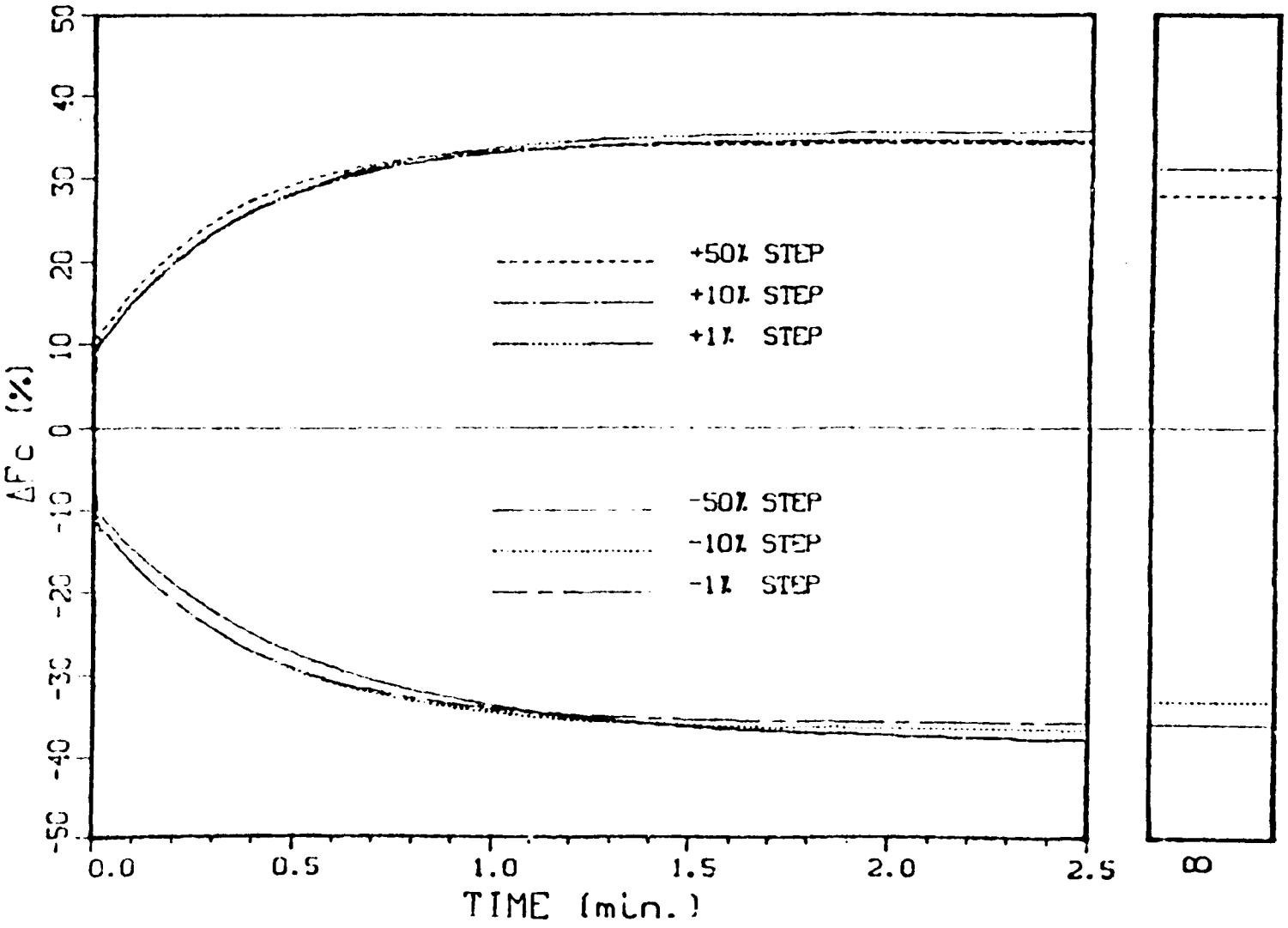

Figure 19e: Open Loop Response of the Coal Feed Rate to Step Inputs in the Air Flow Rate

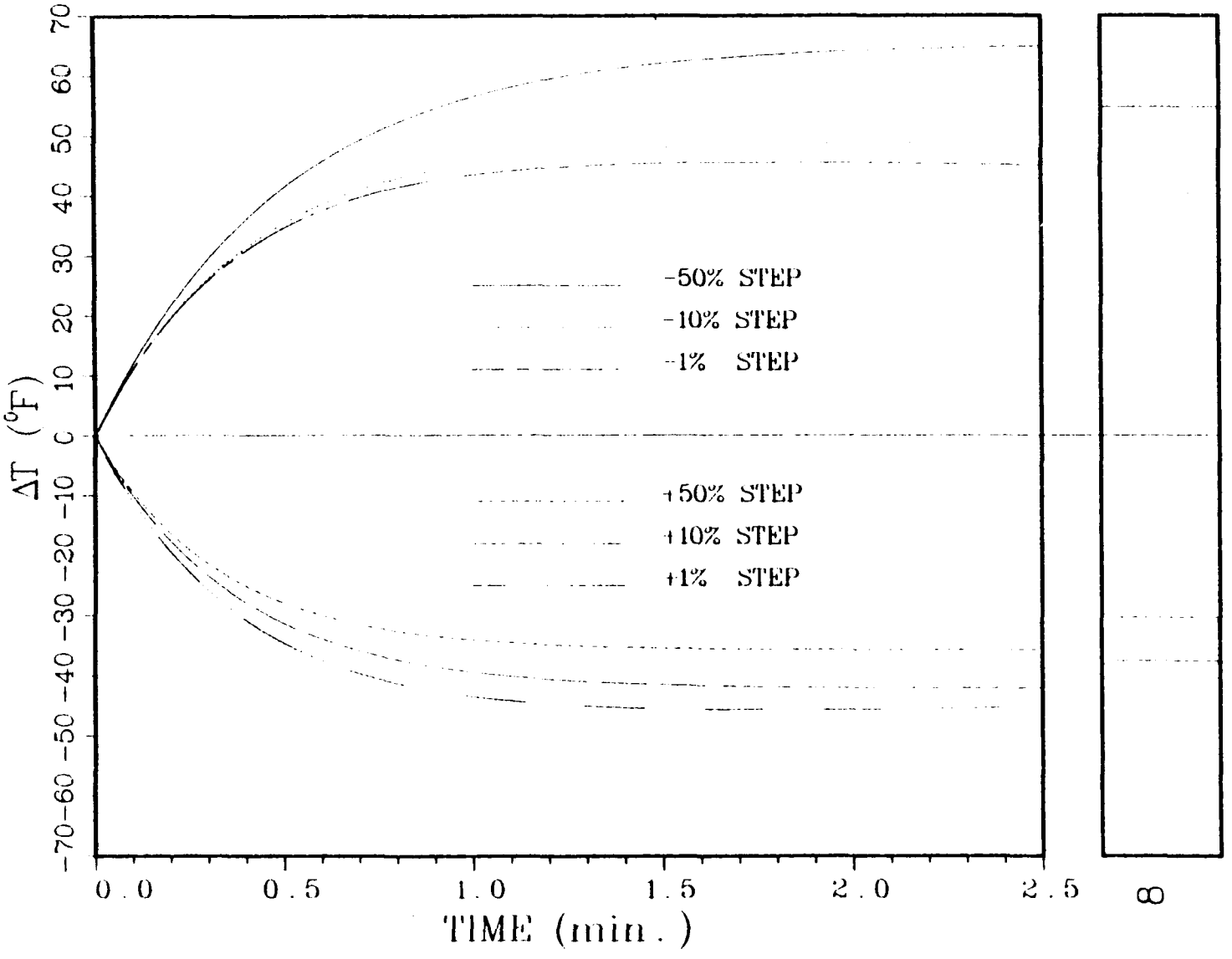

Figure 20a: Open Loop Response of the Temperature to Step Inputs in the Steam Flow Rate

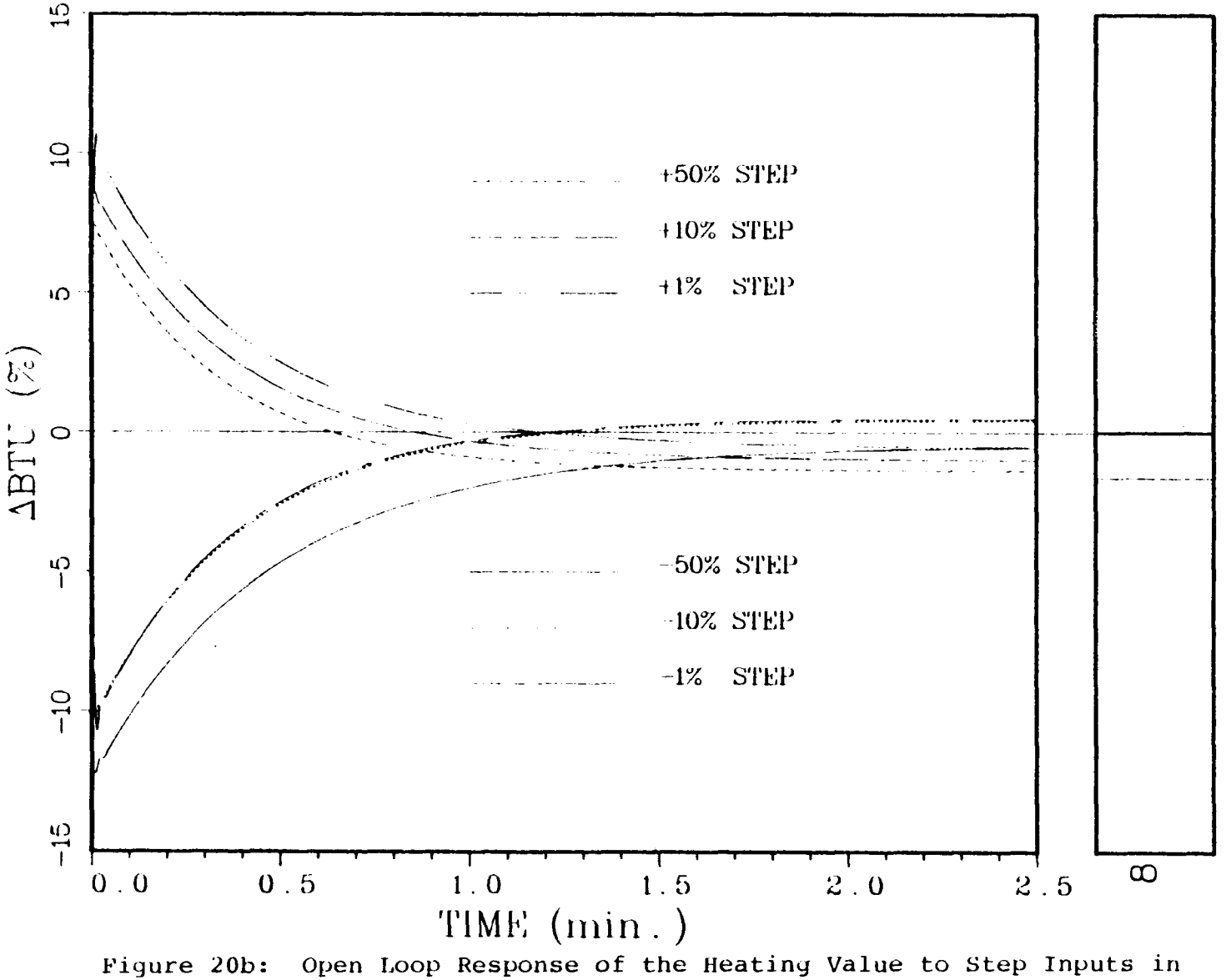

Figure 20b: Open Loop Response of the Heating Value to Step Inputs in the Steam Flow Rate

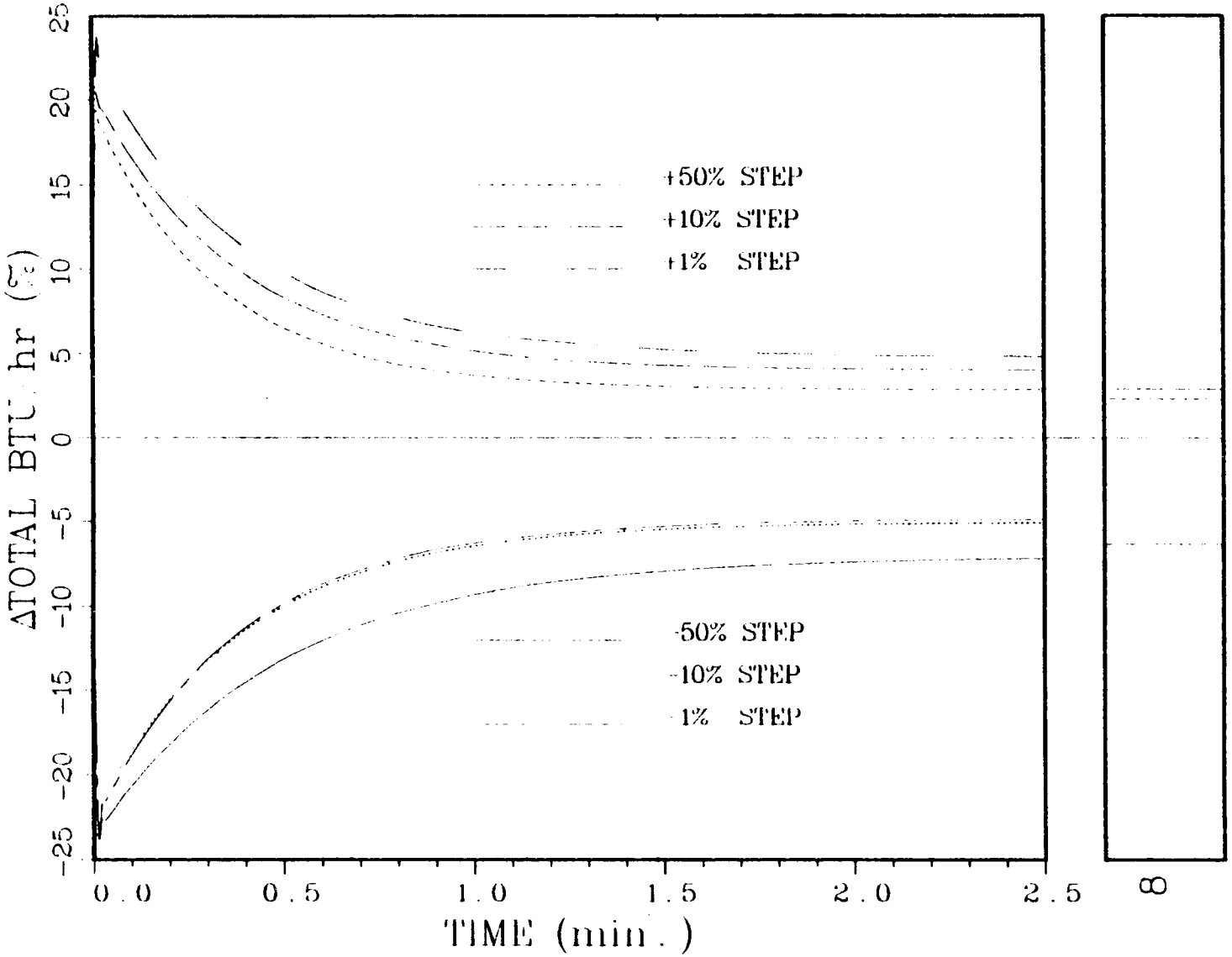

Figure 20c: Open Loop Response of the Total BTU/Hr. to Step Inputs in the Steam Flow Rate

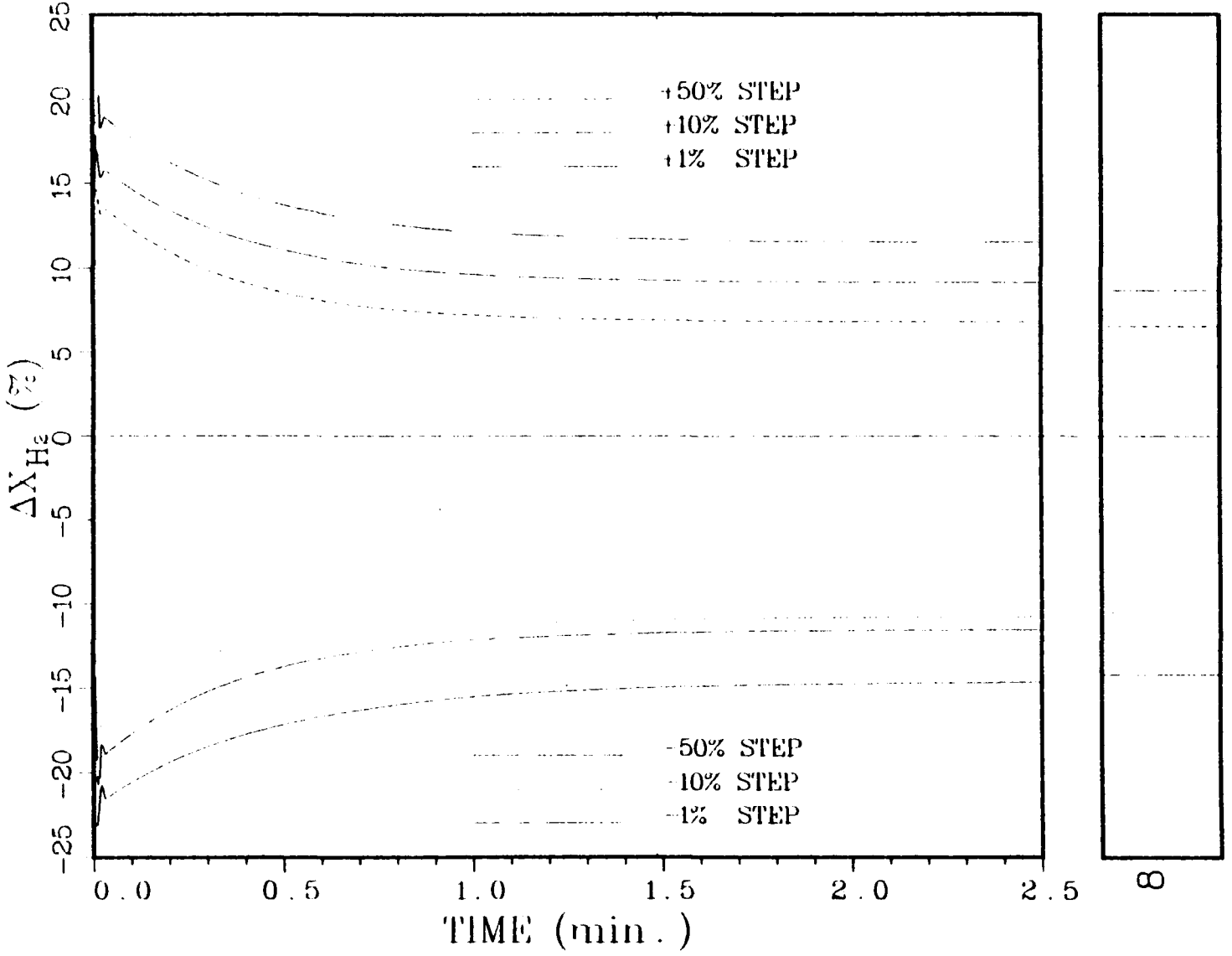

Figure 20d: Open Loop Response of the Hydrogen Content to Step Inputs in the Steam Flow Rate

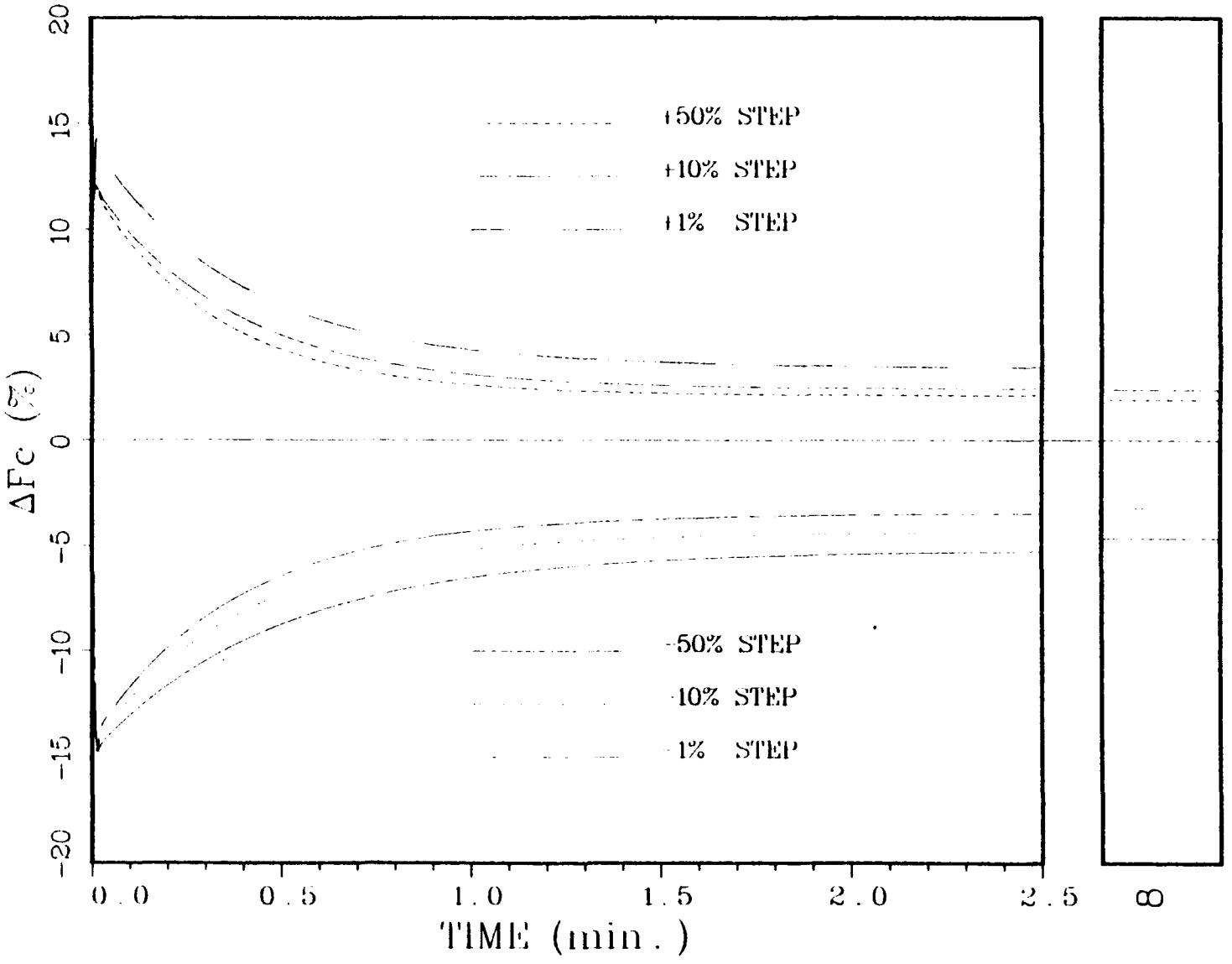

Figure 20e: Open Loop Response of the Coal Feed Rate to Step Inputs in the Steam Flow Rate

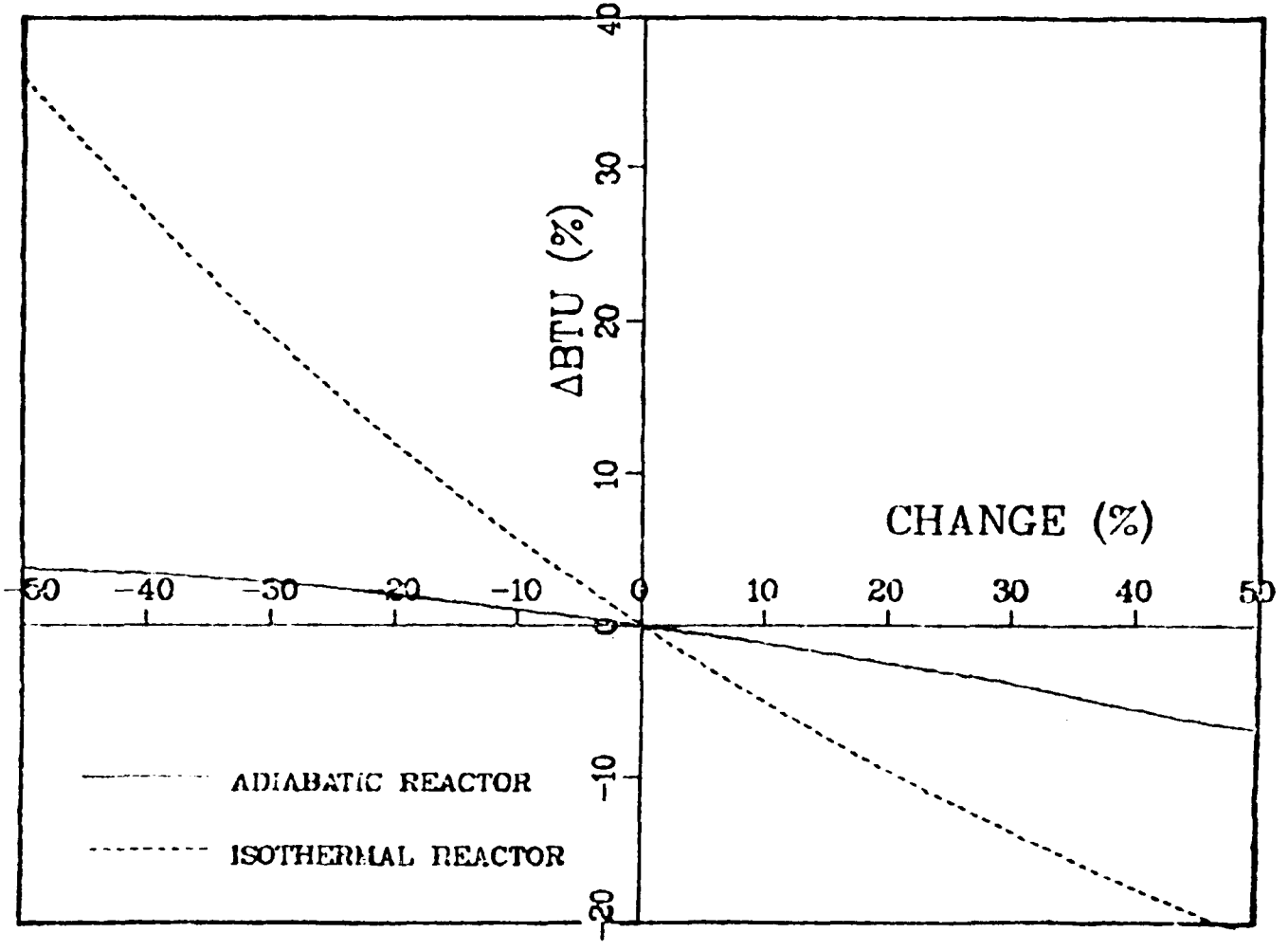

Figure 21: Final Steady States Curves Following Changes in the Air Flow Rate. Isothermal versus Adiabatic Reactors

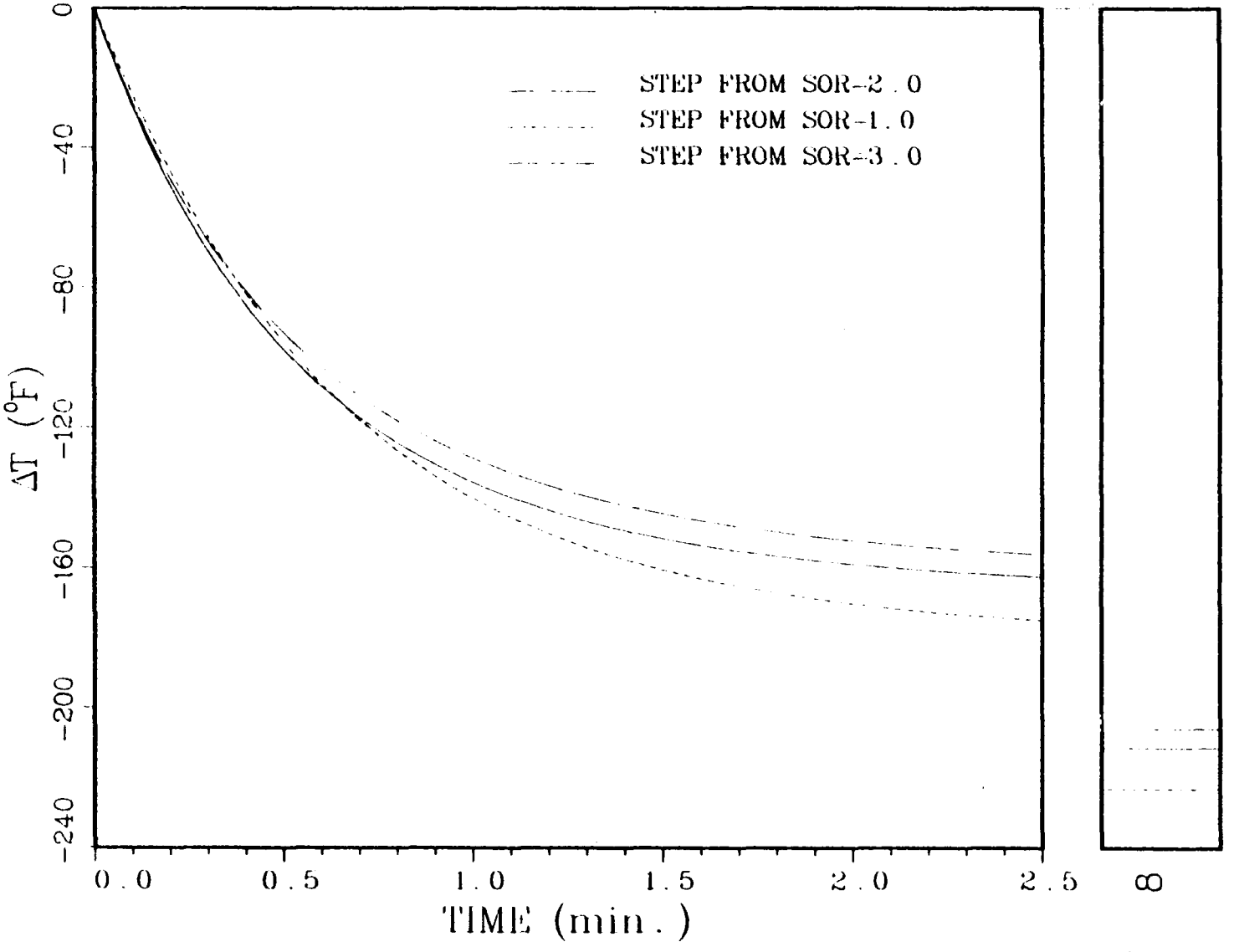

Figure 22a: Open Loop Response of the Temperature to Step Inputs in the Air Flow Rate from Different Initial Steady States.

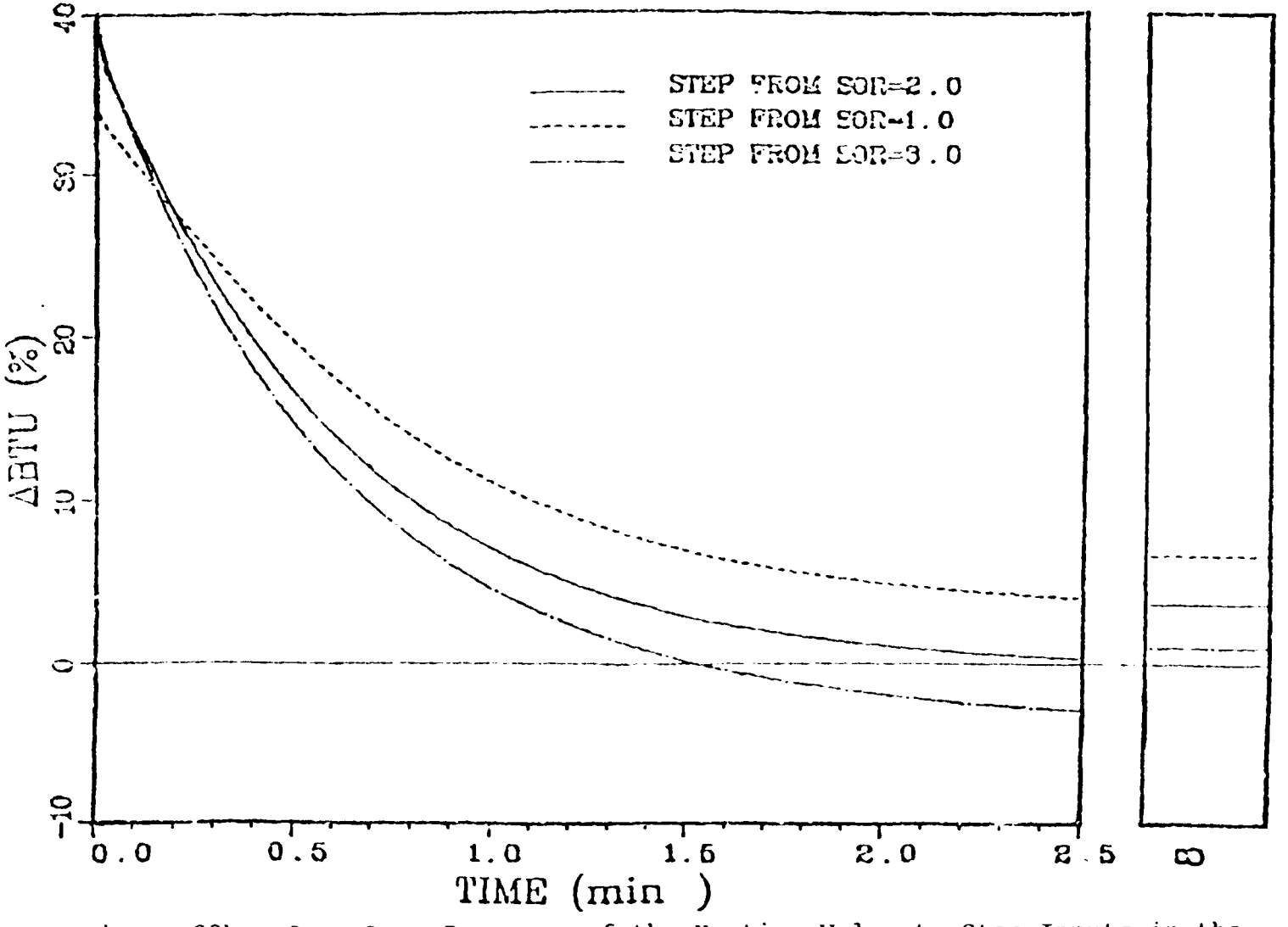

Figure 22b: Open Loop Response of the Heating Value to Step Inputs in the Air Flow Rate from Different Initial Steady States

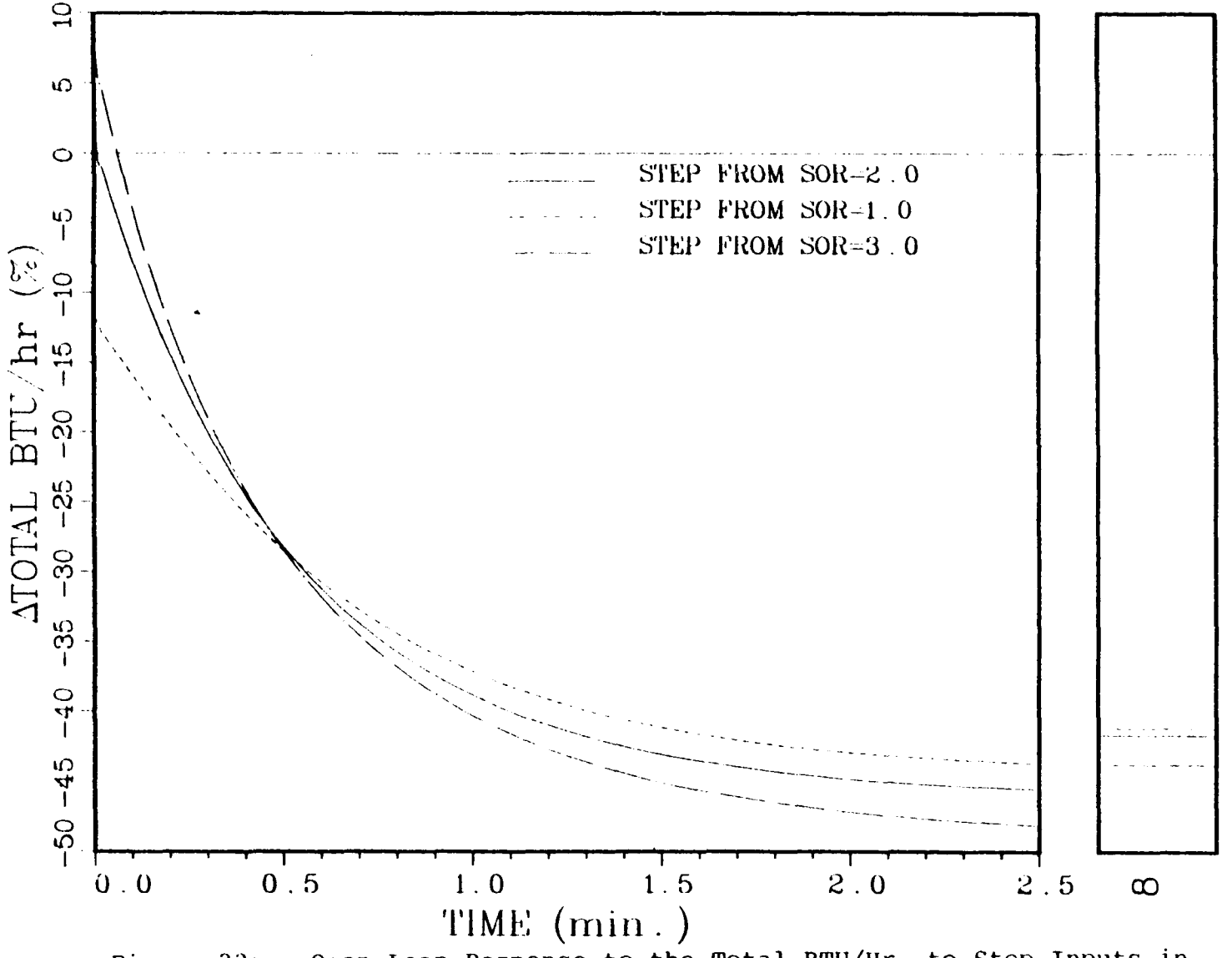

Figure 22c: Open Loop Response to the Total BTU/Hr. to Step Inputs in the Air Flow Rate from Different Initial Steady States

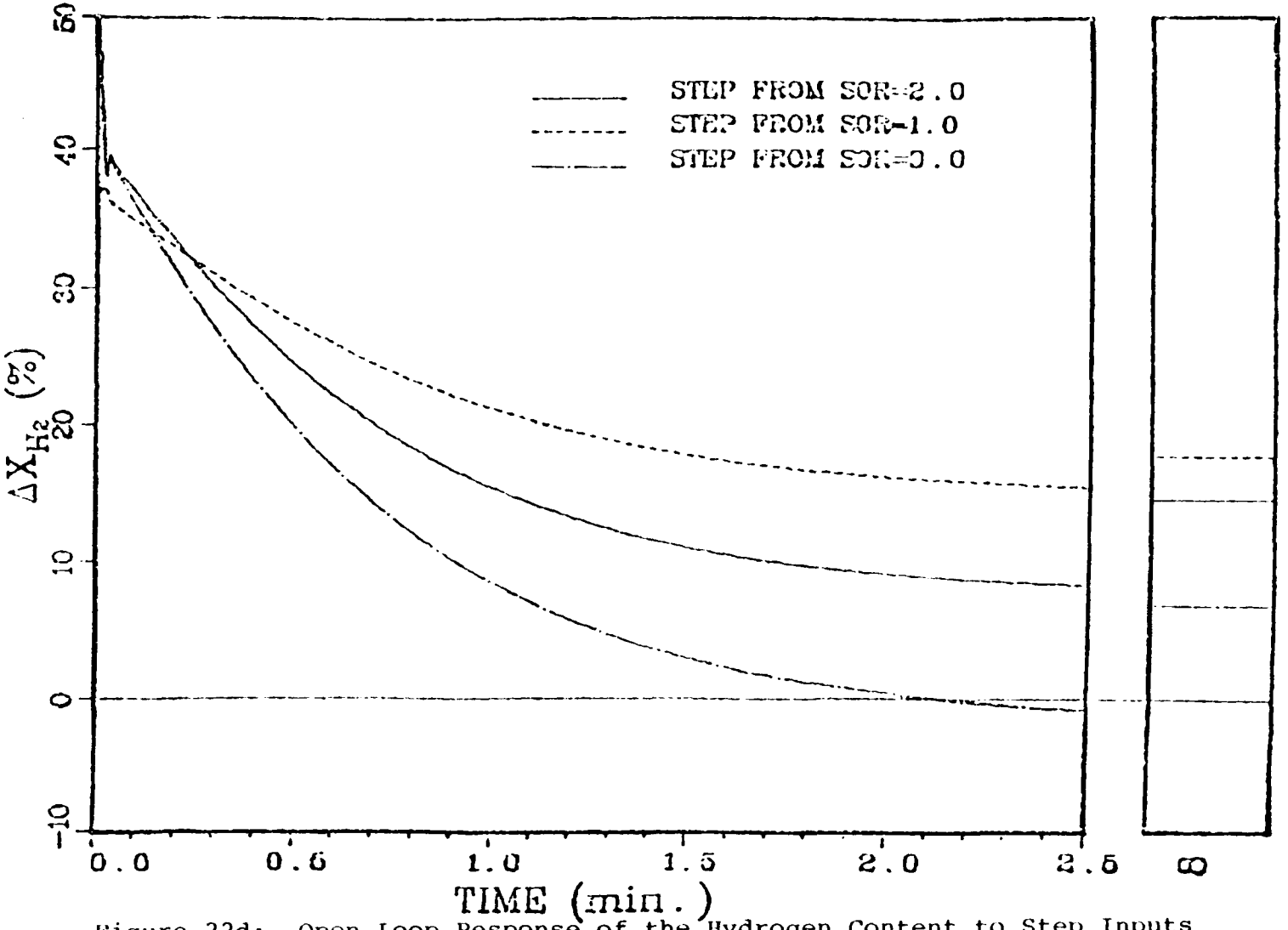

Figure 22d: Open Loop Response of the Hydrogen Content to Step Inputs in the Air Flow Rate from Different Initial Steady States

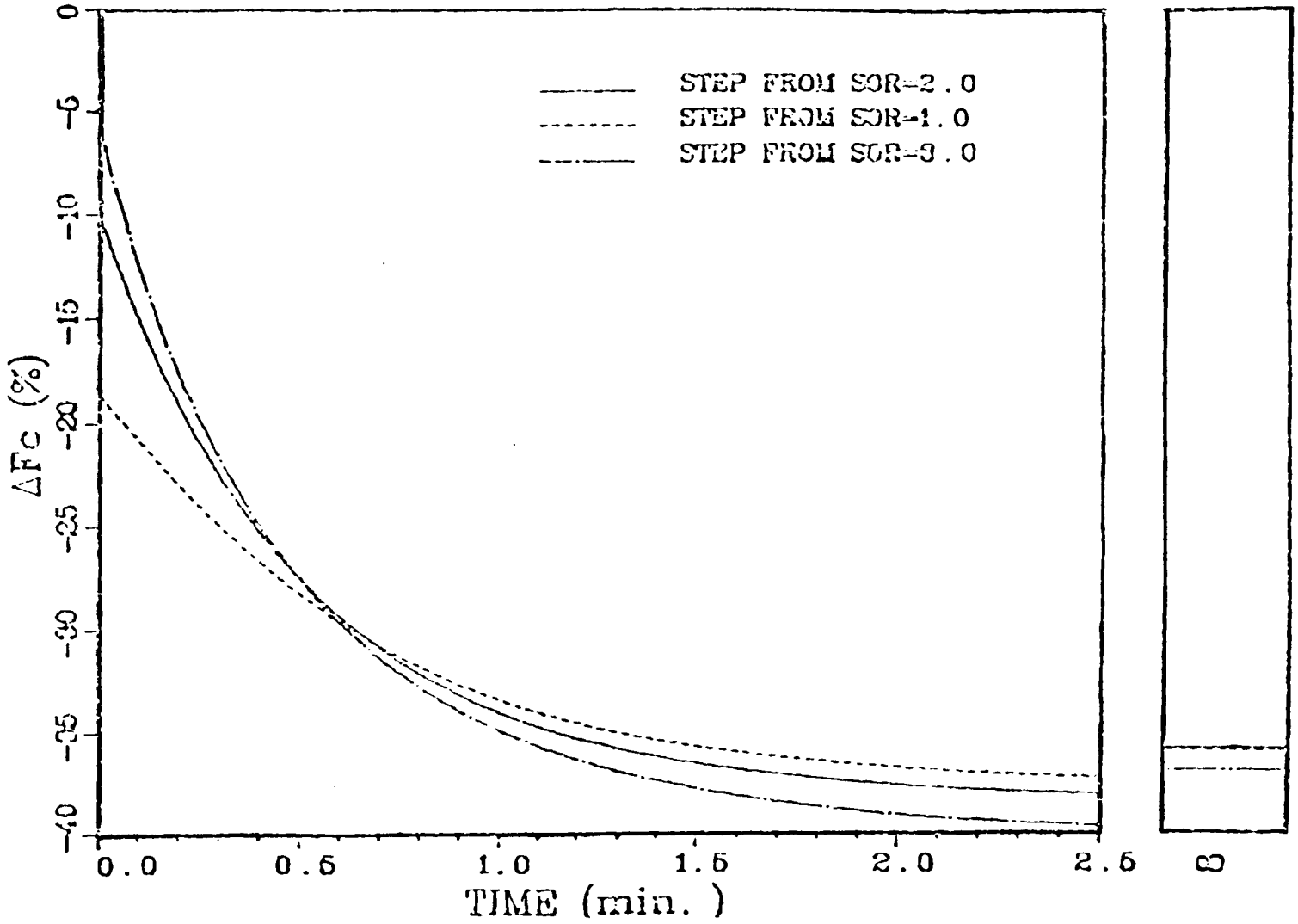

Figure 22e: Open Loop Response of the Coal Feed Rate to Step Inputs in the Air Flow Rate from Different Initial Steady States

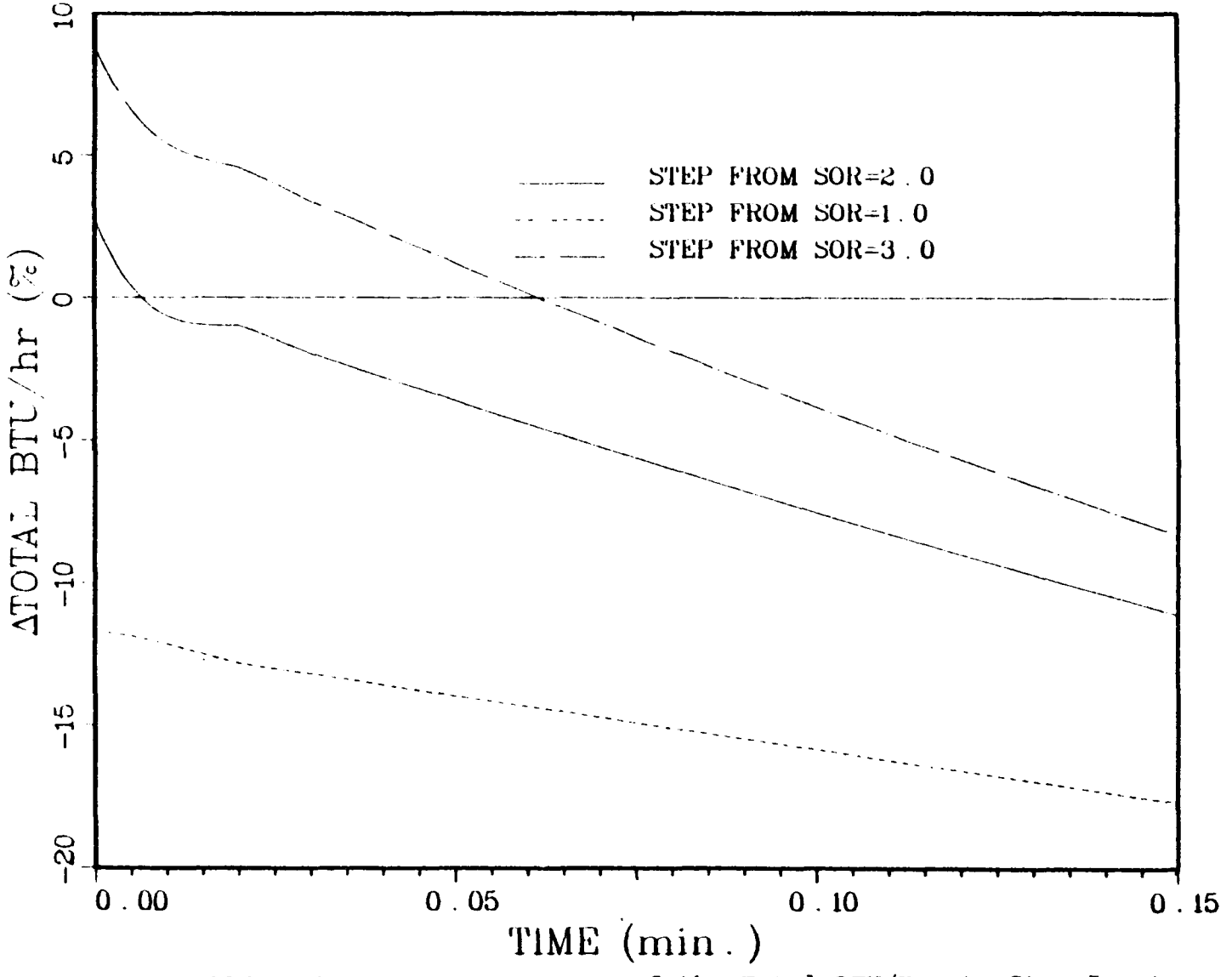

Figure 22f: The Inverse Response of the Total BTU/Hr. to Step Inputs in the Air Flow Rate (Magnified from Figure 22c)

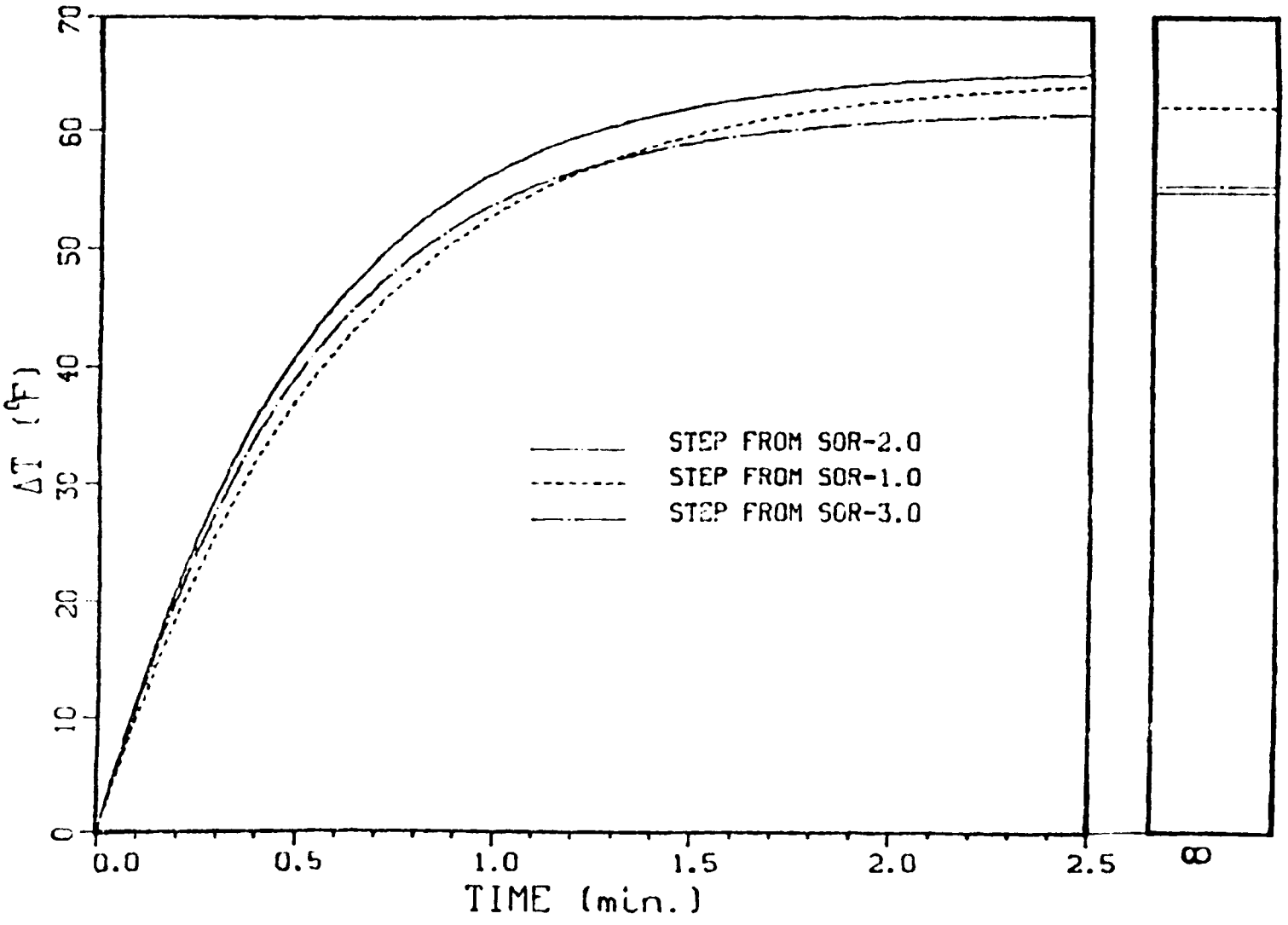

Figure 23a: Open Loop Response of the Temperature to Step Inputs in the Steam Flow Rate from Different Initial Steady States

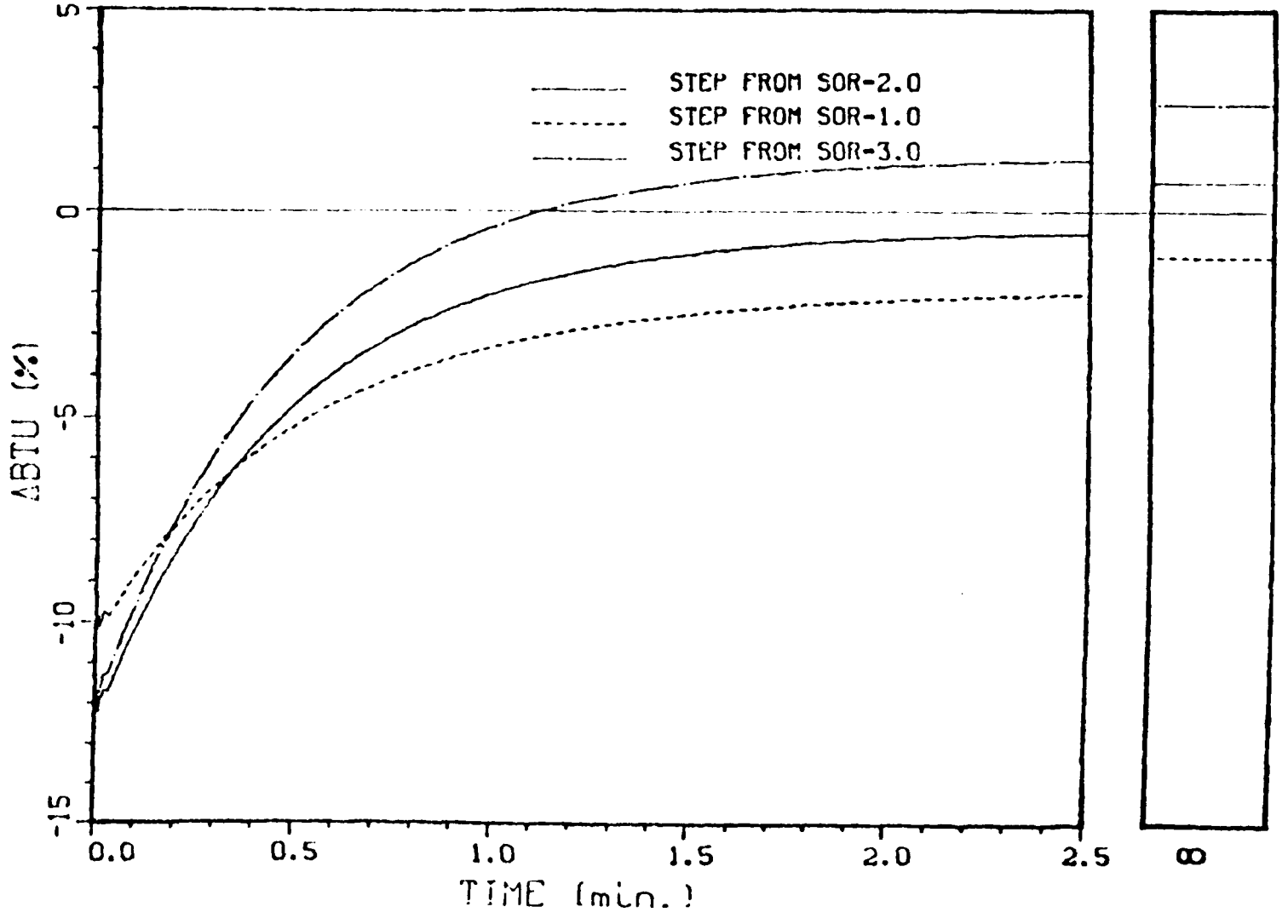

Figure 23b: Open Loop Response of the Heating Value to Step Inputs in the Steam Flow Rate from Different Initial Steady States

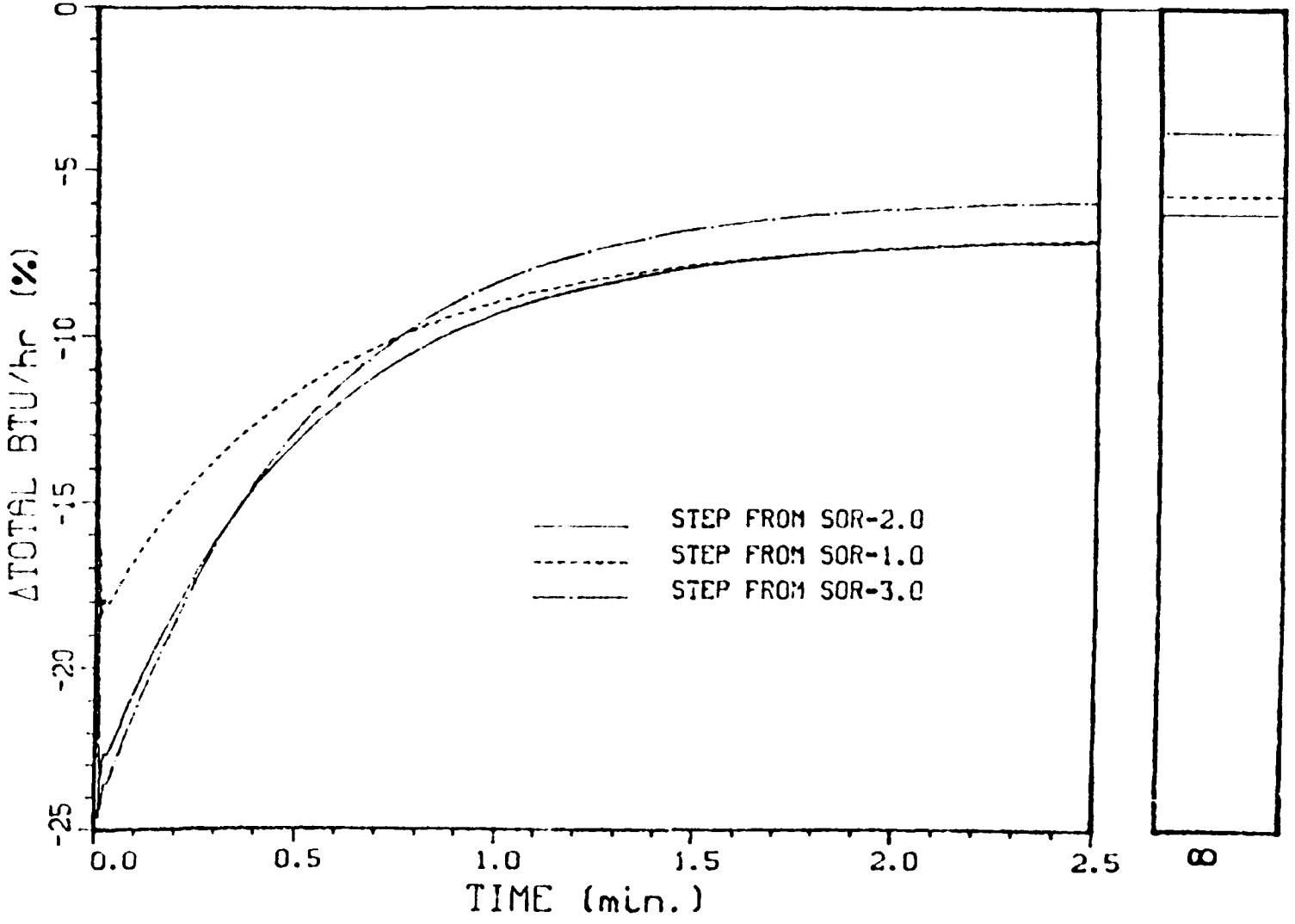

Figure 23c: Open Loop Response of the Total BTU/Hr. to Step Inputs in the Steam Flow Rate from Different Initial Steady States

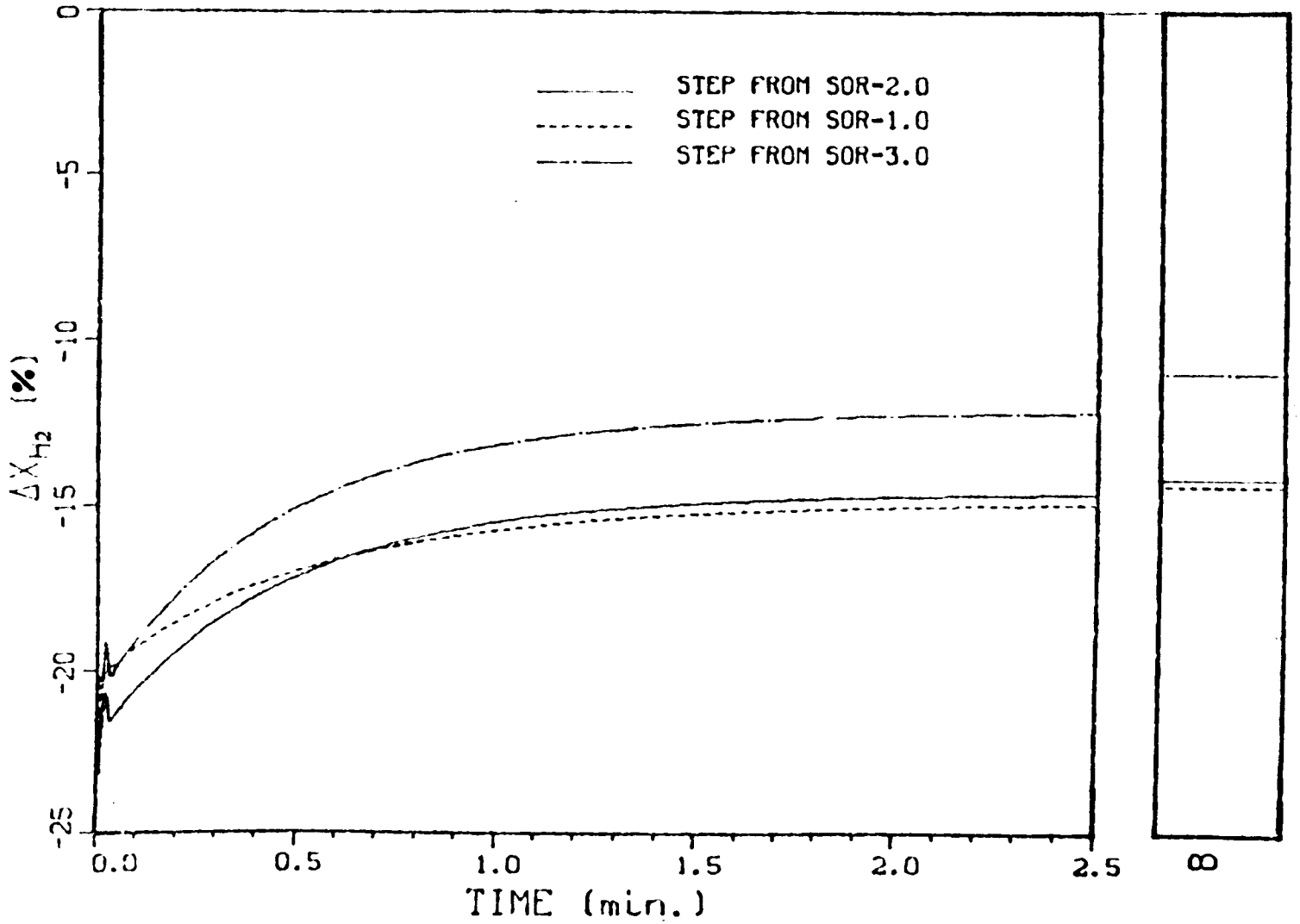

Figure 23d: Open Loop Response of the Hydrogen Content to Step Inputs in the Steam Flow Rate from Different Initial Steady States

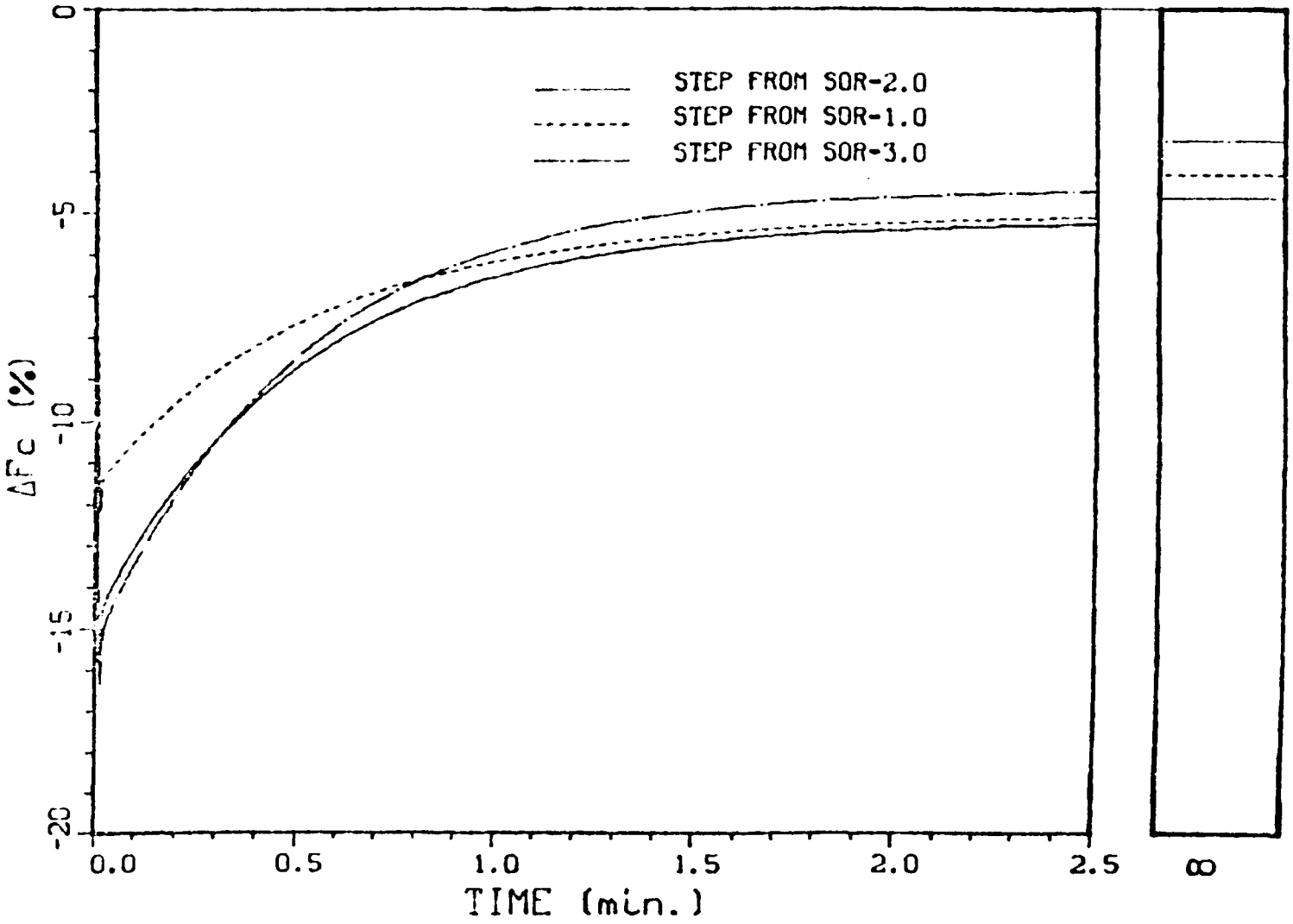

Figure 23e: Open Loop Response of the Coal Feed Rate to Step Inputs in the Steam Flow Rate from Different Initial Steady States

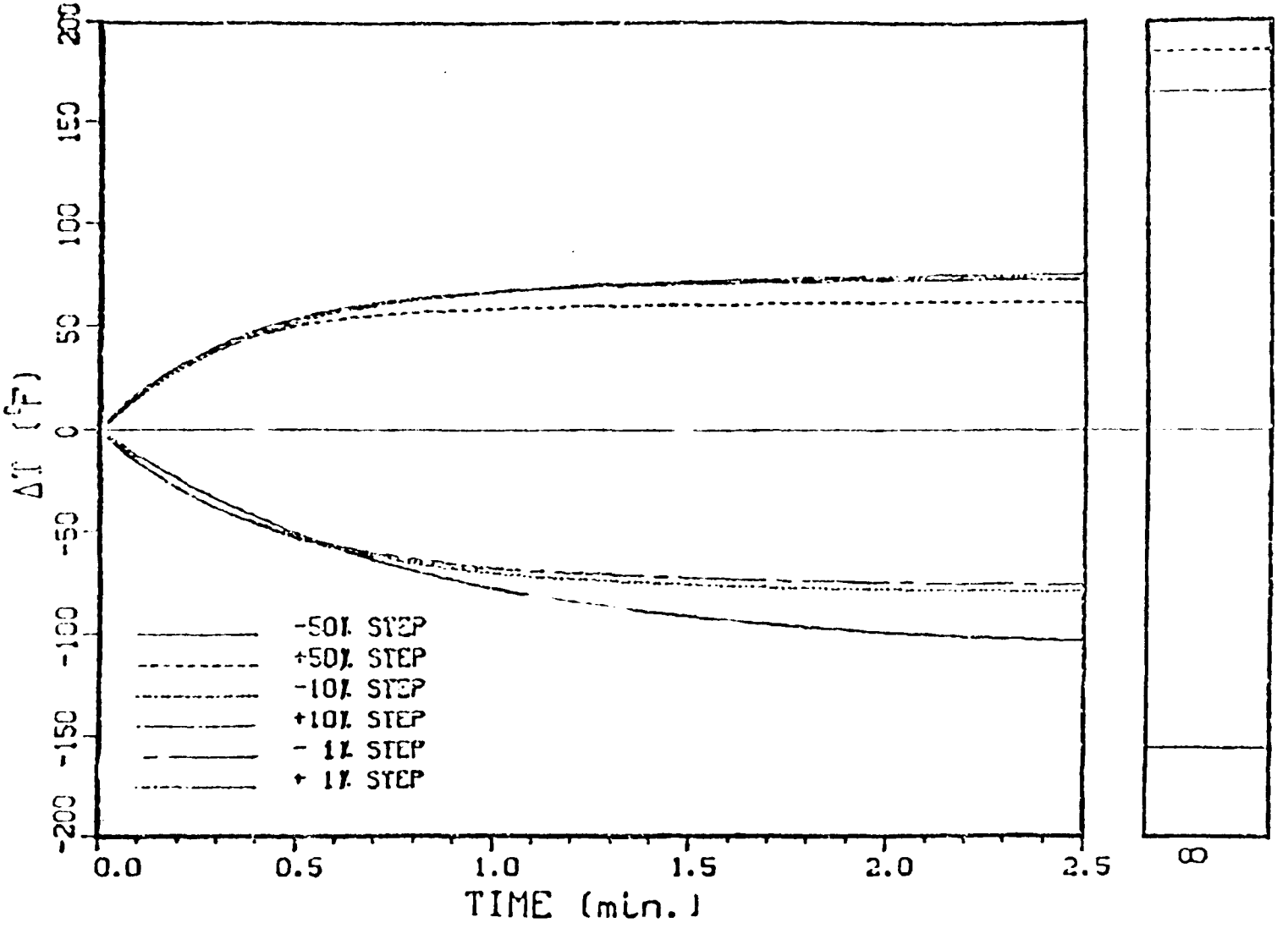

Figure 24a: Open Loop Response of the Temperature to Step Inputs in the Total Flow Rate

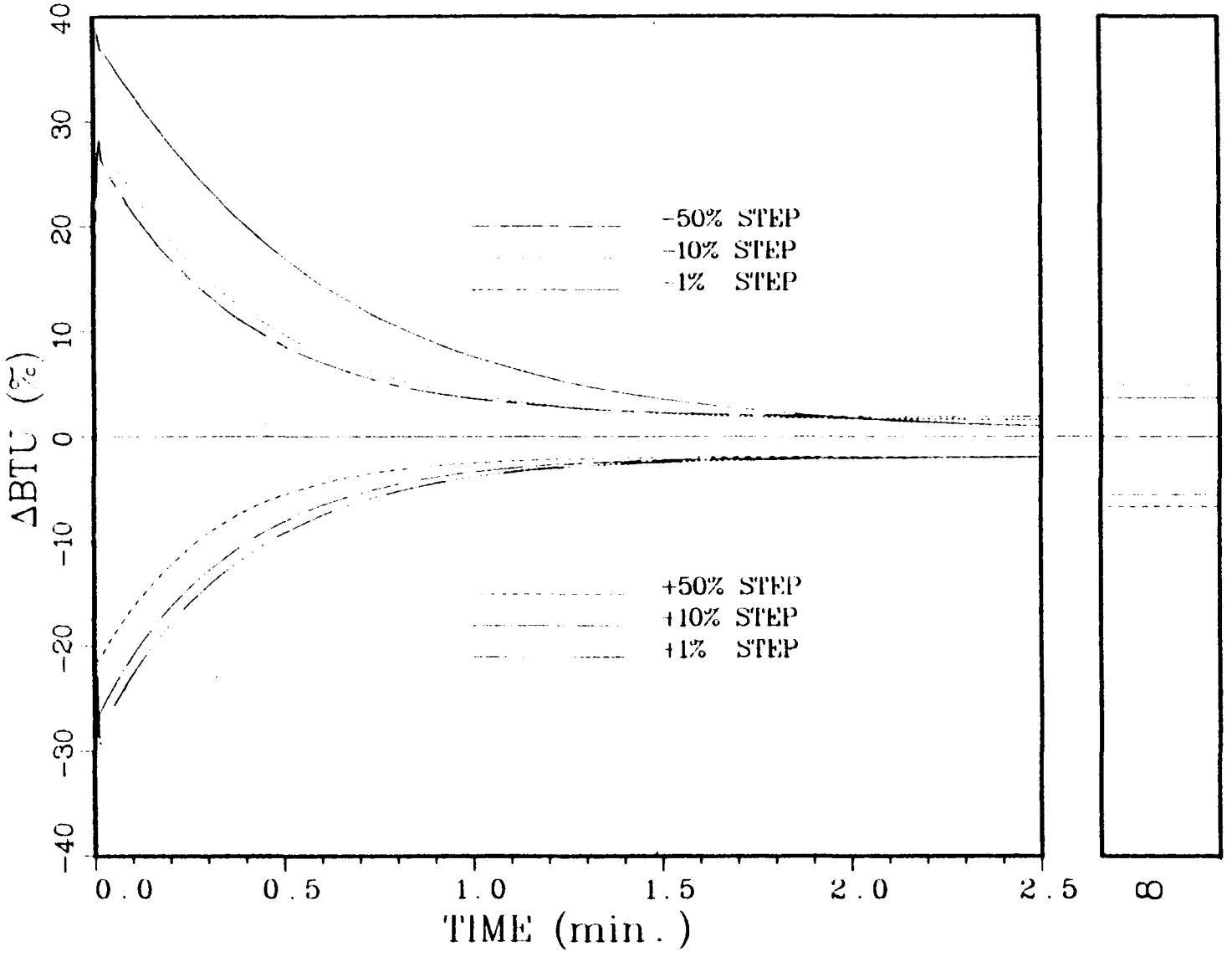

Figure 24b: Open Loop Response of the Heating Value to Step Inputs in the Total Flow Rate

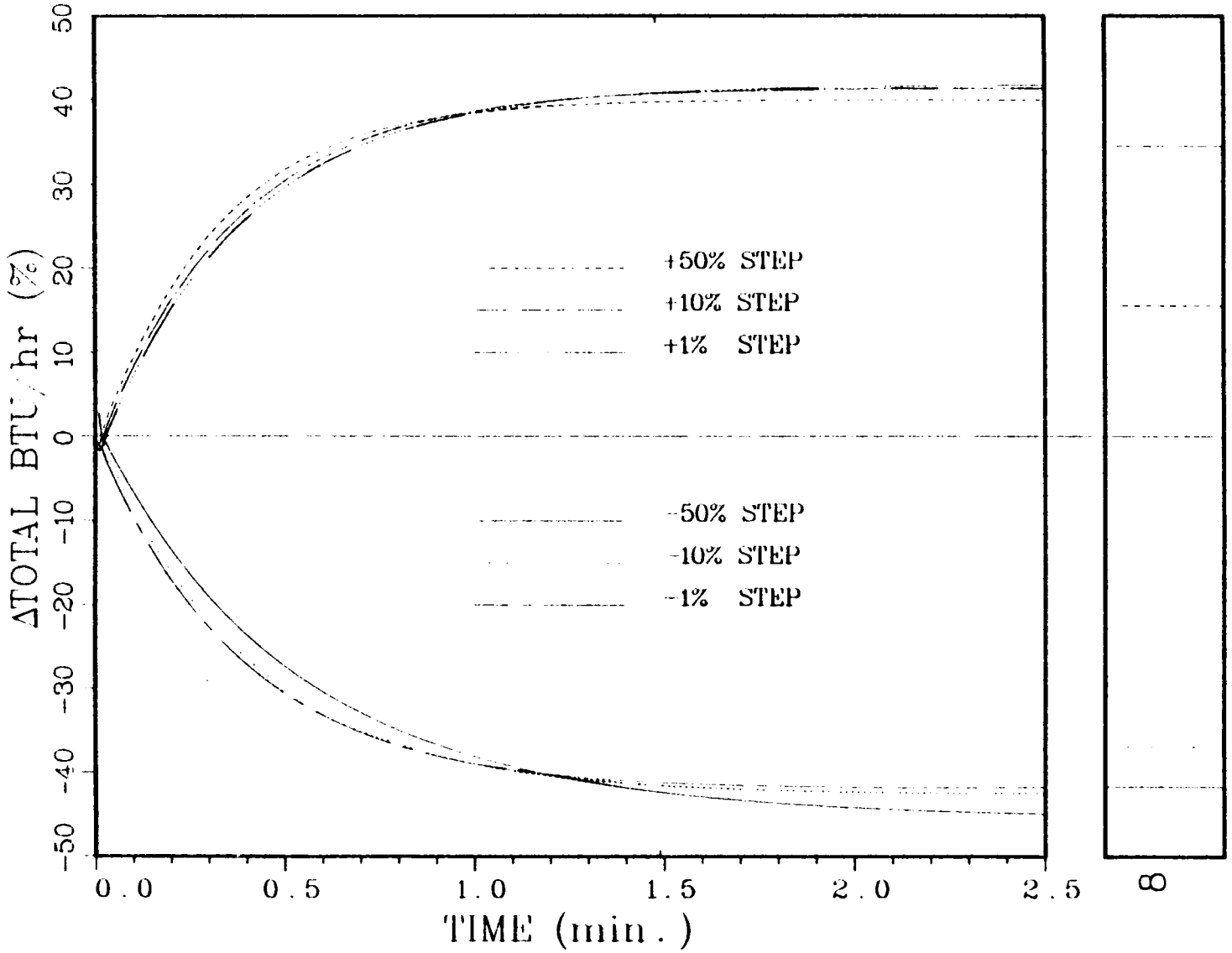

Figure 24c: Open Loop Response of the Total BTU/Hr. to Step Inputs in the Total Flow Rate

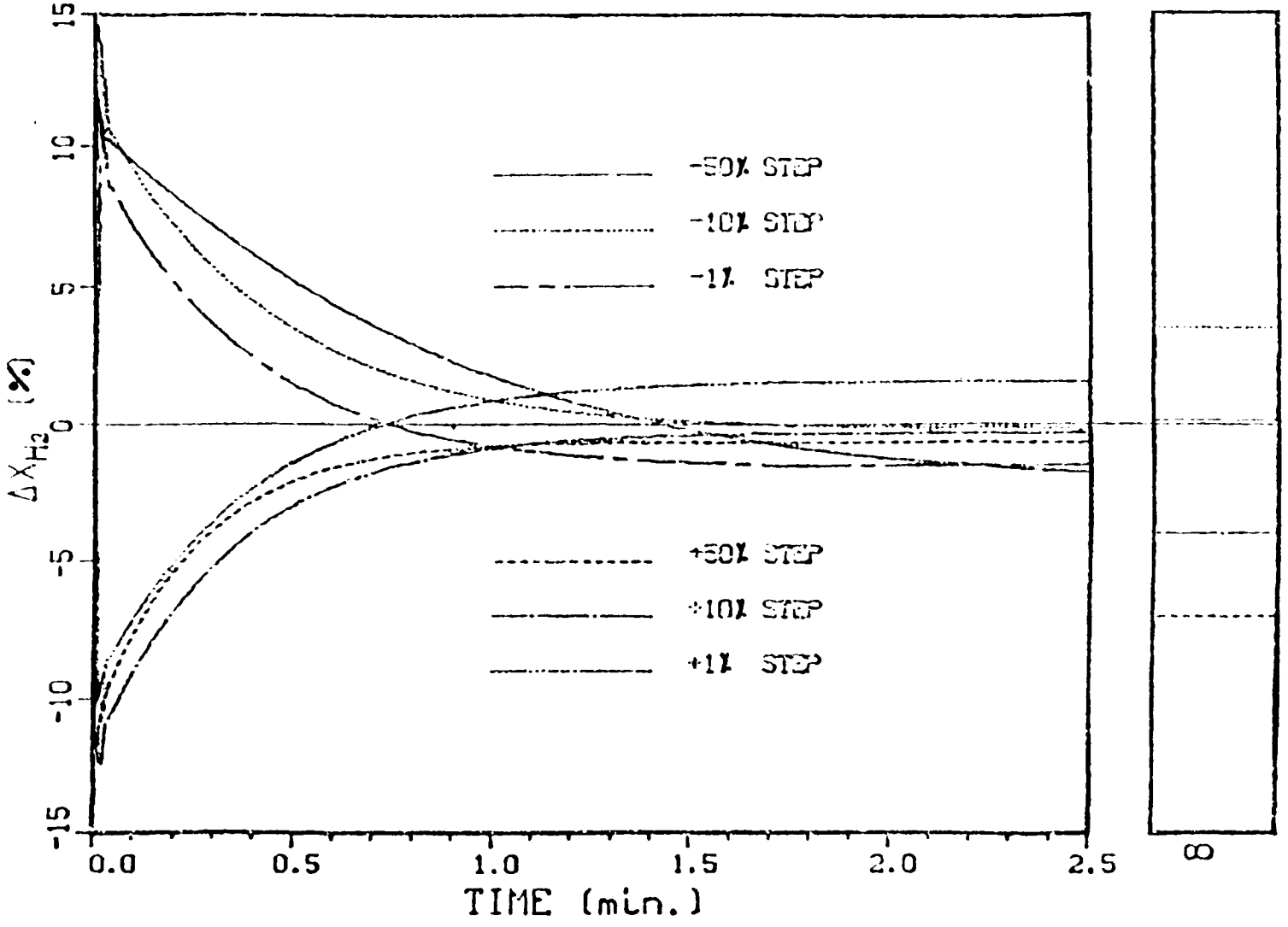

Figure 24d: Open Loop Response of the Hydrogen Content to Step Inputs in the Total Flow Rate

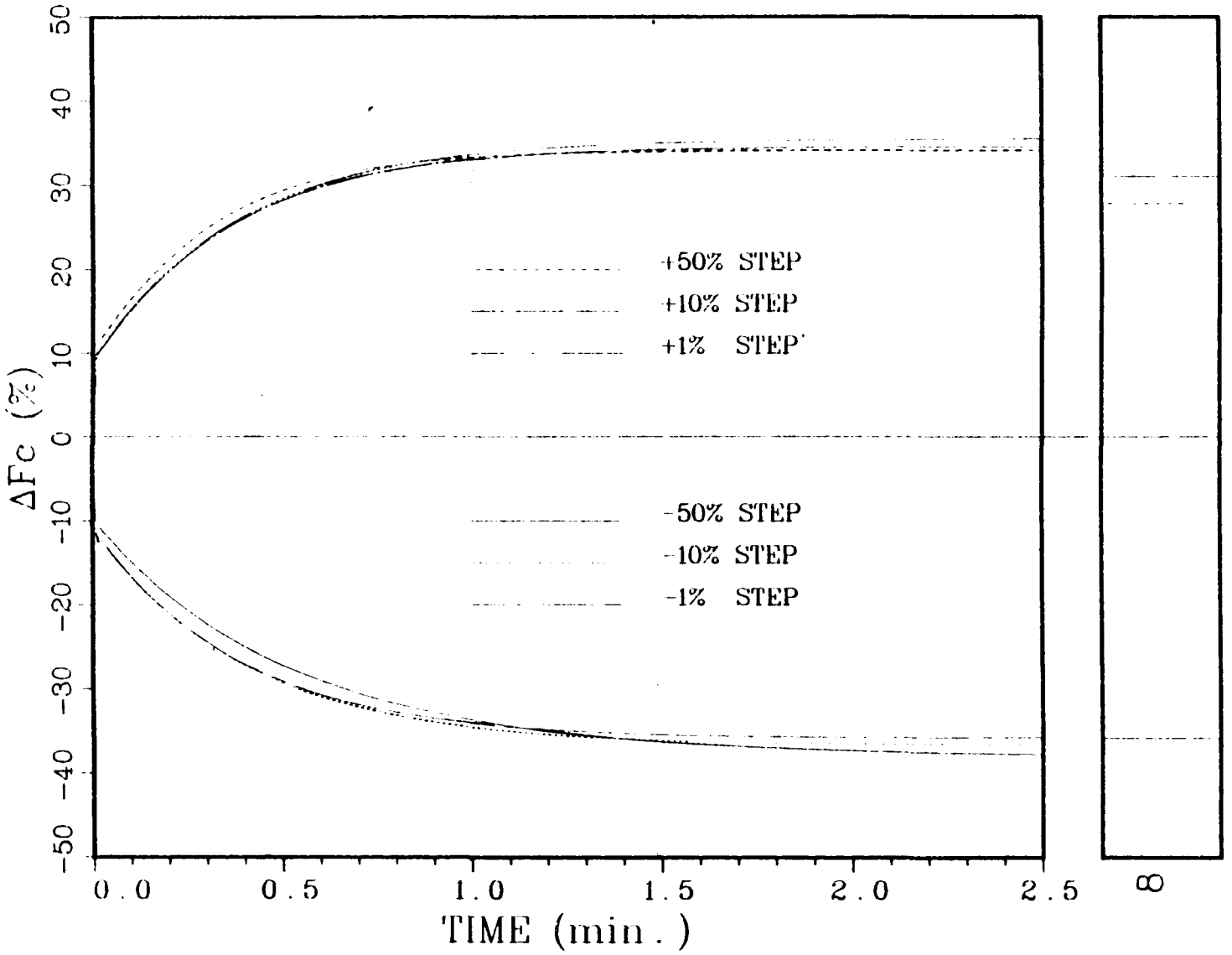

Figure 24e: Open Loop Response of the Coal Feed Rate to Step Inputs in the Total Flow Rate

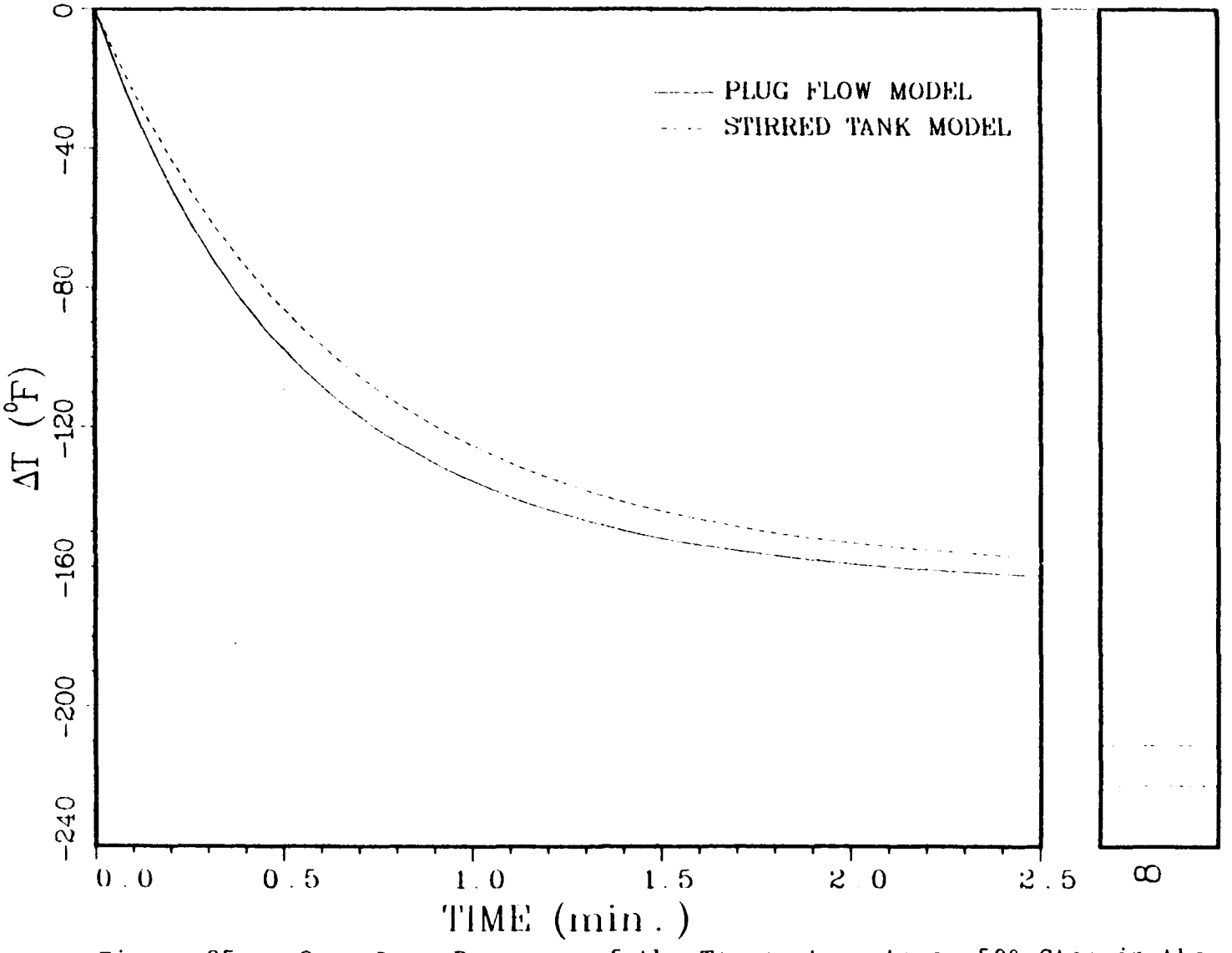

Figure 25a: Open Loop Response of the Temperature to a -50% Step in the Air Flow Rate. A Plug Flow Model versus a Stirred Tank Model

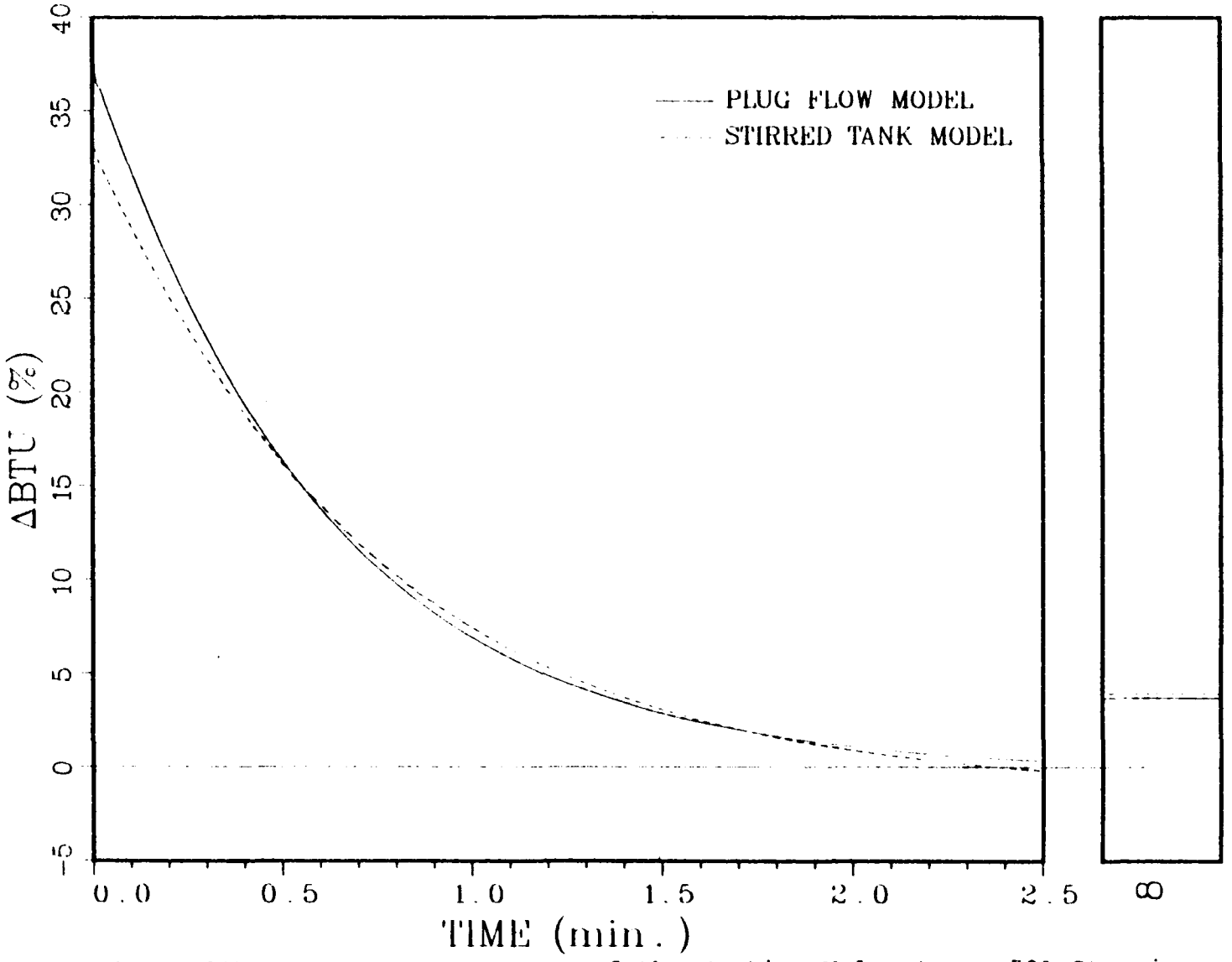

Figure 25b: Open Loop Response of the Heating Value to a -50% Step in the Air Flow Rate. A Plug Flow Model versus a Stirred Tank Model

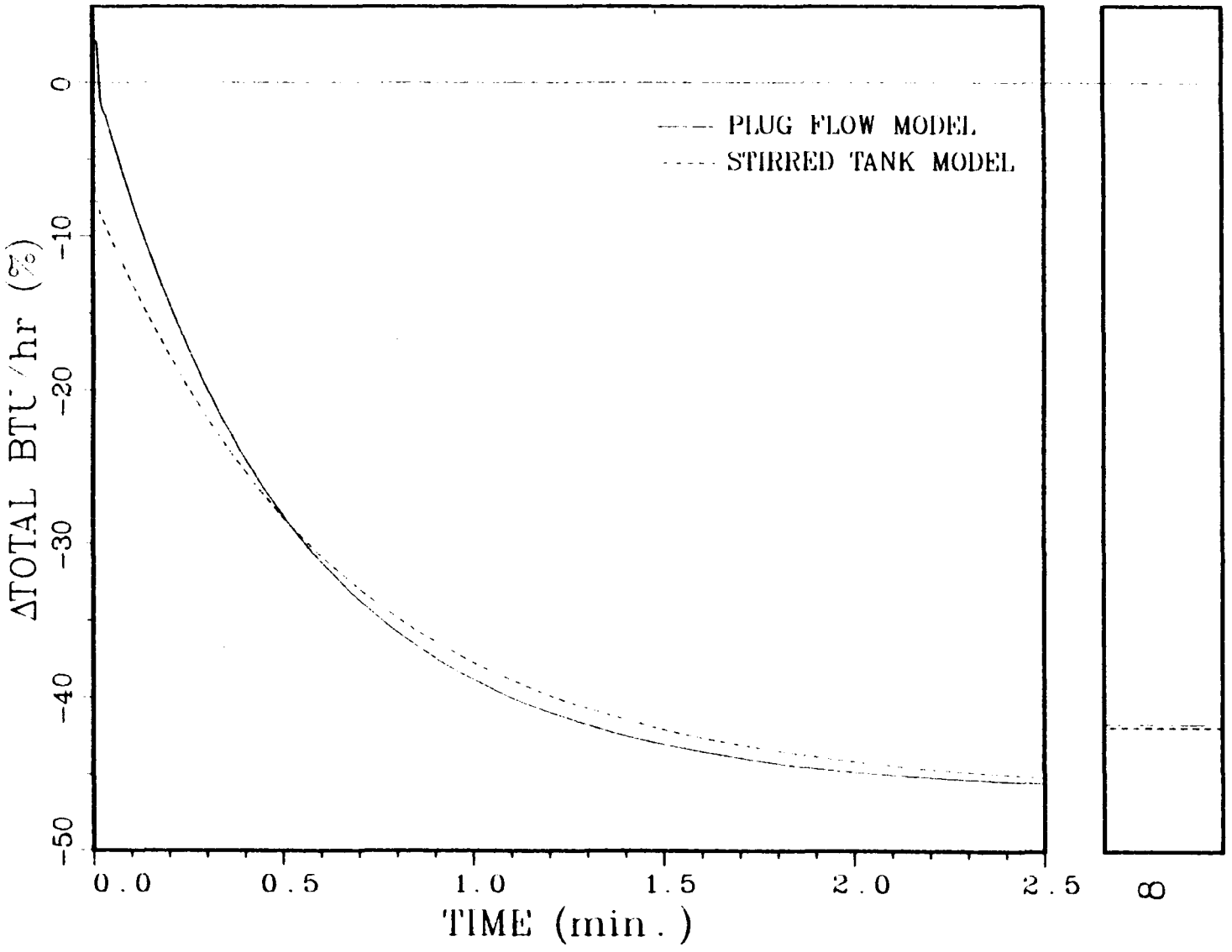

Figure 25c: Open Loop Response of the Total BTU/Hr. to a -50% Step in the Air Flow Rate. A Plug Flow Model versus a Stirred Tank Model

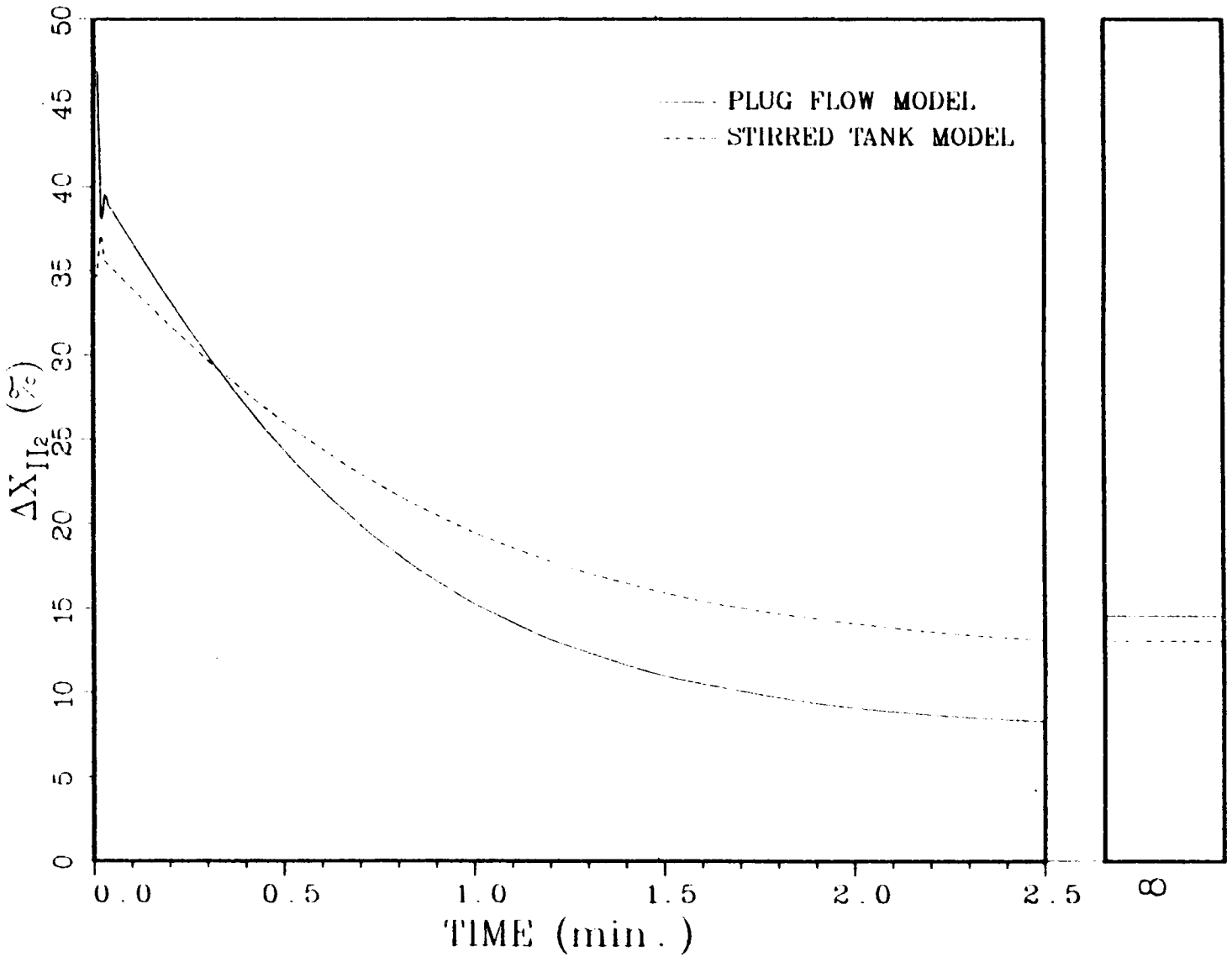

Figure 25d: Open Loop Response of the Hydrogen Content to a -50% Step in the Air Flow Rate. A Plug Flow Model versus a Stirred Tank Model

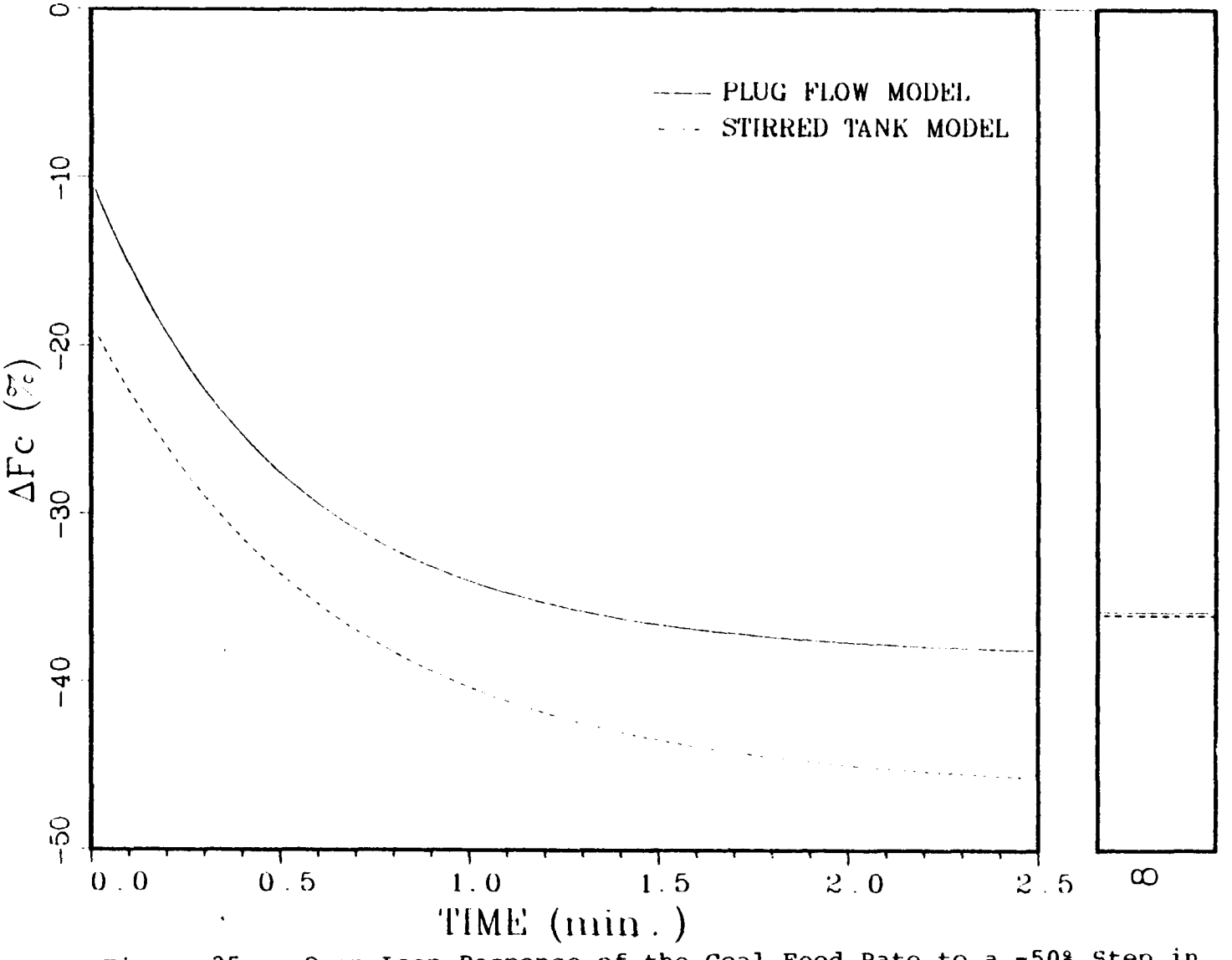

Figure 25e: Open Loop Response of the Coal Feed Rate to a -50% Step in the Air Flow Rate. A Plug Flow Model versus a Stirred Tank Model

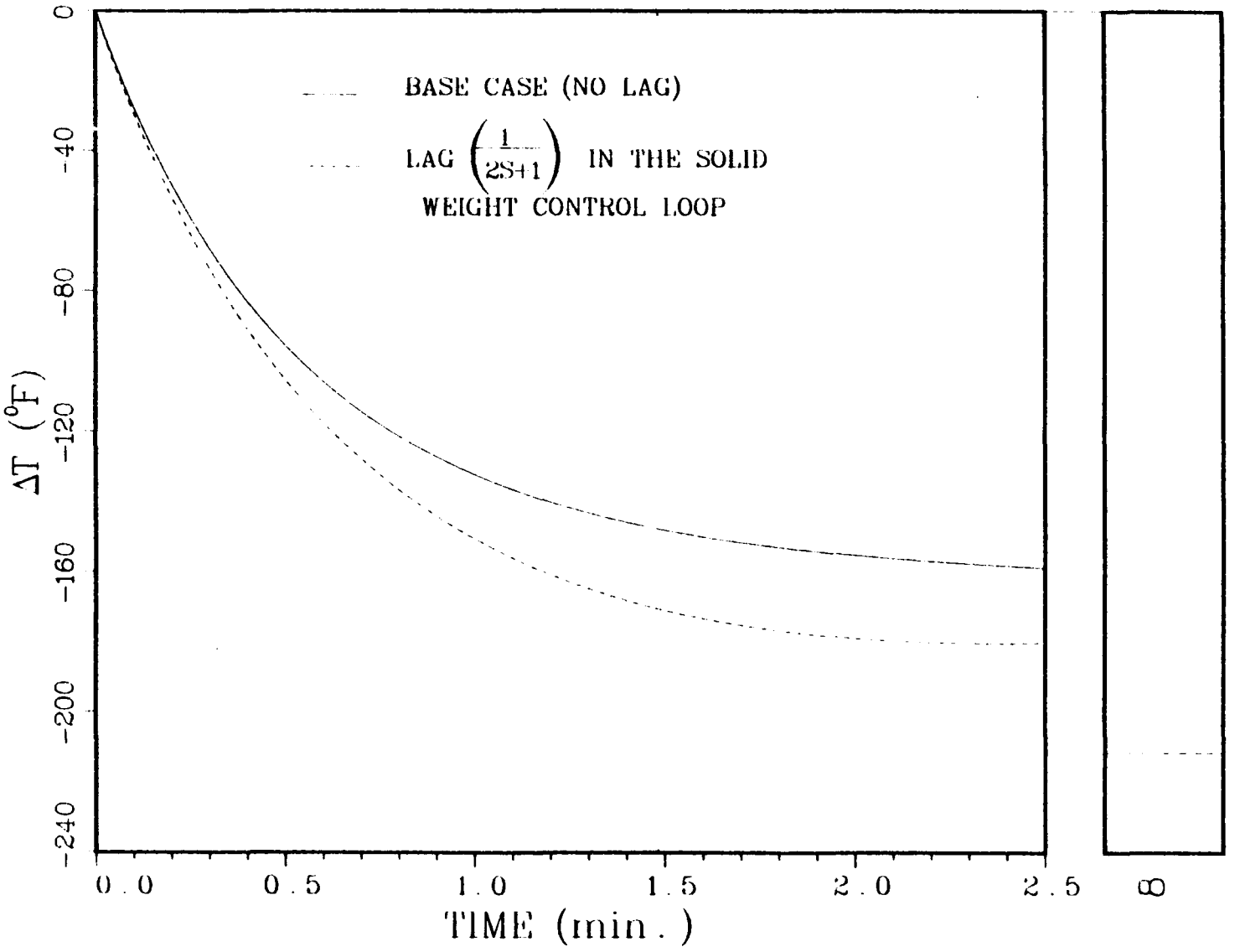

Figure 26a: Open Loop Response of the Temperature to a -50% Step in the Air Flow Rate. Base Case versus the Case where a Lag of $\frac{1}{(2S+1)}$ exists in the Solid Weight Control Loop

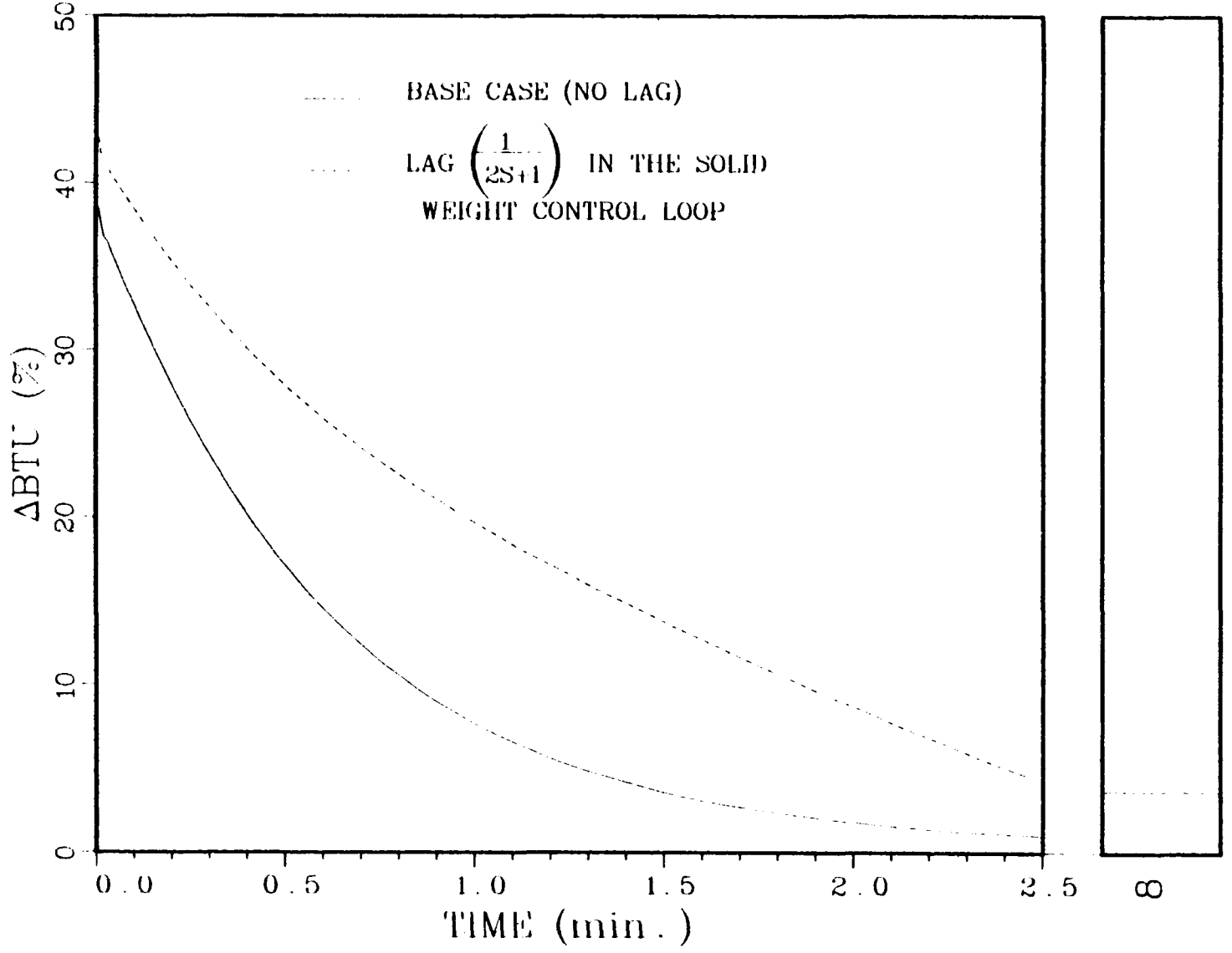

Figure 26b: Open Loop Response of the Heating Value to a -50% Step in the Air Flow Rate. Base Case versus the Case where a Lag of $\frac{1}{(2S+1)}$ exists in the Solid Weight Control Loop

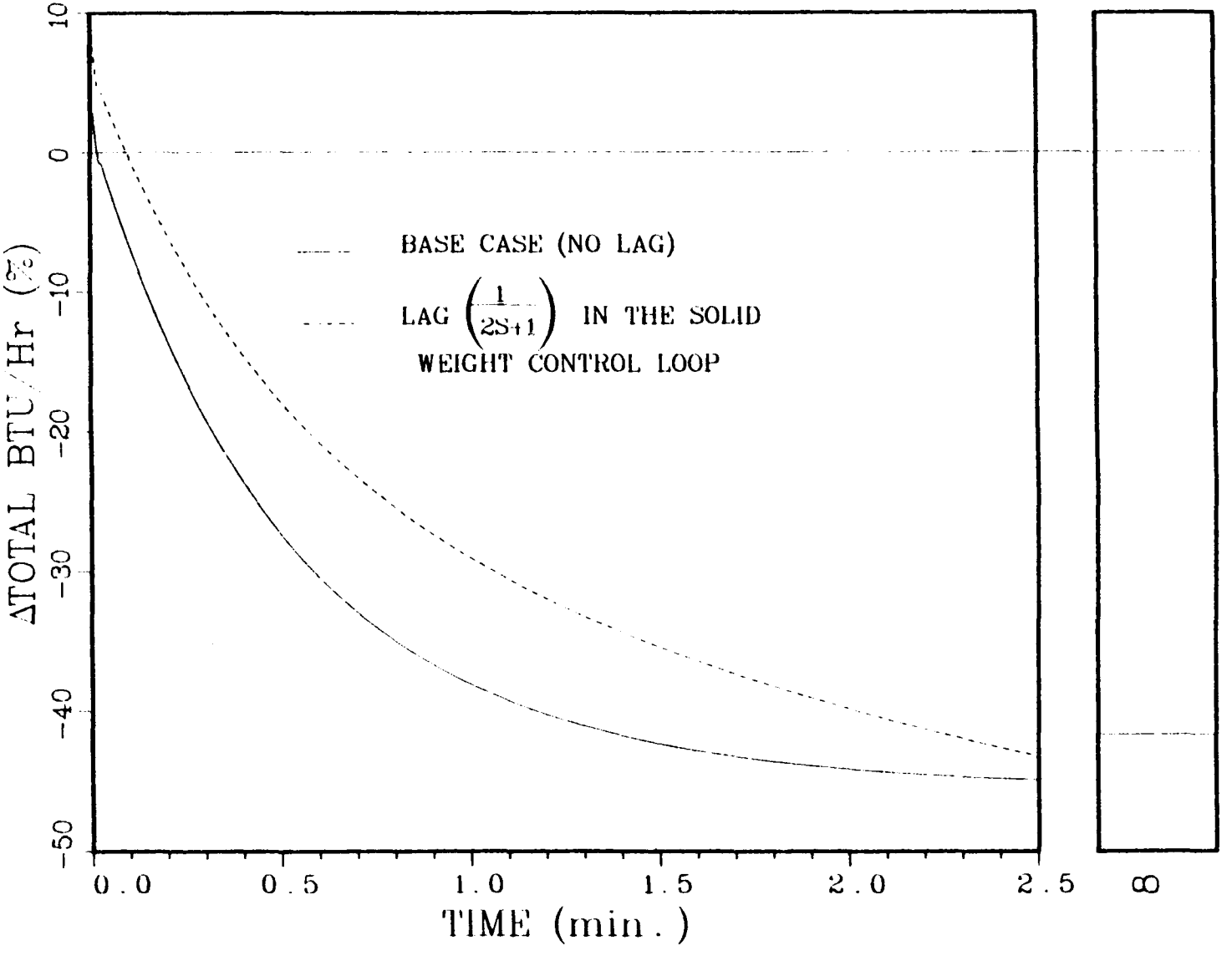

Figure 26c: Open Loop Response of the Total BTU/Hr. to a -50% Step in the Air Flow Rate. Base Case versus the Case where a Lag of $\frac{1}{(2S+1)}$ exists in the Solid Weight Control Loop

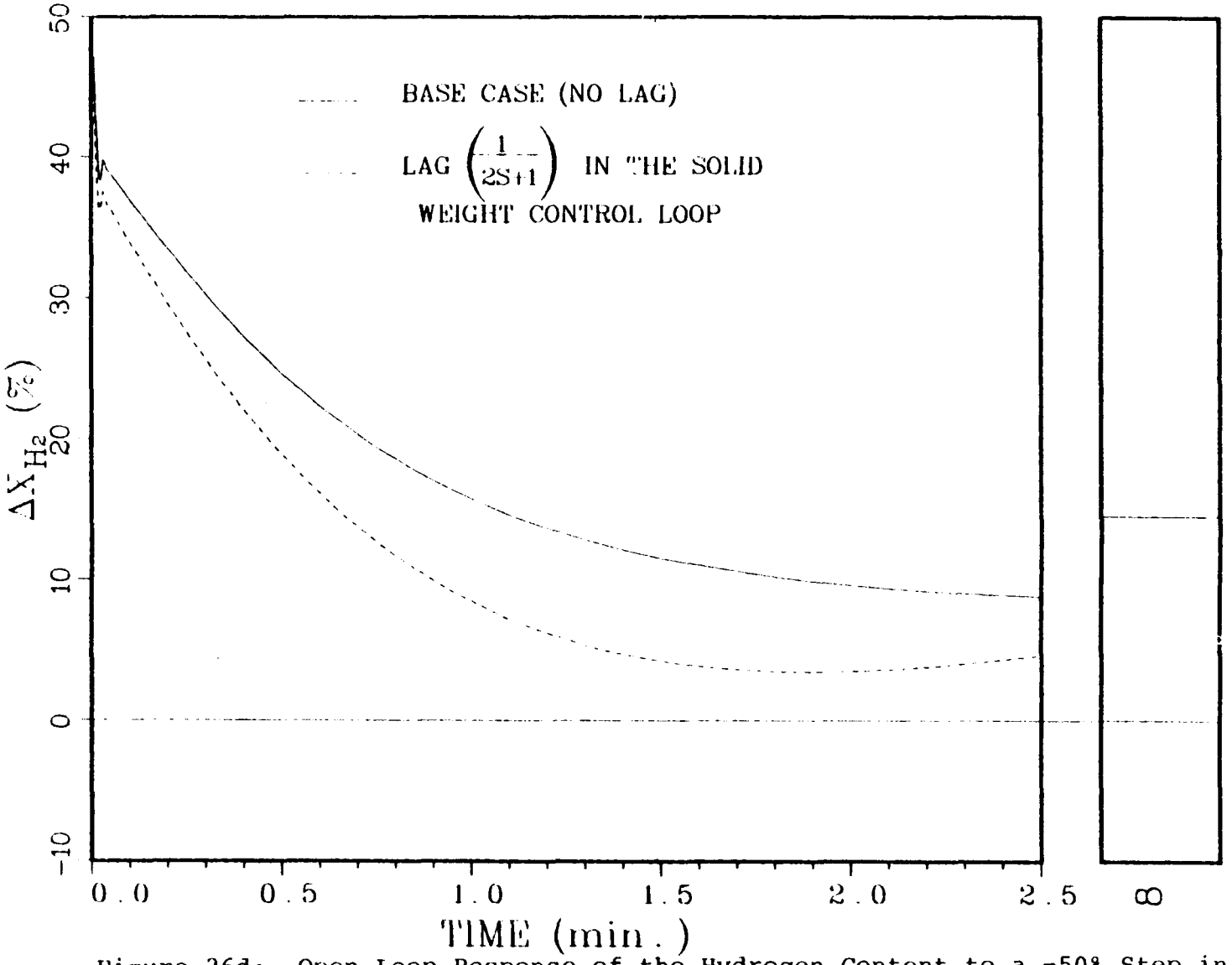

Figure 26d: Open Loop Response of the Hydrogen Content to a -50% Step in the Air Flow Rate. Base Case versus the Case where a Lag of $\frac{1}{(2S+1)}$ exists in the Solid Weight Control Loop

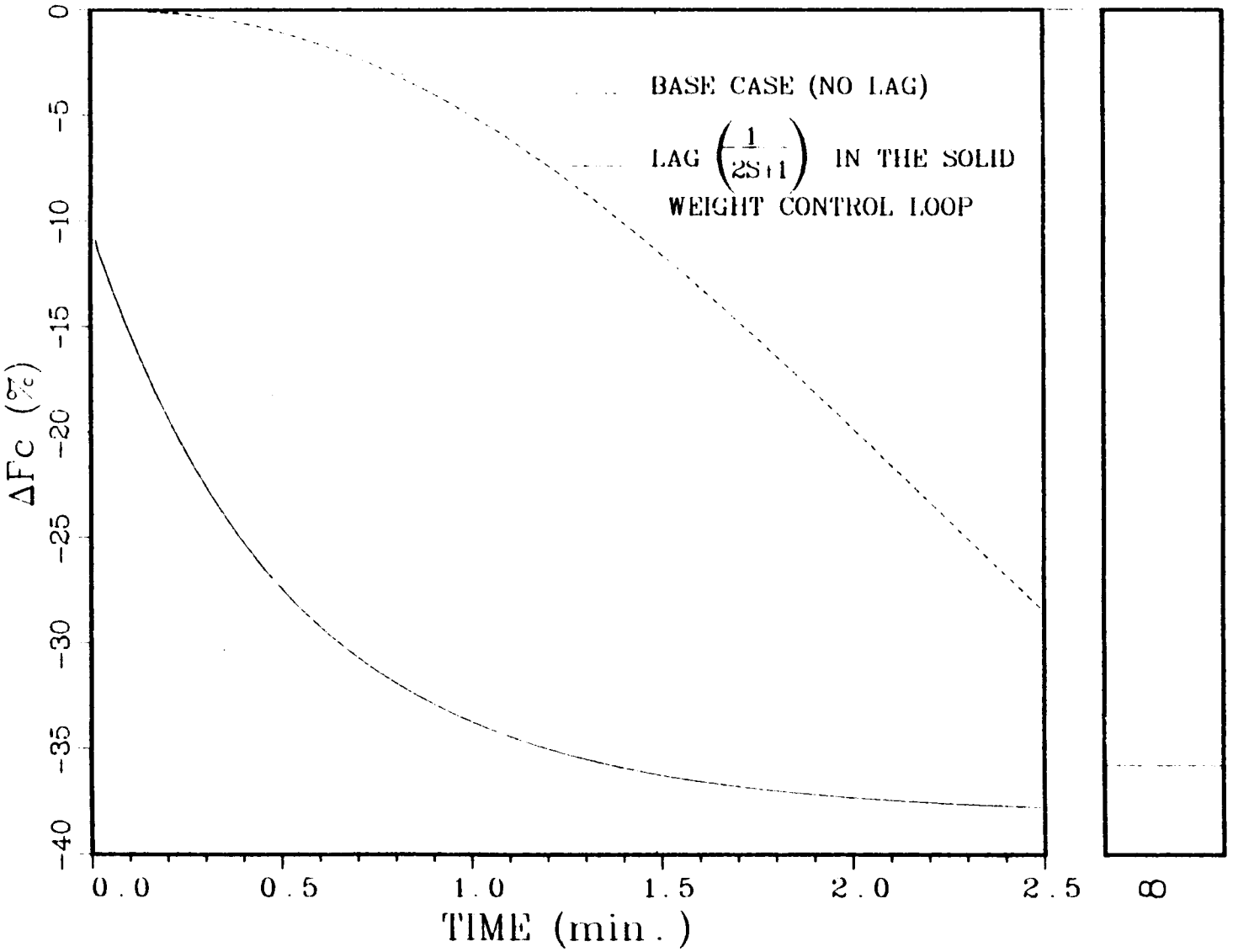

Figure 26e: Open Loop Response of the Coal Feed Rate to a -50% Step in the Air Flow Rate. Base Case versus the Case where a Lag of $\frac{1}{(2S+1)}$ exists in the Solid Weight Control Loop

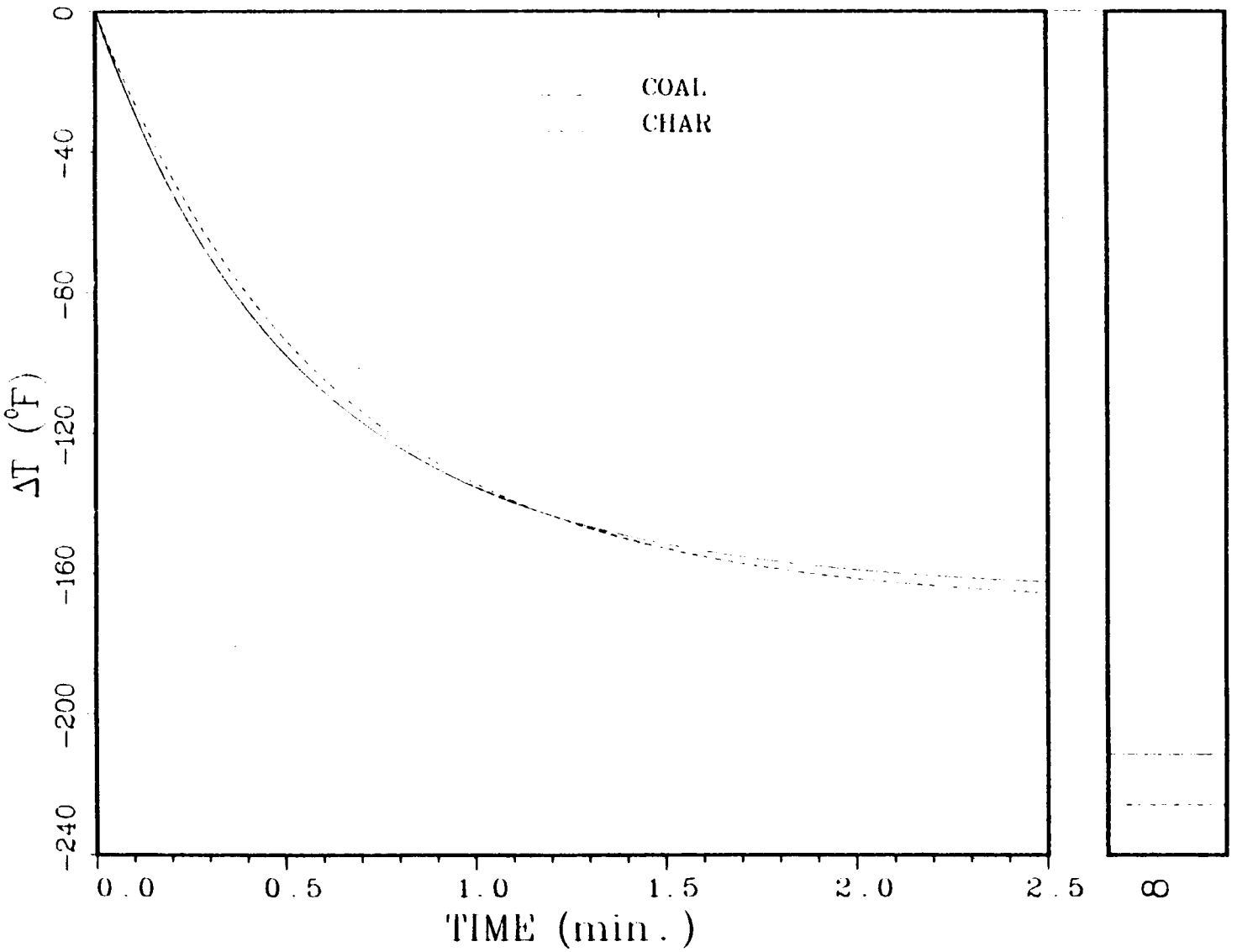

Figure 27a: Open Loop Response of the Temperature to a -50% Step in the Air Flow Rate. Base Case (Coal Feed) versus Char Feed Case

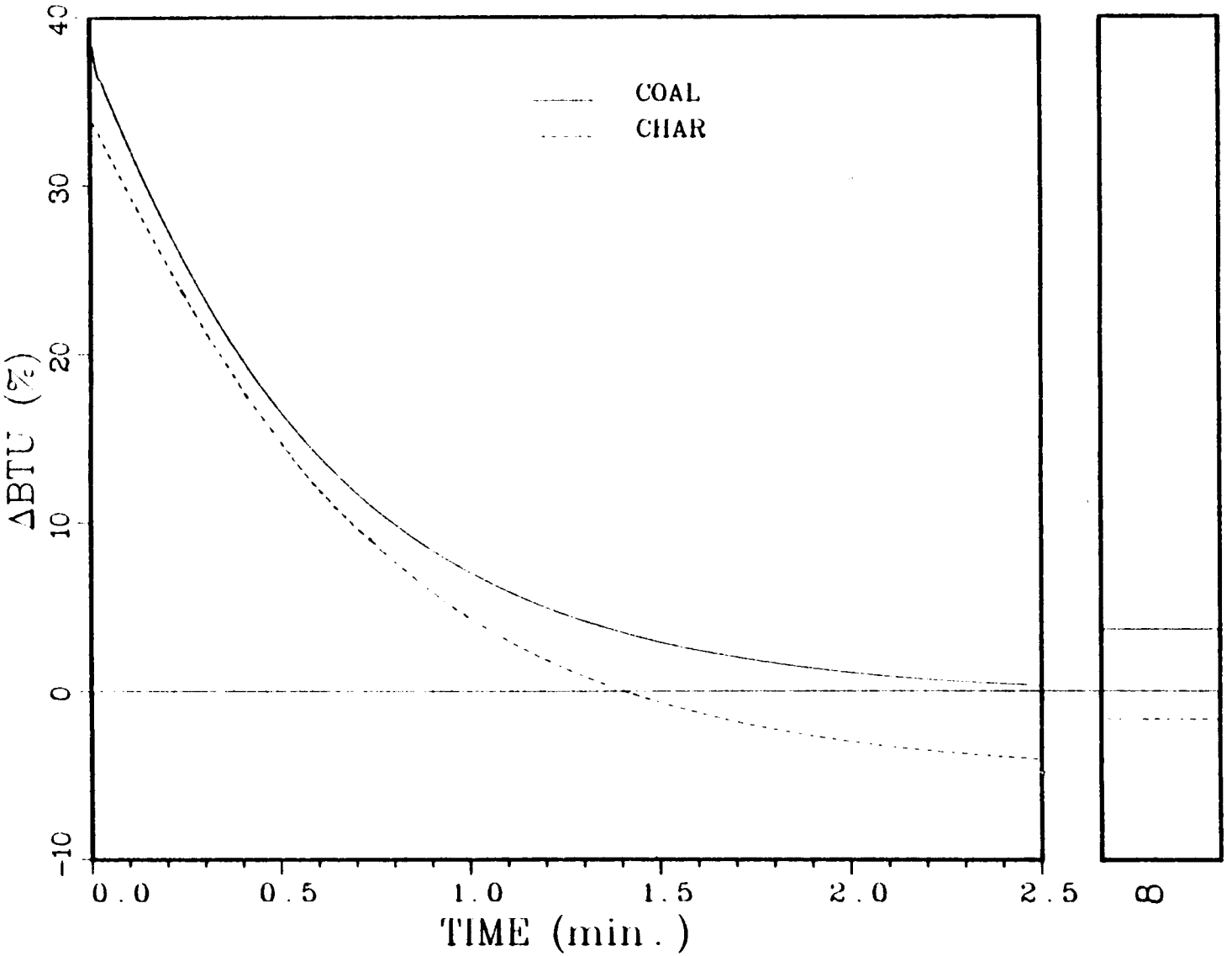

Figure 27b: Open Loop Response of the Heating Value to a -50% Step in the Air Flow Rate. Base Case (Coal Feed) versus Char Feed Case

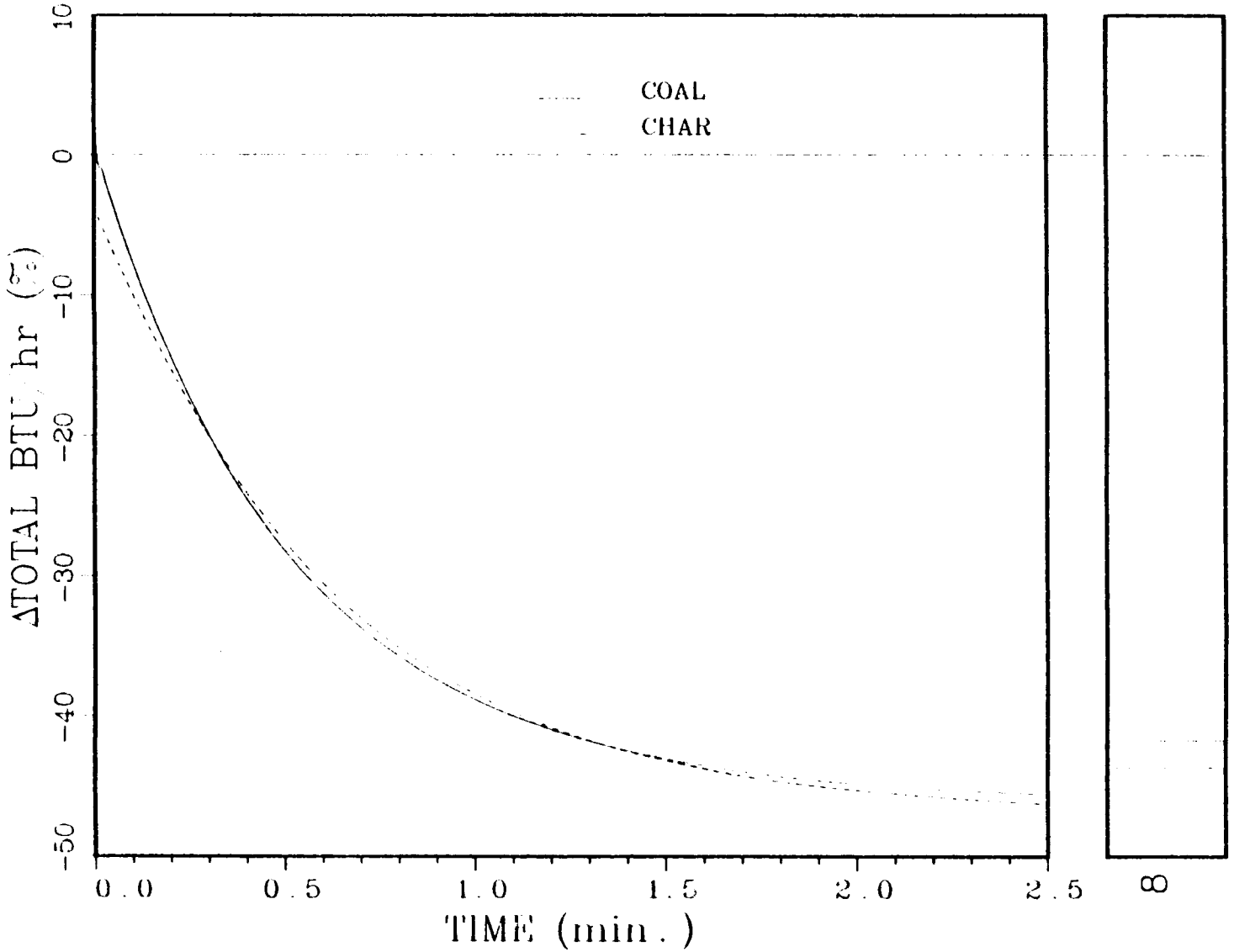

Figure 27c: Open Loop Response of the Total BTU/Hr. to a -50% Step in the Air Flow Rate. Base Case (Coal Feed) versus Char Feed Case.

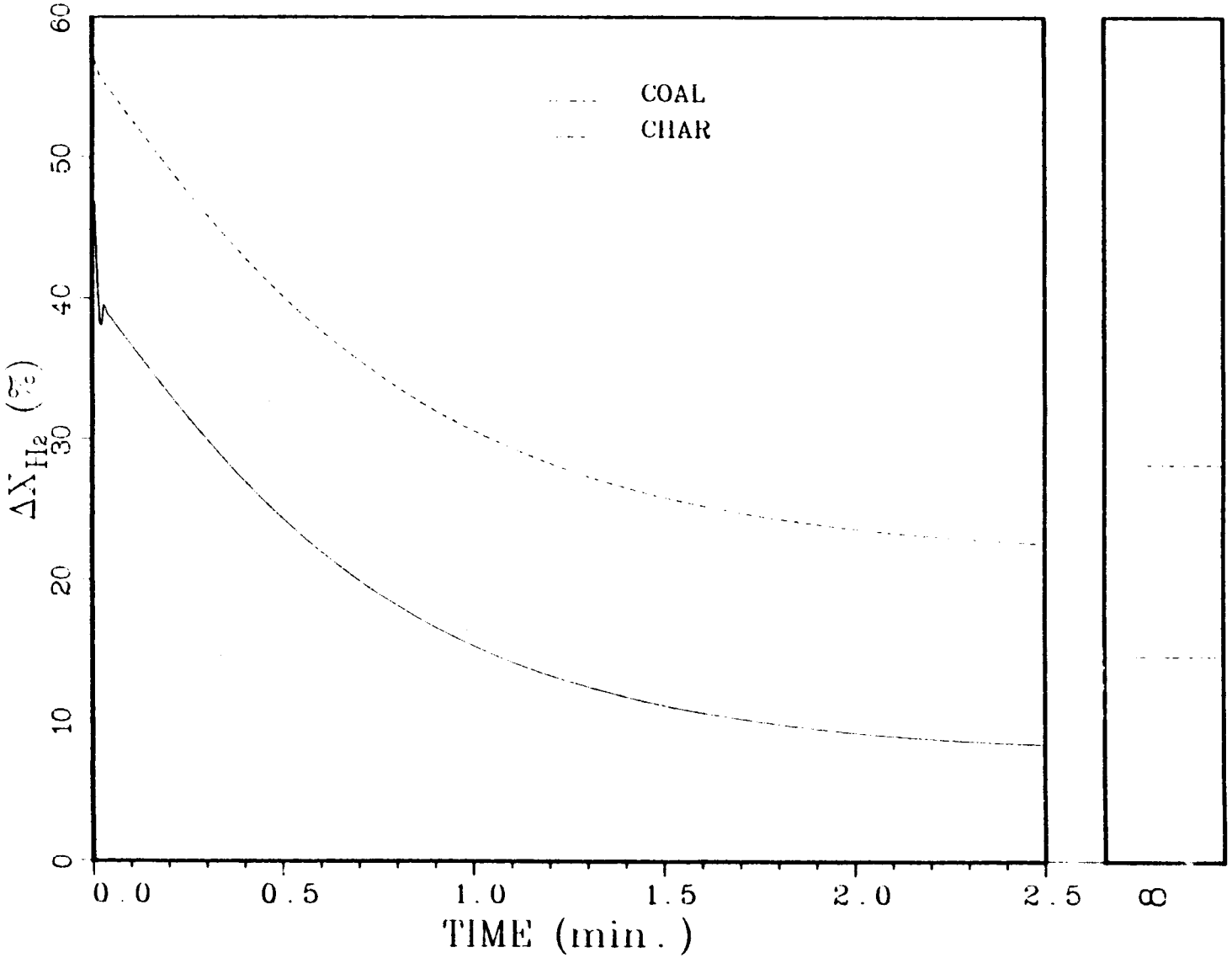

Figure 27d: Open Loop Response of the Hydrogen Content to a -50% Step in the Air Flow Rate. Base Case (Coal Feed) versus Char Feed Case

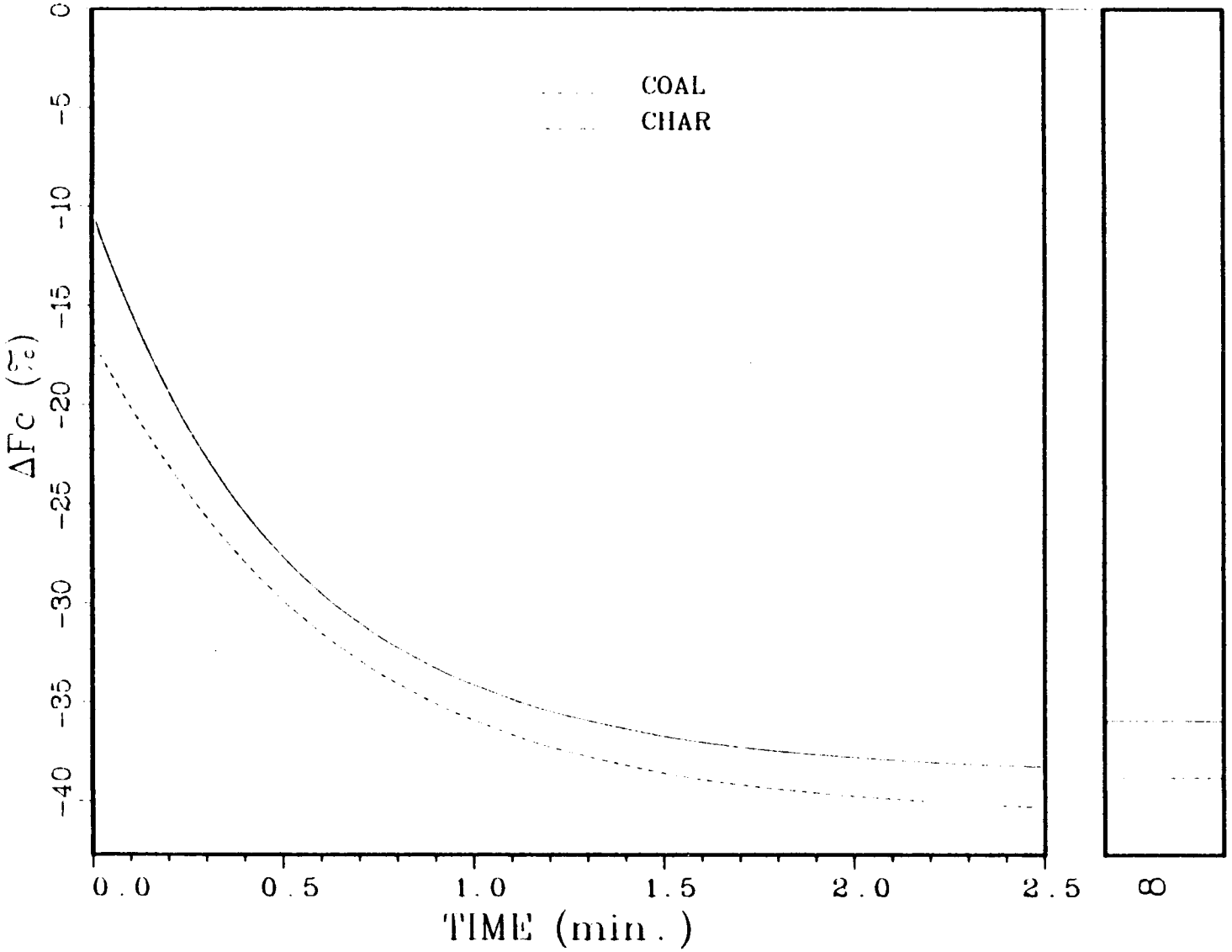

Figure 27e: Open Loop Response of the Solid Feed Rate to a -50% Step in the Air Flow Rate. Base Case (Coal Feed) versus Char Feed Case

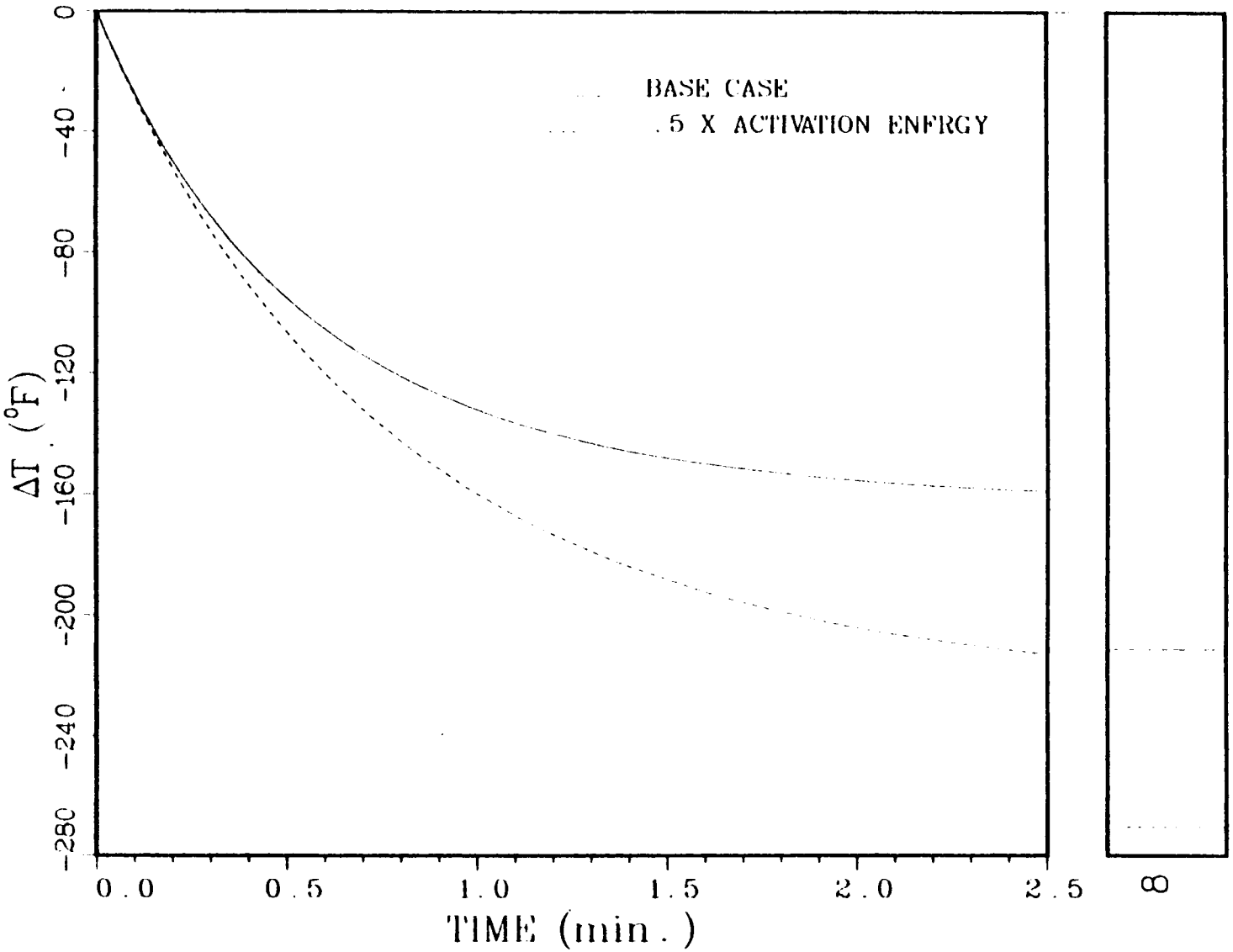

Figure 28a: Open Loop Response of the Temperature to a -50% Step Input in the Air Flow Rate. Base Case versus 50% Activation Energy Case

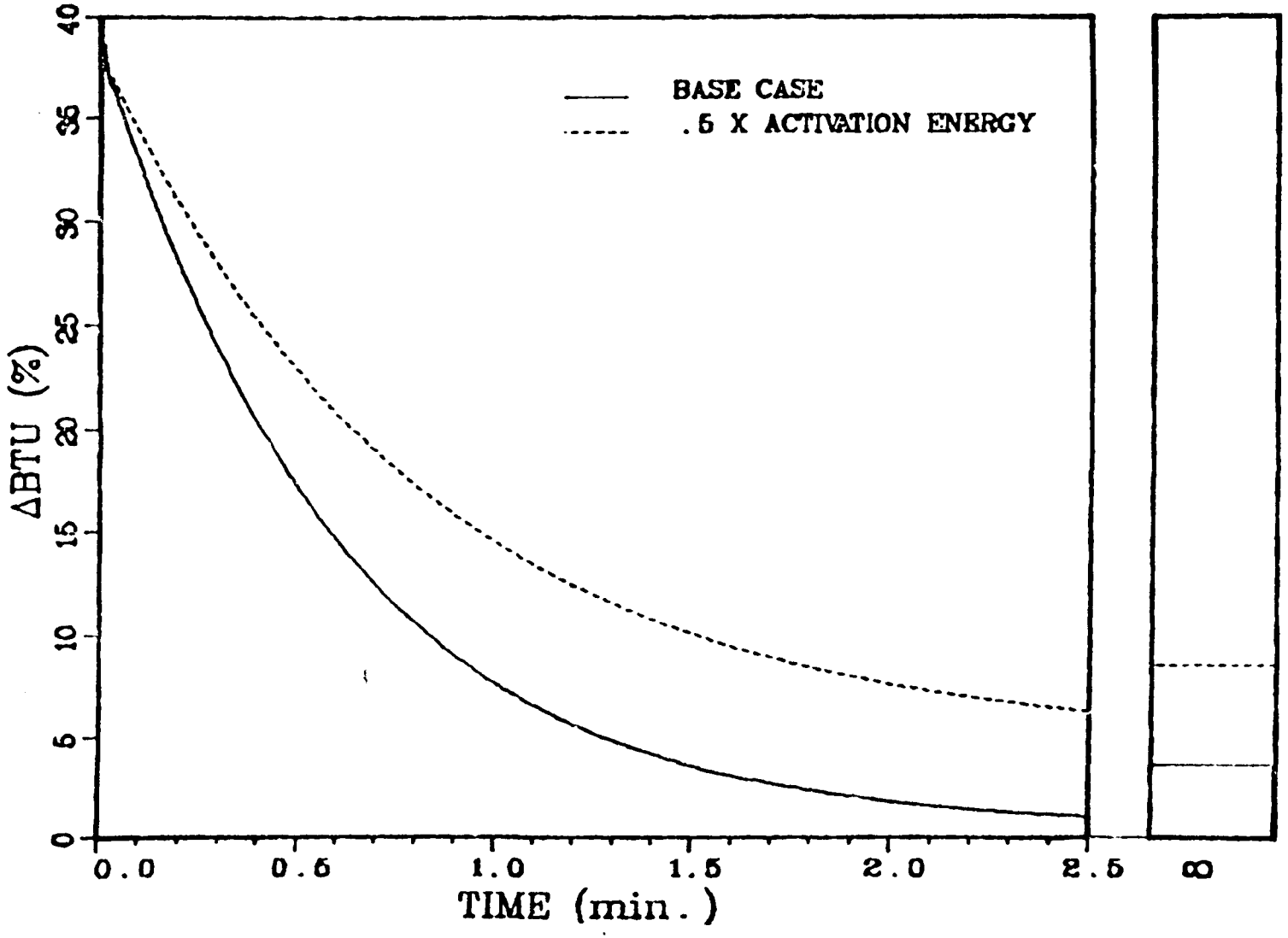

Figure 28b: Open Loop Response of the Heating Value to a -50% Step Input in the Air Flow Rate. Base Case versus 50% Activation Energy Case

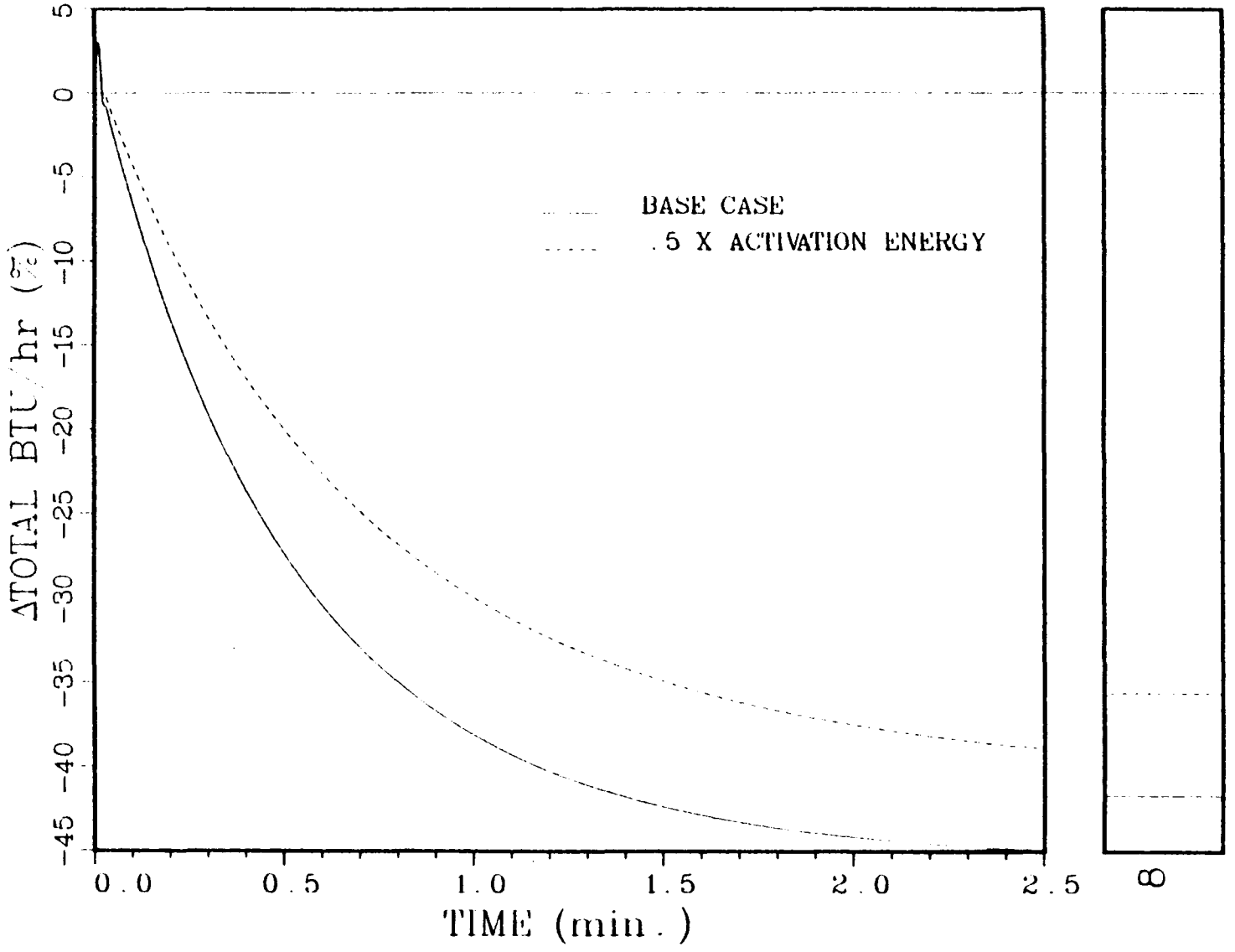

Figure 28c: Open Loop Response of the Total BTU/Hr. to a -50% Step Input in the Air Flow Rate. Base Case versus 50% Activation Energy Case

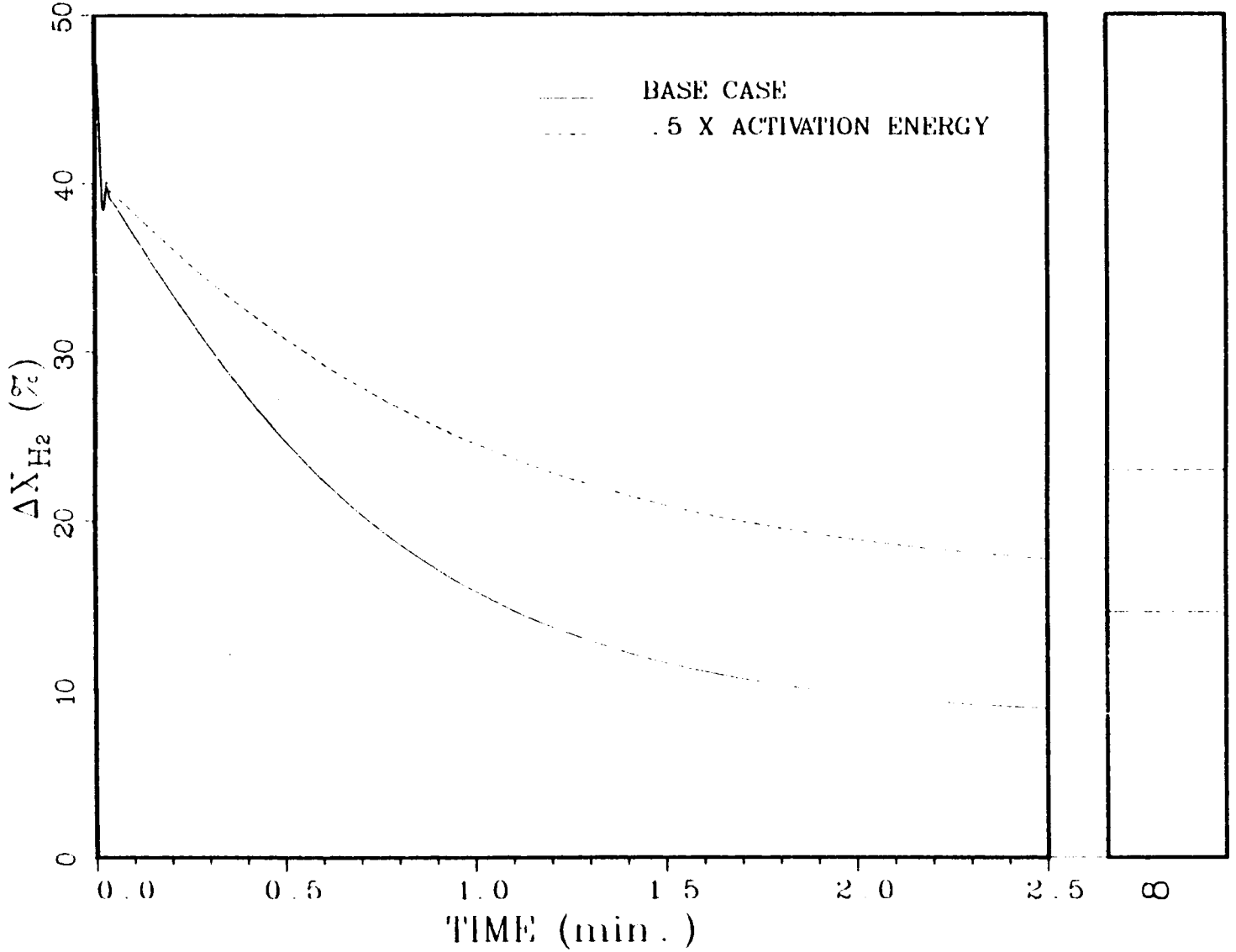

Figure 28d: Open Loop Response of the Hydrogen Content to a -50% Step Input in the Air Flow Rate. Base Case versus 50% Activation Energy Case

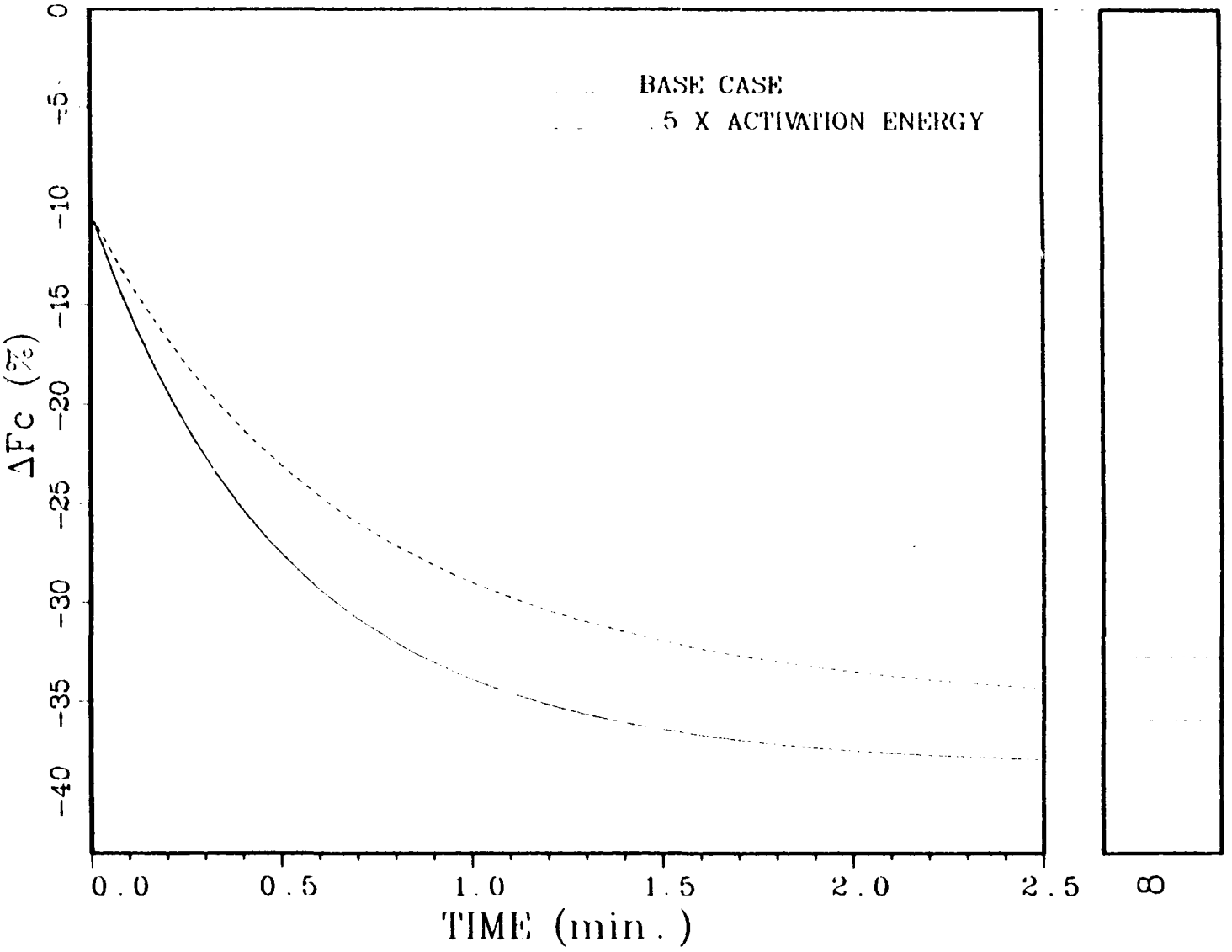

Figure 28e: Open Loop Response of the Coal Feed Rate to a -50% Step Input in the Air Flow Rate. Base Case versus 50% Activation Energy Case

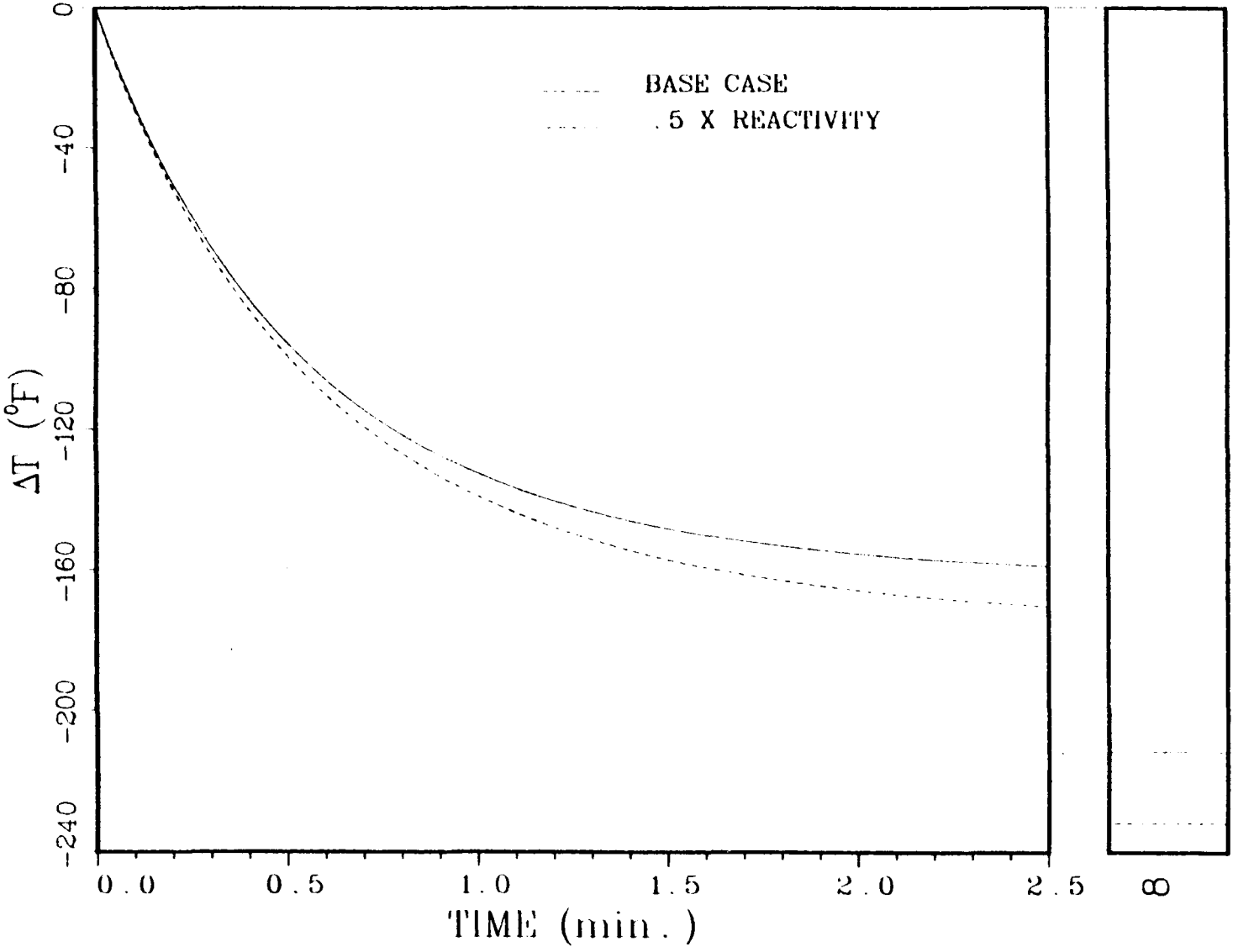

Figure 29a: Open Loop Response of the Temperature to a -50% Step Input in the Air Flow Rate. Base Case versus 50% Reactivity Case

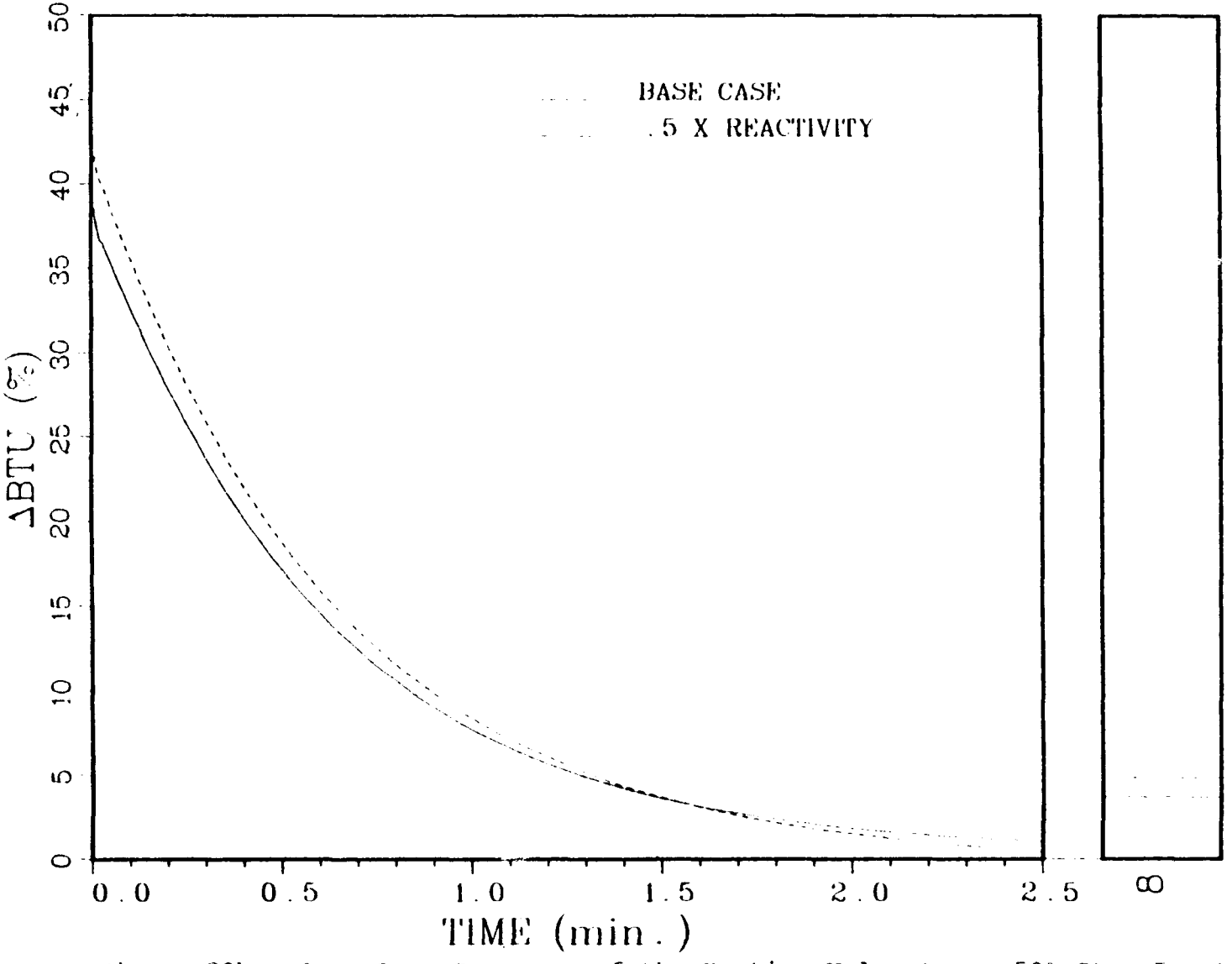

Figure 29b: Open Loop Response of the Heating Value to a -50% Step Input in the Air Flow Rate. Base Case versus 50% Reactivity Case

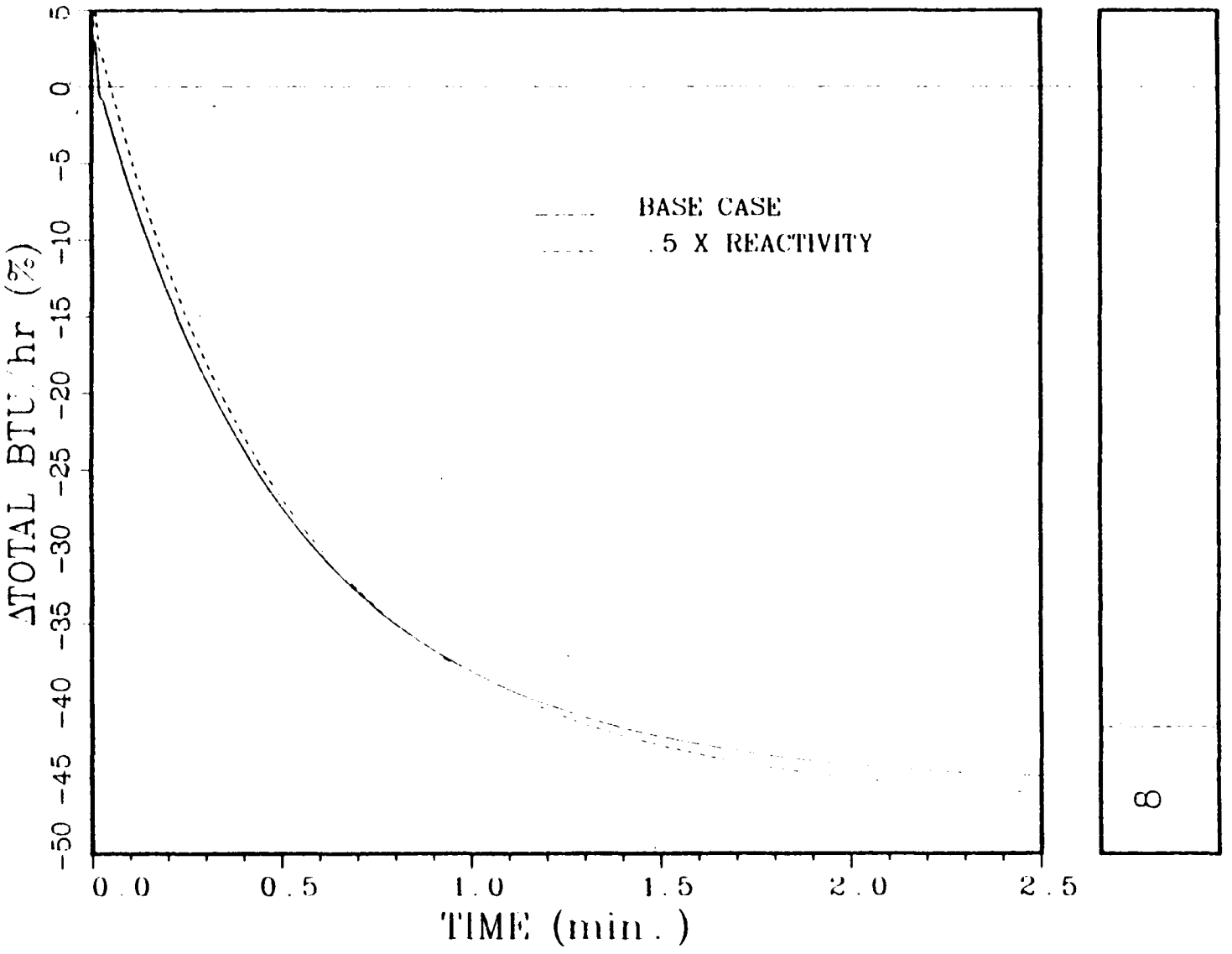

Figure 29c: Open Loop Response of the Total BTU/Hr. to a -50% Step Input in the Air Flow Rate. Base Case versus 50% Reactivity Case

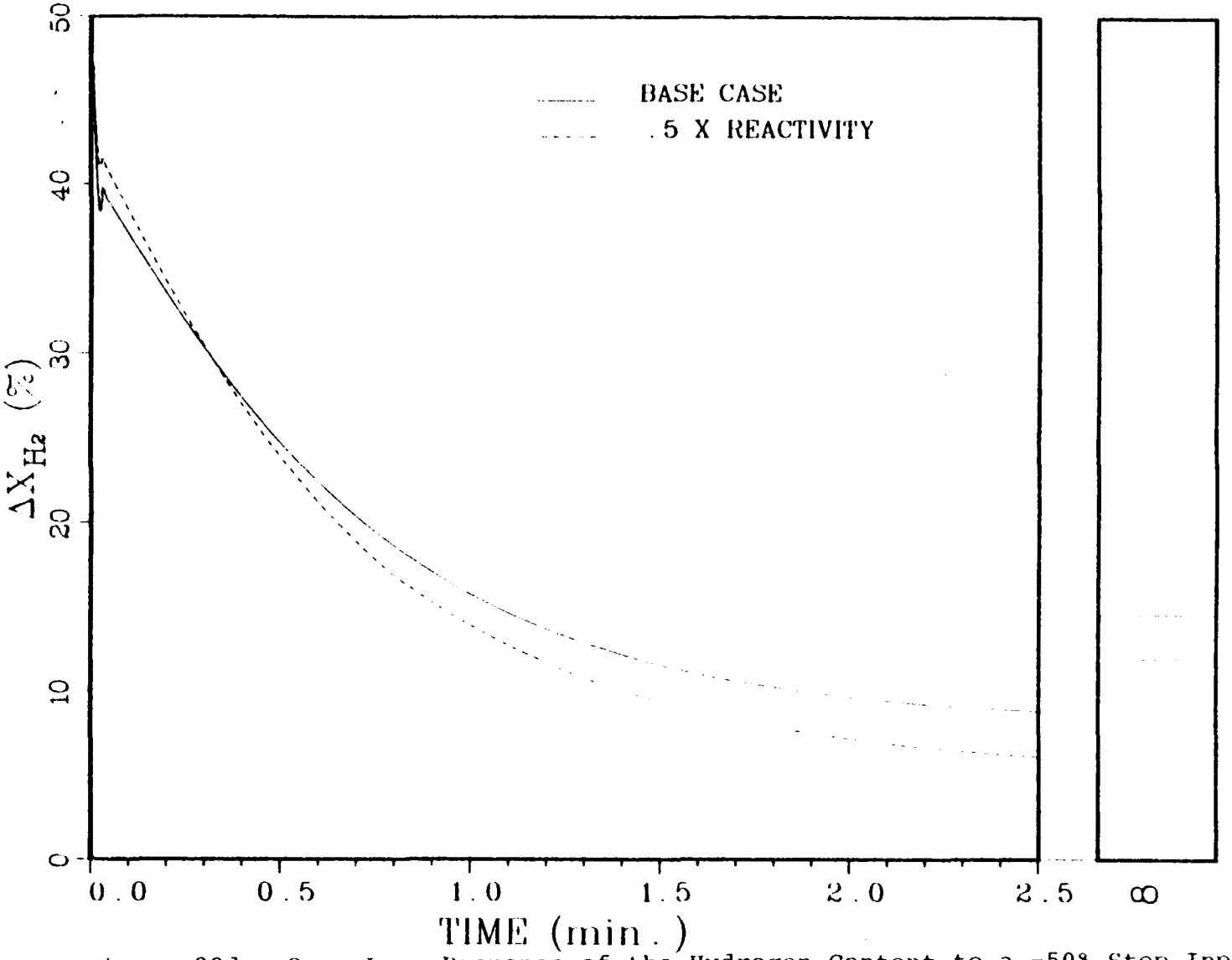

Figure 29d: Open Loop Response of the Hydrogen Content to a -50% Step Input in the Air Flow Rate. Base Case versus 50% Reactivity Case

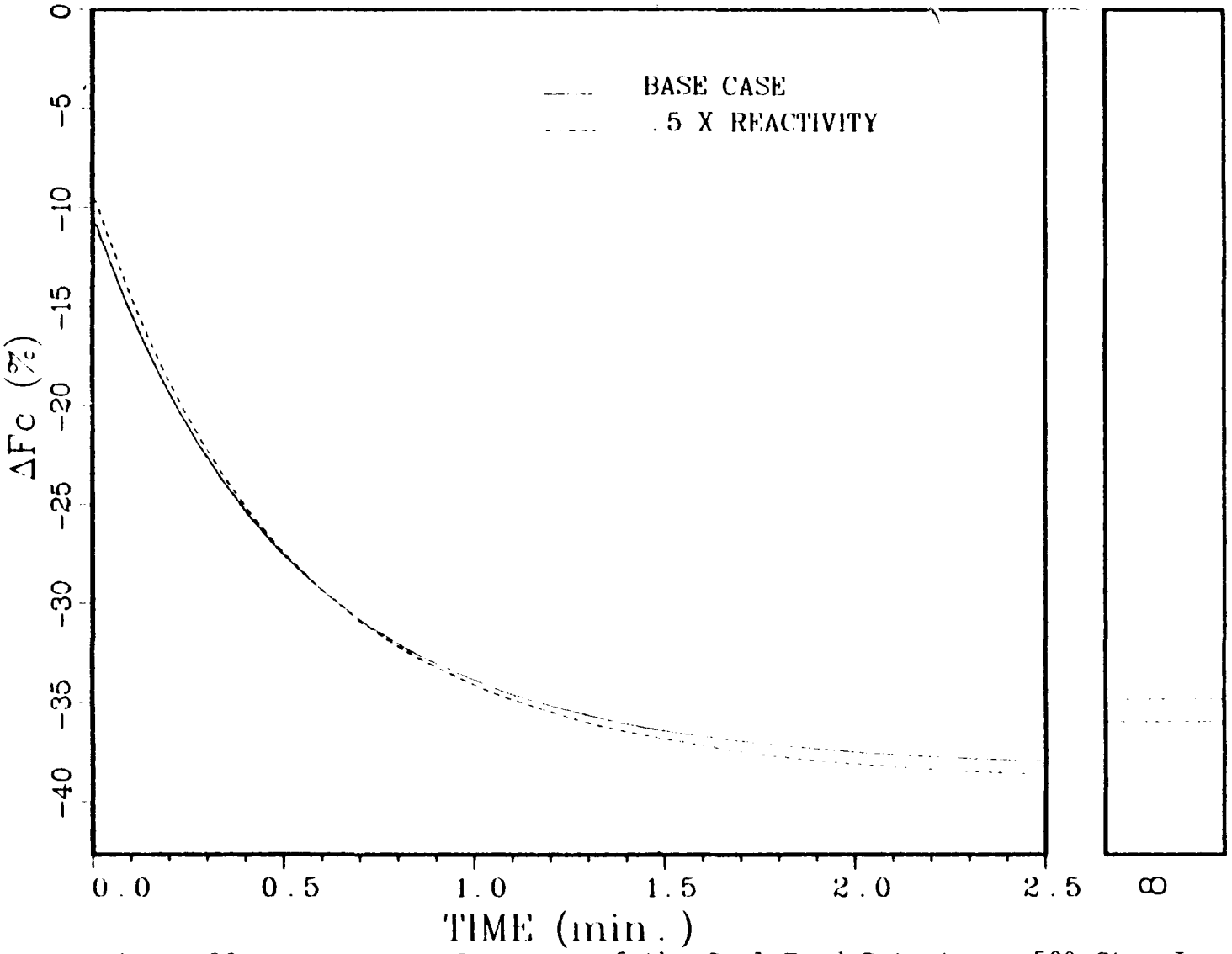

Figure 29e: Open Loop Response of the Coal Feed Rate to a -50% Step Input in the Air Flow Rate. Base Case versus 50% Reactivity Case

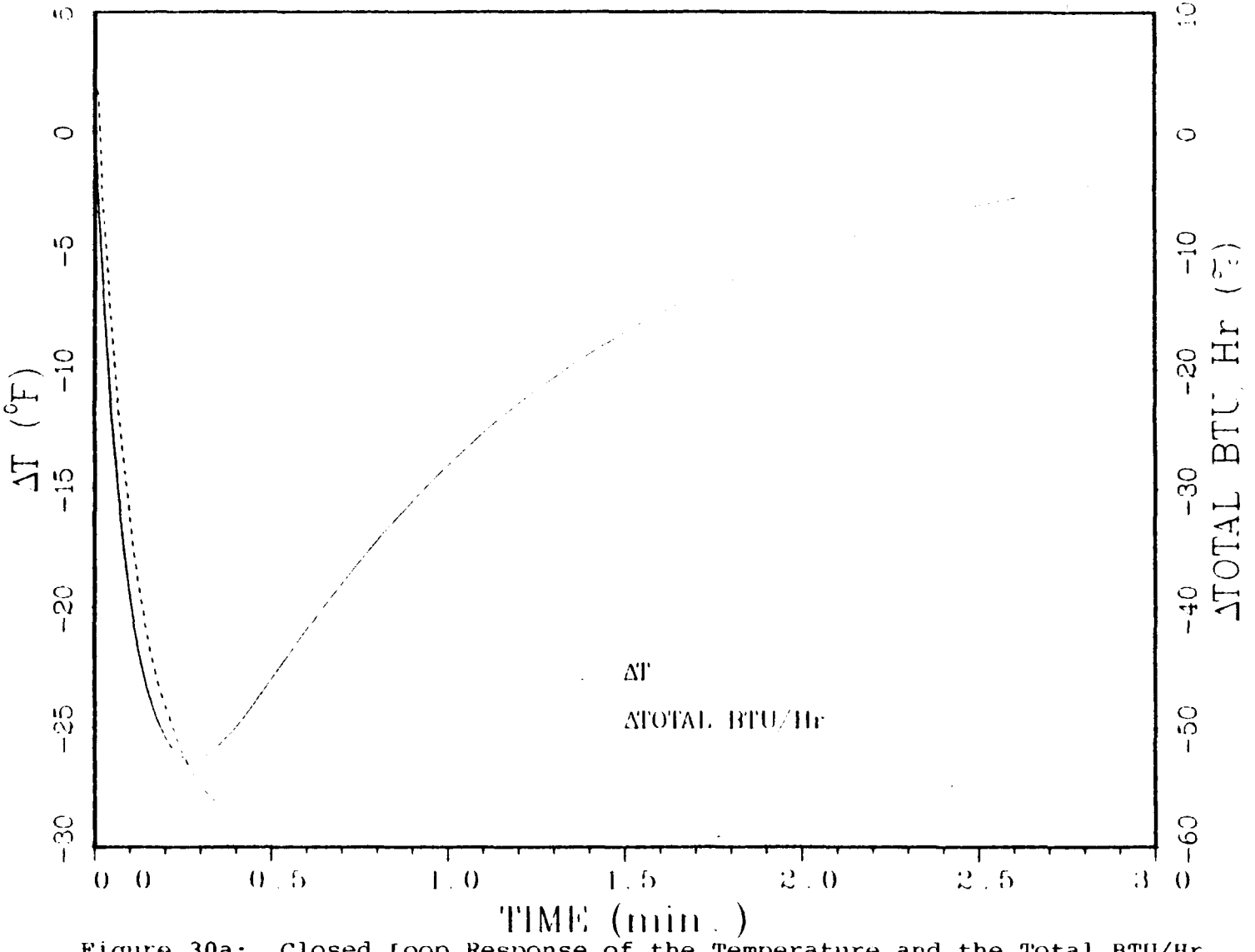

Figure 30a: Closed Loop Response of the Temperature and the Total BTU/Hr. to a -50% Step Input in the Air Flow Rate. Temperature is P.I.D. Controlled by Manipulation of the Steam Flow Rate

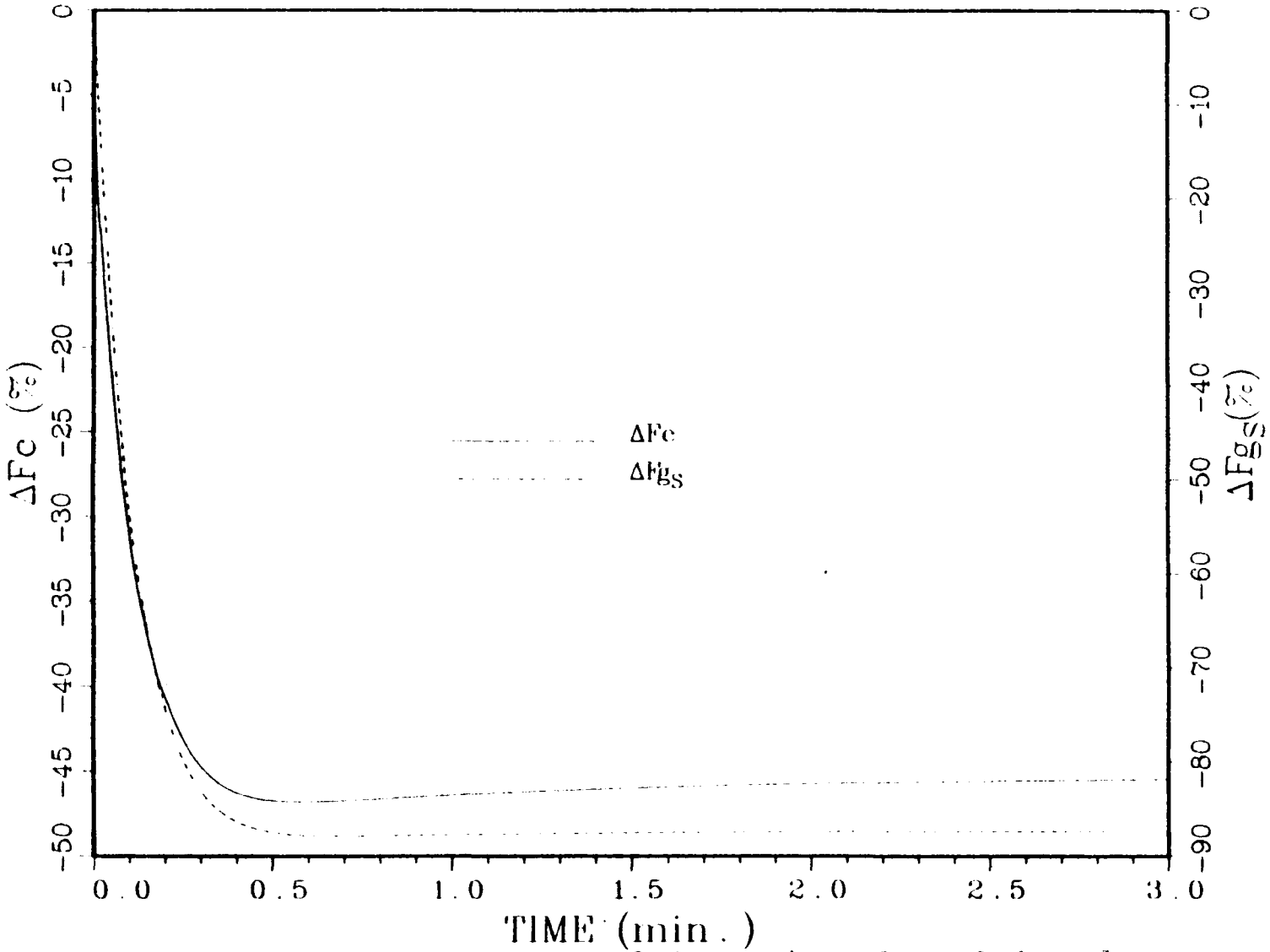

Figure 30b: Closed Loop Response of the Heating Value and the Hydrogen Content to a -50% Step Input in the Air Flow Rate. Temperature is P.I.D. Controlled by Manipulation of the Steam Flow Rate

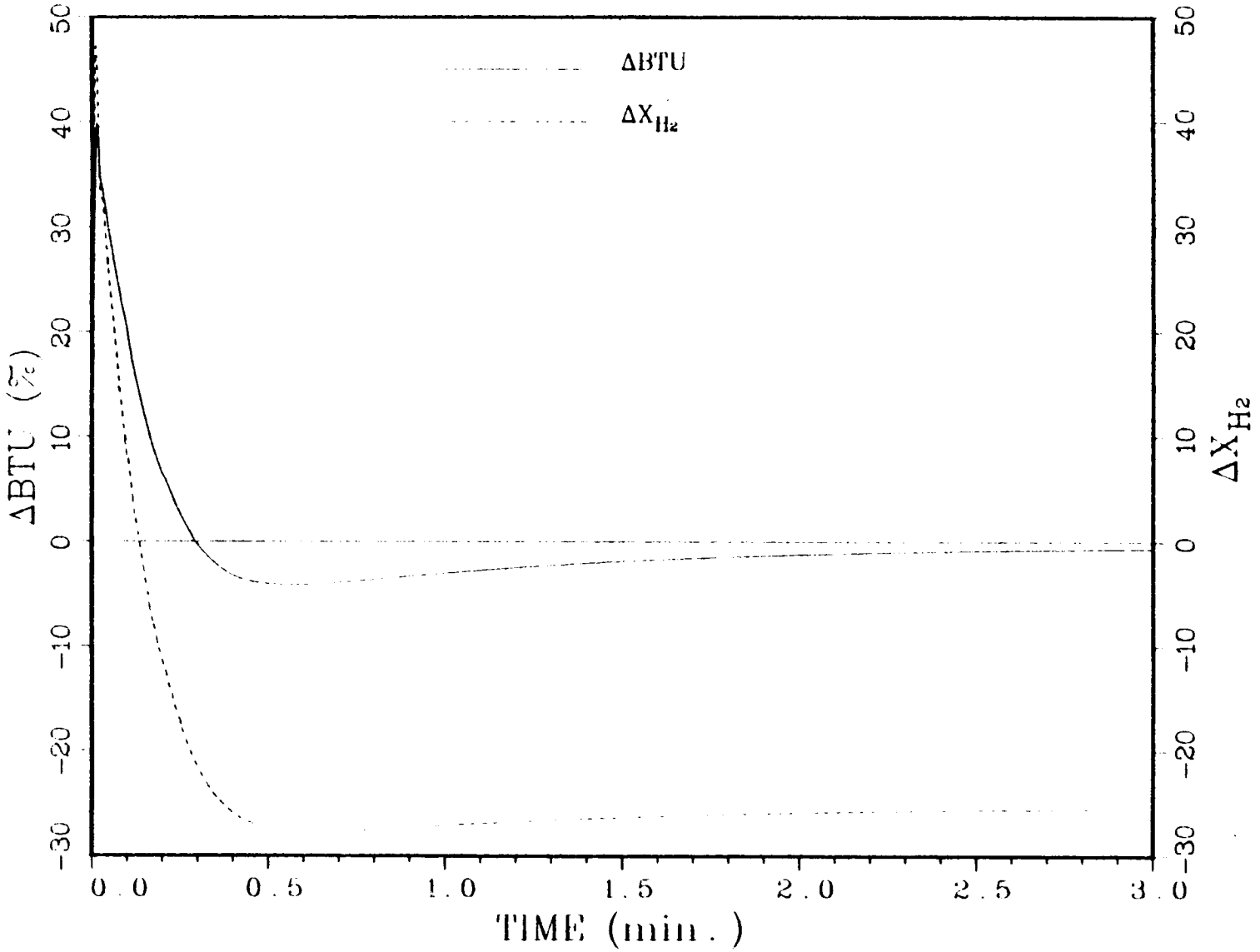

Figure 30c: Closed Loop Response of the Coal Feed Rate and the Steam Flow Rate to a -50% Step Input in the Air Flow Rate. Temperature is P.I.D. Controlled by Manipulation of the Steam Flow Rate

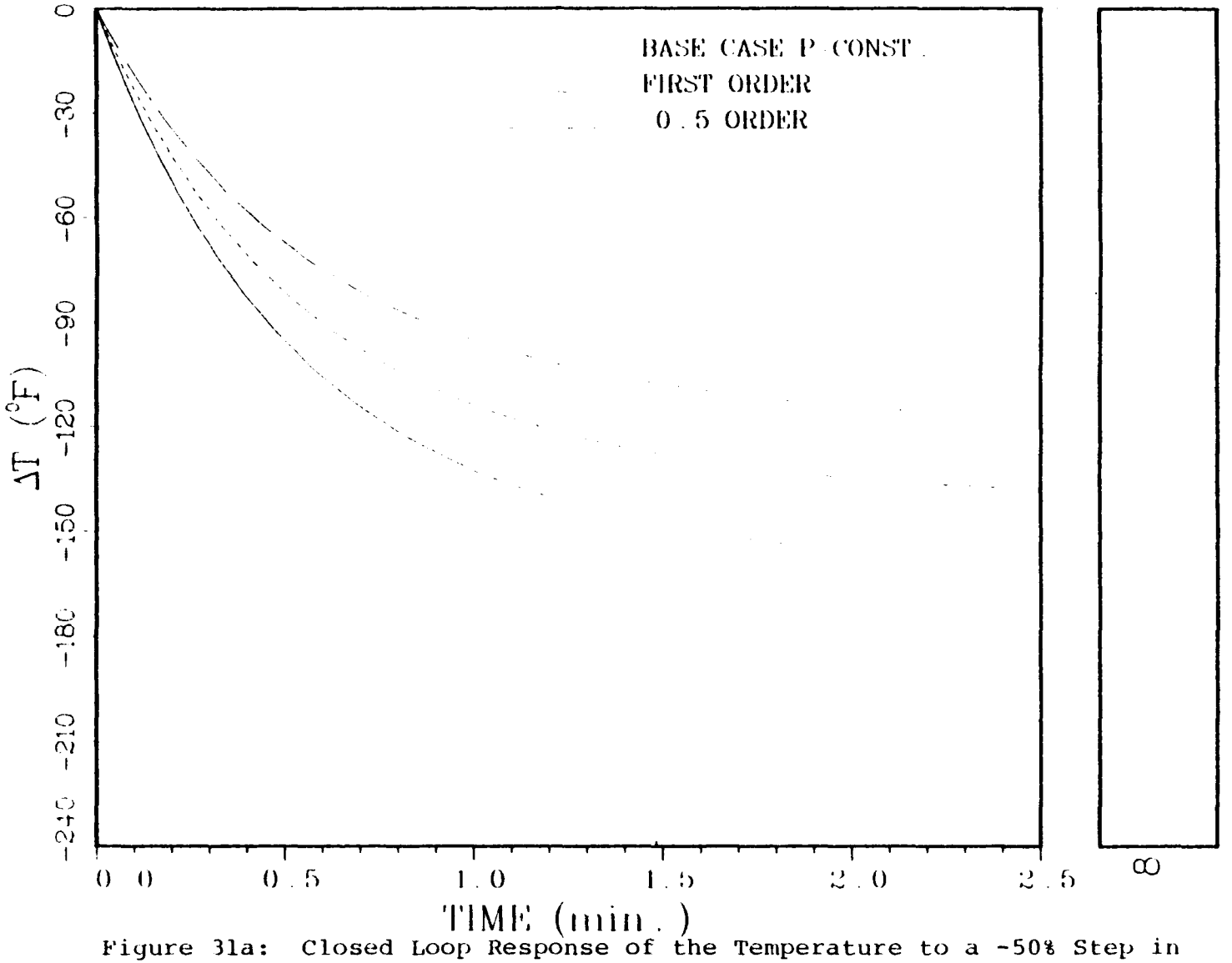

Figure 31a: Closed Loop Response of the Temperature to a -50% Step in the Air Flow Rate. Constant Linear Velocity (Adjusted Pressure) Control Loop

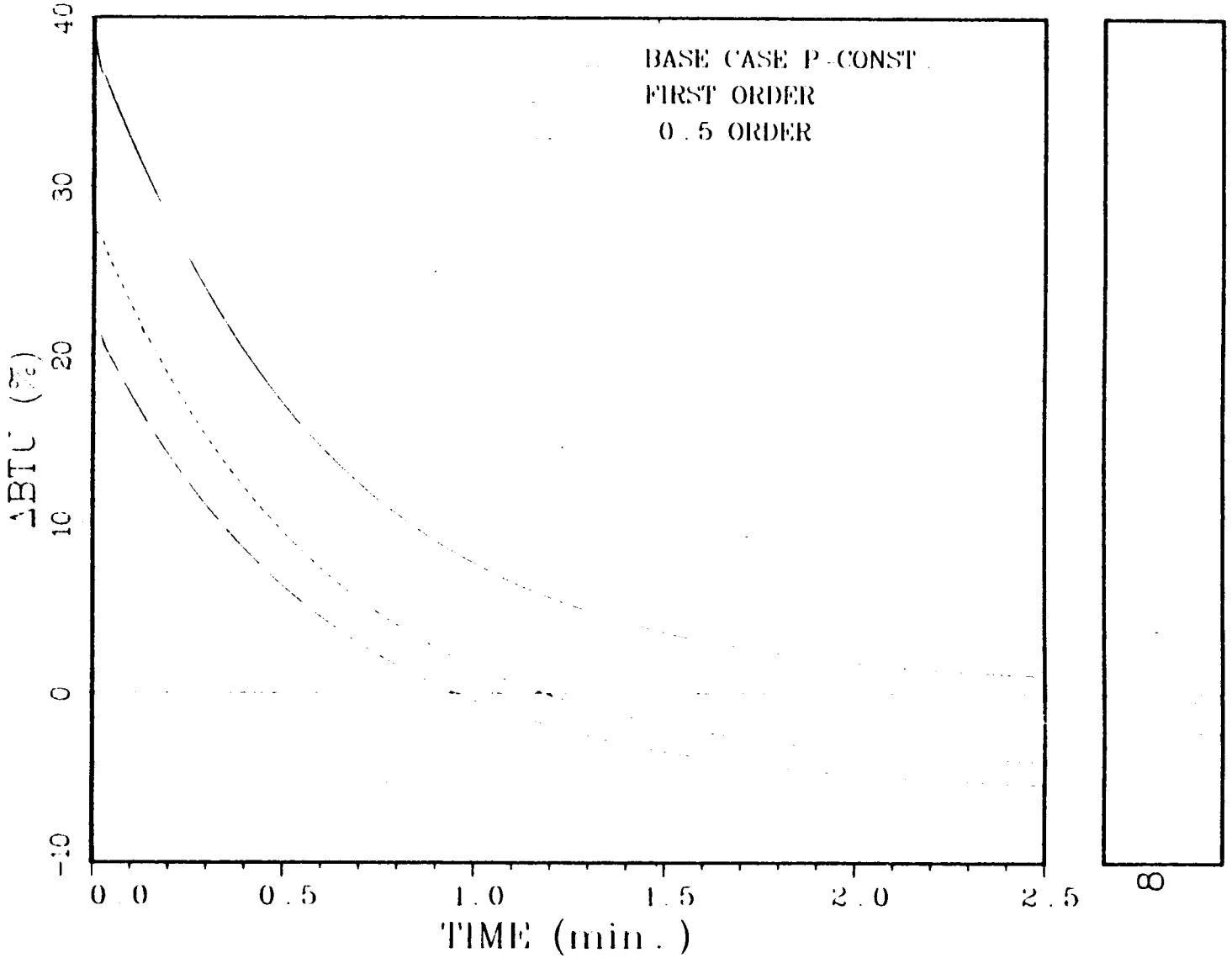

Figure 31b: Closed Loop Response of the Heating Value to a -50% Step in the Air Flow Rate. Constant Linear Velocity (Adjusted Pressure) Control Loop

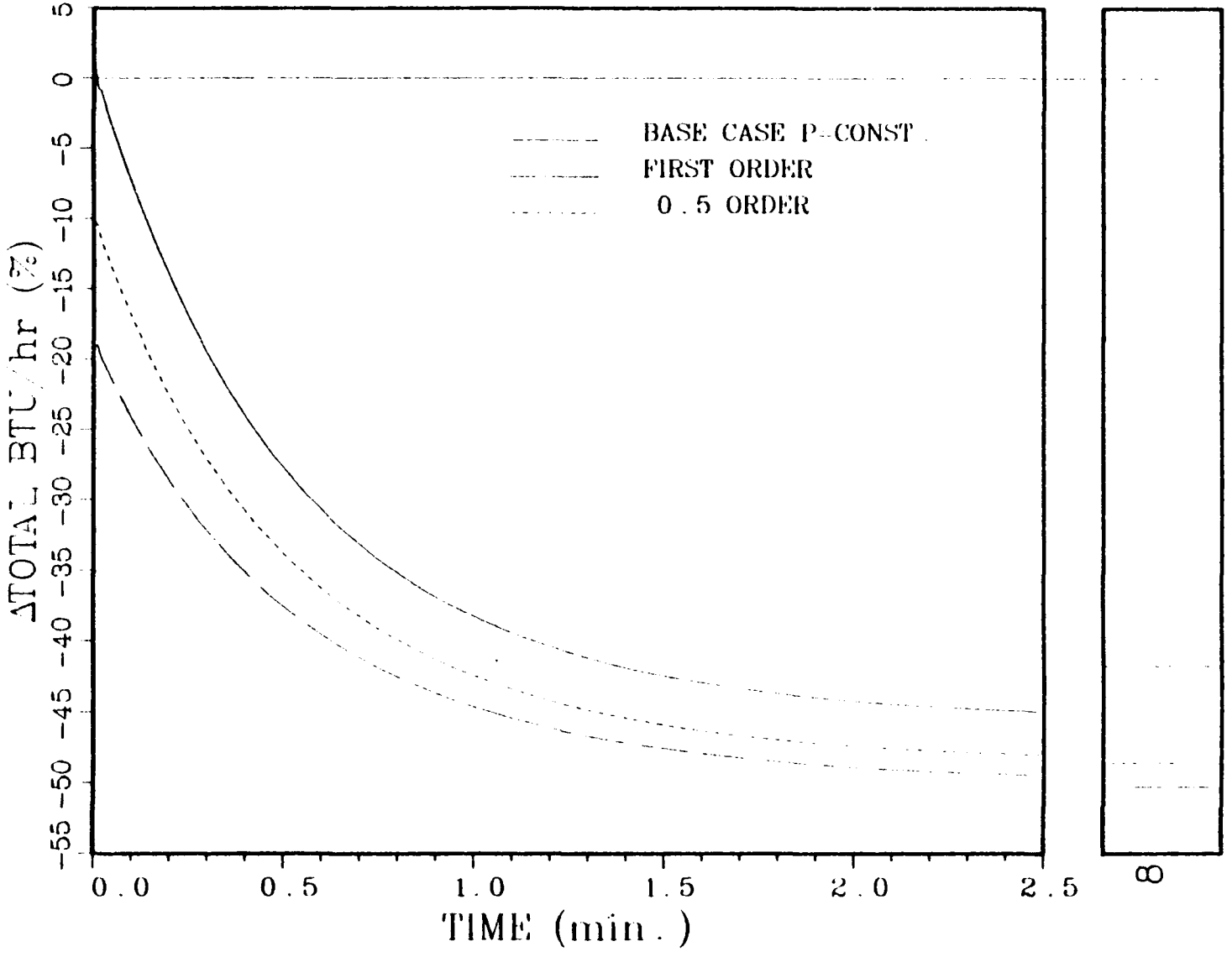

Figure 31c: Closed Loop Response of the Total BTU/Hr. to a -50% Step in the Air Flow Rate. Constant Linear Velocity (Adjusted Pressure) Control Loop

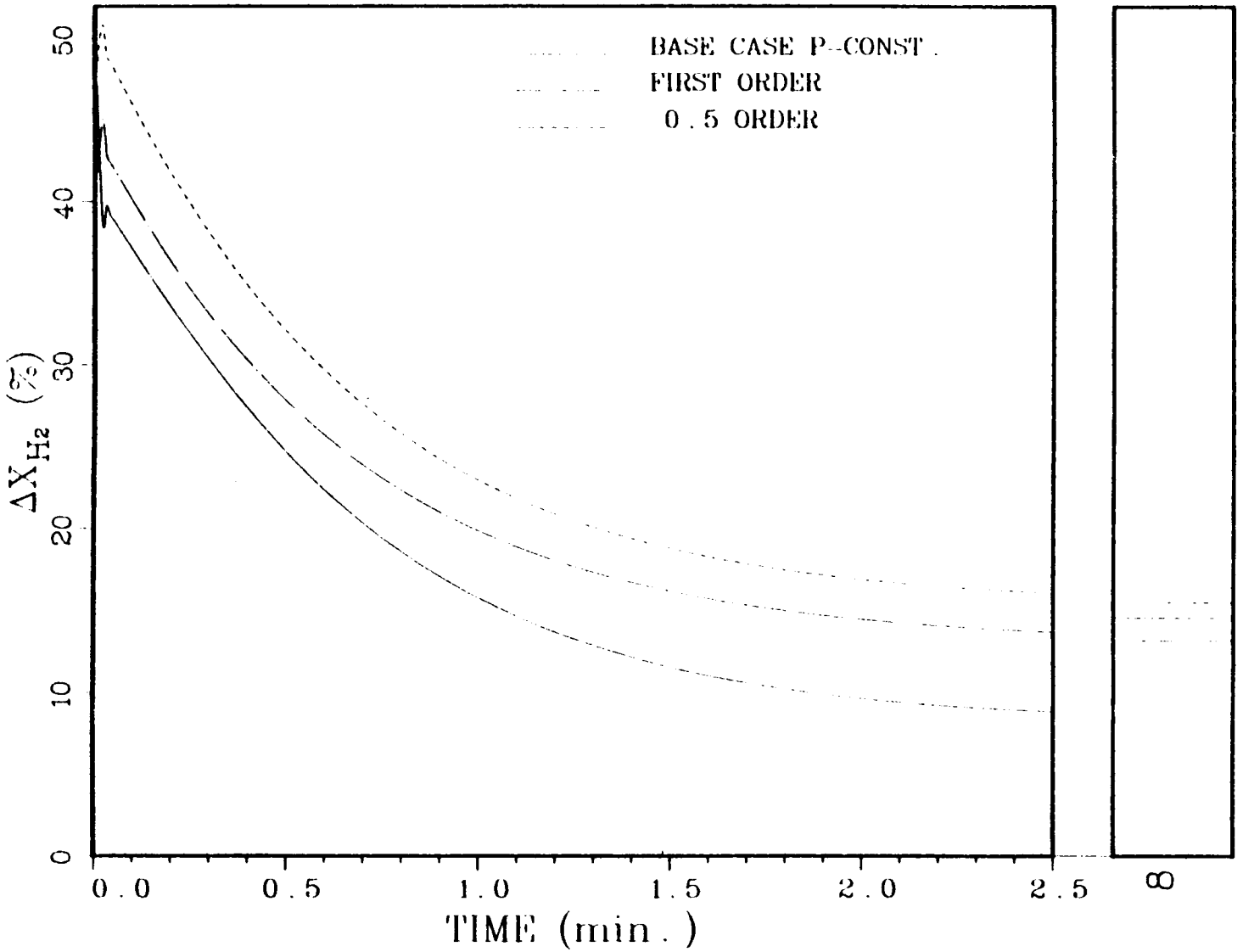

Figure 31d: Closed Loop Response of the Hydrogen Content to a -50% Step in the Air Flow Rate. Constant Linear Velocity (Adjusted Pressure) Control Loop

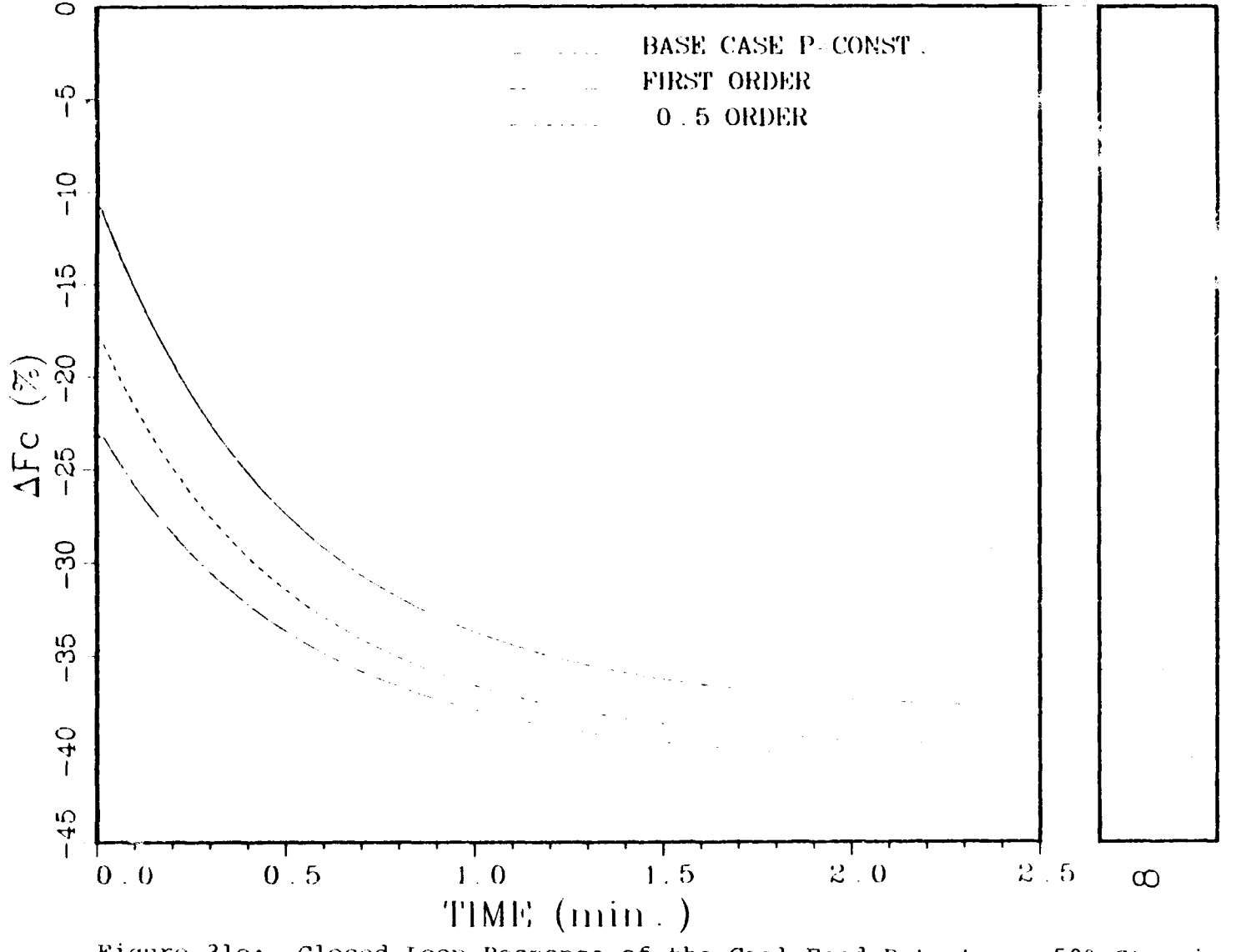

Figure 31e: Closed Loop Response of the Coal Feed Rate to a -50% Step in the Air Flow Rate. Constant Linear Velocity (Adjusted Pressure) Control Loop